DOCTORAL THESIS

Arsenic (V) Adsorption on Iron Oxide

Implications for Soil Remediation and Water Purification

Ivan Carabante

LULEÅ UNIVERSITY OF TECHNOLOGY

Arsenic (V) Adsorption on Iron Oxide

Implications for Soil Remediation and Water Purification

Ivan Carabante

Chemical Technology
Division of Sustainable Process Engineering
Department of Civil, Environmental and Natural Resources Engineering

Luleå University of Technology
SE- 971 87 Luleå
Sweden

October 2012

Cover illustration: the Pumpkin Springs, known as arsenic's pool, in The Grand Canyon shows high levels of arsenic, copper, zinc and lead.

Photo taken from: www.flickr.com/photos/alanenglish/3744877954/in/photostream

Printed by Universitetstryckeriet, Luleå 2012

ISSN: 1402-1544
ISBN 978-91-7439-485-6

Luleå 2012

www.ltu.se

Abstract

Addition of iron oxide based adsorbents to arsenic contaminated soils has been proposed as a mean to reduce the mobility of arsenic in the soil. However, the conditions in the soil such as pH value, the presence of phosphate after addition of fertilizer to the soil or the presence of Zn (II) as a co-contaminant may affect the adsorption of arsenate on the iron oxide and may therefore have implications for the mobility of arsenic in the remediated soil.

In the present work, a new flow method was developed to study the adsorption of arsenate on synthetic iron oxide with high surface area (ferrihydrite) in situ by means of Attenuated Total Reflection – Fourier Transform Infrared (ATR – FTIR) spectroscopy and the method was used for studying how the adsorption of arsenate was affected by the pH/pD value, the presence of phosphate and Zn (II) in the system.

The highest adsorption of arsenate was found at pD 4 and decreased as the pD value increased. The arsenate complexes formed on ferrihydrite appeared to be very stable at pD 4, while the stability decreased as the pD value increased.

Arsenate showed a higher adsorption affinity than phosphate on ferrihydrite under the conditions studied. However, phosphate was able to replace about 10 % of pre-adsorbed arsenate on ferrihydrite at pD 4 and about 20 % of the pre-adsorbed arsenate at pD 8.5 in equimolar concentrations of phosphate and arsenate. Phosphate replaced 30 % of pre-adsorbed arsenate at pD 4 and up to 50 % of pre-adsorbed arsenate at pD 8.5 when the concentration of phosphate in the system was 5 times higher than that of arsenate.

Batch adsorption experiments indicated an enhancement in the arsenate removal from a ferrihydrite suspension in the presence of Zn (II) at pH 8 in accordance with previous reports. However, no adsorption of arsenate on ferrihydrite in the presence of high concentrations of Zn (II) in the system was observed by infrared spectroscopy. Instead, precipitation of zinc hydroxide carbonate followed by arsenate adsorption on the zinc precipitate was found to be the most likely explanation of these results.

Although iron oxides are selective towards arsenate, high specific surface areas are required to achieve sufficiently high adsorption capacity. A method of increasing the specific surface area of coarse hematite particles to obtain a good adsorbent was also developed in the present work. The method comprises an acid treatment to produce iron ions followed by hydrolysis to

precipitate an iron oxy-hydroxide coating on the hematite particles. While the arsenate adsorption capacity of the original coarse hematite particles was found to be negligible, the sintered coarse hematite particles showed good potential as an adsorbent for arsenate with an adsorption capacity of about 0.65 mg[As]/g.

The method developed for studying adsorption on iron oxides by in situ ATR – FTIR spectroscopy was further developed for studying the adsorption of flotation collectors on iron oxides. Iron ore is often separated from gangue minerals by means of reverse flotation in which a surfactant should selectively adsorb on the gangue mineral rendering it hydrophobic. However, unwanted adsorption of the surfactants on the iron oxide has been reported to affect the production of iron ore pellets. A method was developed to study the adsorption of the surfactant Atrac 1563 on synthetic hematite in situ by means of ATR – FTIR spectroscopy. The adsorption of Atrac 1563 on hematite at pH 8.5 was found to mostly occur via interactions between the polar ester and ethoxy groups of the surfactant and the hematite surface.

Acknowledgements

The Swedish Research Council Formas, the Hjalmar Lundbohm Research Center (HLRC) and Luossavaara-Kiirunavaara AB (LKAB) are acknowledged for their finantial support.

I would like to thank my supervisors, Prof. Jonas Hedlund and Assoc. Prof. Mattias Grahn, for guiding me during this journey.

I thank Assoc. Prof. Allan Holmgren, Assoc. Prof. Jurate Kumpiene, Dr. Elisaveta Potapova, Dr. Andreas Fredriksson and Dr. Johanne Mouzon for their valuable contribution to this work.

I offer my thanks to Dr. Anna Maria Vilinska, Dr. Alessandra Mosca, Lic. Eng. Iftekhar Bhuiyan, Lic. Eng. Danil Korelskyi, Eng. Maine Ranheimer and Dr. Evelina Brännvall for their generous help in the laboratory during this time.

All the friends I made during this time at Luleå University of Technology are acknowledged for our time spent together.

I thank my parents, brother, relatives and friends who have always supported me.

Finally, I want to thank my wife Jenni and my sons, Cristian and Mathias, for their loving support and for being my main source of energy.

List of papers

The thesis is based on the following papers.

Paper I: Studies of Collector Adsorption on Iron Oxides by in Situ ATR-FTIR Spectroscopy. E. Potatova, I. Carabante, M. Grahn, A. Holmgren, J. Hedlund. Industrial & Engineering Chemistry Research, 49 (2010) 1493-1502

Paper II: Adsorption of As(V) on iron oxide nanoparticle films studied by in situ ATR-FTIR spectroscopy. I. Carabante, J. Kumpiene, M. Grahn, A. Holmgren, J. Hedlund. Colloids and Surfaces A. Physicochemical and Engineering Aspects, 346, 1-3 (2009) 106–113

Paper III: In Situ ATR-FTIR Studies of Competitive Adsorption of Arsenate and Phosphate on Ferrihydrite. I. Carabante, M. Grahn, A. Holmgren, J. Hedlund. Manuscript Journal of Colloid and Interface Science, 351, (2010) 523-531

Paper IV: Influence of Zn(II) on the adsorption of arsenate onto ferrihydrite. I. Carabante, M. Grahn, A. Holmgren, J. Kumpiene, J. Hedlund. Submitted to Environmental Science and Technology.

Paper V: An Effective Adsorbent prepared from Hematite for Removal of Arsenic (V) from Water. I. Carabante, J. Mouzon, J Kumpiene, M. Grahn, A. Fredriksson, J. Hedlund. Manuscript in preparation.

Contribution of the defendant to the papers

Paper I: contribution to the planning, performance of experimental work regarding film characterisation and contribution to the evaluation of the data.

Paper II - V: Most of planning, experimental work, evaluation of data and writing of papers.

Contents

1 Introduction

1.1 Arsenic in the environment

Arsenic is the 20th most abundant element in natural environment, the 14th in seawater and the 12th in the human body [1, 2]. However, arsenic is very toxic at sufficiently high levels. Long-term exposure to low levels of arsenic may lead to cancer or skin diseases such as blackfoot disease, whilst exposure to high levels of arsenic is lethal [1].

Inorganic arsenic is the predominant form found in natural waters [3] and can be found in two different oxidation states: As (III), the main species of which are arsenic trioxide, sodium arsenite and arsenic trichloride; and As (V), with the main species being arsenic pentoxide, arsenic acid and arsenates. In comparison, As (III) shows higher mobility in soils and higher toxicity for human beings than As (V). However, As (V) is the predominant specie under oxidizing conditions and may thus generally be found more frequently than As (III) species in natural waters such as seawater, lakes and rivers [4 – 7]. The presence of As (III) might, nevertheless, vary in rain water according to the arsenic source [8] and in groundwater since reducing conditions in soils are likely [9]. Organic arsenic species, such as monomethylarsenic acid (MMAA) and dimethylarsenic acid (DMAA), can also be found in natural water, but rarely at concentrations above 1 μg/l [3].

From 2001 the maximum arsenic concentration recommended in drinking water by the World Health Organization (WHO) was changed from 50 μg/l to 10 μg/l [2]. However, no studies on the toxicity of arsenic at concentrations in water below 50 μg/l have been reported [2]. Most countries changed their legislation to follow the WHO recommendation. As a result, areas considered to be contaminated by arsenic increased significantly. Countries such as Argentina, Bangladesh, China, Chile, Mexico and Nepal have retained their limit at 50 μg/l due to the high arsenic content in natural water and also due to the technical and the economic challenges associated with reducing the arsenic levels in drinking water [10].

West Bengal in India and Bangladesh are the areas in the world where the greatest population is exposed to high arsenic concentrations in ground water. However, many countries such as China, Mexico, Argentina, Nepal, Chile, USA or Vietnam also have areas with high arsenic concentrations in the ground water [1].

The origin of arsenic contamination is often natural abundance in the environment [2]. However, contamination can also be a result of human activities, such as carbon combustion, mining activities or from arsenic based pesticides used in many countries [2, 7].

CCA (copper, chromate and arsenate) is a wood preservative based on a copper, chromium and arsenic mixture that was introduced in the 1930s. As a consequence of inappropriate industrial methods of CCA wood preservative impregnation, many of the impregnation sites are now contaminated with high concentrations of arsenic in the soil. Remediation of arsenic contaminated soils is typically done by excavating the soil followed by controlled land filling. However, this method has a negative effect on the environment and is also expensive [11]. Chemical amendment is an alternative to this method. Arsenic mobility and bioavailability is reduced in the soil by the addition of an appropriate chemical to avoid leaching of the contaminant to the environment. The addition of iron compounds, aluminium oxides and to a lesser extent manganese oxides to the soil has been reported as potential inexpensive amendment to reduce leaching of arsenate to the environment [11]. Amorphous aluminium oxides showed a higher specific arsenic adsorption capacity than did iron oxides [12]. However, the still high affinity of iron oxides for arsenic in combination with its abundance and low cost (they may be produced from cheap industrial by-products or wastes) have made them an interesting adsorbent material for arsenic contaminated soil remediation but also for arsenic removal from water [1].

Although promising initial results have been obtained in the different investigations regarding the use of iron compounds as soil amendments to arsenic contaminated soils [13 – 17], this method is still at a development stage and more data is needed to establish both the preferred conditions as well as the conditions to be avoided [11]. The effect of parameters such as pH, redox potential and the presence of other species are examples of important issues to be understood, as is the long-term stability of arsenic in the soil. The influence of these parameters needs to be established before chemical amendment can be accepted as a commercial remediation method [11].

The addition of fertilizers to improve plant growth is often needed after the contaminated soil has been stabilized. Phosphates are one of the principal soil nutrients and are a main component in most fertilizers. The presence of phosphate in the soil water, either due to natural abundance, or as a result of external addition, e.g. from fertilizers, will compete with arsenate species for the adsorption sites of the iron oxide and may therefore affect the stability of the arsenate complexes on the metal oxide [18 – 24].

Soils exposed to leaching water from mine tailings often contain high concentrations of both zinc and arsenic [25]. Soils at old CCA treatment plants, on the other hand, contains high concentrations of chromium, copper, and arsenate, but may also show high concentrations of Zn compounds [26]. The presence of zinc may affect the mobility of arsenate in the soil by affecting the adsorption of arsenate on iron oxides. Previous studies reported an enhancement of arsenic removal from aqueous solution by iron oxides in the presence of Zn (II) in the system [25]. Further studies regarding the Zn (II) / arsenate / iron oxide system could provide valuable information when amending an As and Zn co-contaminated soil by the addition of iron compounds.

1.2 Iron oxides

Two oxidation states of iron, Fe (II) and Fe (III), can be found in the different phases of iron oxides, -hydroxides and -oxy-hydroxides. Hereafter, the term iron oxide will, for the sake of simplicity, be used to refer to iron oxides, iron-hydroxides and iron-oxy-hydroxides. Iron oxides are relatively abundant in natural systems, such as soils, rocks and ground water [27]. There are 16 known different structures of iron oxides. The most relevant iron oxides for the present thesis work are presented in Table 1.

Table 1. Most relevant iron oxides [27].

Oxy-hydroxides and hydroxides		Oxides	
Goethite	α-FeOOH	Hematite	α-Fe_2O_3
Ferrihydrite	$Fe_5O_8H{\cdot}4H_2O$	Maghemite	β -Fe_2O_3
		Magnetite	Fe_3O_4

Goethite (α-FeOOH) is one of the iron oxides with high thermodynamic stability at room temperature. Consequently, it is by far the most common iron oxide found in soils and rocks. It has a hexagonal close packing (hcp) of anions (O^{2-} and OH^-). Despite its high stability at room temperature, goethite transforms to hematite at temperatures above 200 – 400 °C [27]. Ferrihydrite ($Fe_5O_8H \cdot 4H_2O$) is sometimes denoted amorphous iron oxide, even though it has an hcp anion crystalline structure. It is widely abundant in surface environments, but it is only present as nanoparticles being poorly XRD crystalline. Ferrihydrite may recombine to a more stable iron oxide phase, e.g goethite or hematite. Magnetite (Fe_3O_4) is one of the three iron oxides containing iron in the divalent state, Fe (II); however, it also contains trivalent iron Fe (III) in its structure. Magnetite is well known for its magnetic properties and it is an important iron ore. Magnetite has a face-centred cubic crystal (fcc) structure. Magnetite may oxidize by air even at room temperatures, transforming into Maghemite (β-Fe_2O_3) which is isostructural with magnetite. In contrast, only iron in the trivalent state is present in the structure of maghemite. Maghemite occurs in soils as an oxidation product from magnetite and it can further transform into hematite (Fe_2O_3) at temperatures above 300 °C. Hematite presents a very similar structure to goethite based on a hexagonal close packing of the anion (O^{2-}). Hematite is the most thermodynamically stable iron oxide, and it is consequently very abundant in natural systems. Most of the thermal transformations of the different iron oxides lead ultimately to hematite [27].

The main applications of iron oxides are as pigments, as catalysts, as raw material for the iron and steel industry and as an adsorbent for water or gas purification [27, 28].

The iron oxides have also shown good properties as adsorbents for ions, for instance, they have relatively high affinity for several inorganic oxoanions such as sulphate, phosphate or arsenate [27]. Gold particles have been shown to adsorb on synthetic hematite [28]. Goethite, in combination with activated carbon fibre, has been used for NO, SO_2 and NH_3 adsorption [28]. The cosmetics industry has been taking advantage of the adsorption capacity of hematite to remove any arsenic trace elements and thus to reduce the toxicity of their products [28]. Hematite has also been assessed in sensor applications e.g. for detecting fluor or water (humidity) in gases [28].

From the applications listed above it is clear that the adsorption properties of iron oxides make them interesting in a wide range of applications. However, when producing a pure iron oxide concentrate from ore by reverse flotation, some unwanted adsorption of surfactants on the iron oxide may occur under certain conditions, affecting the production of iron ore pellets. In the reverse flotation process, a flotation collector selectively adsorbs on the surface of the gangue mineral (e.g. apatite), to render the surface of that mineral hydrophobic. The gangue mineral then float upon introduction of air in the form of bubbles in the flotation cell, forming a froth rich in the gangue mineral which subsequently may be removed from the flotation vessel. Ideally, no collector should adsorb on the iron oxide and thus the surface of the iron oxide should remain hydrophilic. Therefore the iron oxide fraction will remain in the flotation vessel and can thus be separated from the floating gangue mineral. However, a slight adsorption of the collector agent may occur under certain conditions, e.g. at high concentrations of calcium ions in the process water [29]. The presence of collector agent adsorbed on the iron oxide surface would affect the efficiency of the flotation process, but perhaps more importantly, it may have an adverse effect on the production of iron ore pellets [30]. The adsorption of collector agent on iron oxide during reverse floatation of iron ore is therefore unwanted.

1.3 Adsorption

In the adsorption process, species from a gas or a liquid bind to the surface of a solid or a liquid. The molecules which are extracted from a phase and concentrated at the surface of a solid or liquid are called adsorbate. When the adsorbate adsorbs on a solid surface, the solid material is called adsorbent. The reverse process, in which the molecules detach from the surface of a solid or liquid to a gas or a liquid is called desorption [31].

Two main kinds of adsorption processes occur: chemical adsorption and physical adsorption. Chemical adsorption implies a (covalent) chemical bond between a specific adsorption site of the adsorbent and the adsorbate. On the other hand, in physical adsorption, weak chemical interactions, such as van der Waals and hydrogen bonding occur between adsorbent and adsorbate. Therefore, in physical adsorption, the chemical structure of the adsorbate and adsorbent do not undergo any major chemical changes as a result of the adsorption. Chemical adsorption is normally associated with a higher enthalpy of adsorption and slower kinetics of adsorption than physical adsorption [31 – 32]. Since chemical adsorption implies that the adsorbent reacts with a specific adsorption site of the adsorbent, there is an upper limit to the

quantity which may adsorb on the surface i.e. when the adsorbate has covered all the sites available resulting in a monolayer covering the surface. On the other hand, in physical adsorption, multilayers are frequently formed [32]. This is because the adsorbate molecules can adsorb on each other via van der Waals- or hydrogen bonding forces.

1.3.1 Adsorption isotherms

The amount of adsorbate that adsorbs on a particular adsorbent depends basically on the affinity of the adsorbate for the adsorbent, the concentration of the adsorbate, and the temperature at which the adsorption takes place, as well as the presence of any other molecules that could adsorb simultaneously [31]. To measure or study the adsorption process, adsorption isotherms are typically recorded. Adsorption isotherms show the amount adsorbed at equilibrium as a function of the concentration of the adsorbate in the fluid at a fixed temperature.

The shape of the isotherm has been used to classify the adsorption process into five different classes [32]. The type I adsorption isotherm shown in Figure 1 is a typical adsorption isotherm for a chemical adsorption. However, certain physical adsorption processes may also present this type of isotherm, e.g. adsorption in microporous materials. At low concentrations, the amount adsorbed increases quickly as the concentration of the adsorbate is increased in the fluid. At a certain point, the adsorbate covers the whole surface of the adsorbent and any increase in the concentration does not lead to an increase in the amount adsorbed, this corresponds to a monolayer covering the surface of the adsorbent. The other type of curves shown in Figure 1 illustrates different isotherms encountered where multilayer adsorption occurs. A type II isotherm corresponds to formation of a monolayer on the adsorbent surface, either by chemical or physical adsorption, followed by the formation of a multilayer at higher concentrations. A type III isotherm represents a process in which the adsorbate has a low affinity for the adsorbent. Type IV and V adsorption isotherms usually occur due to multilayer adsorption onto the surfaces of pores in the adsorbent [31].

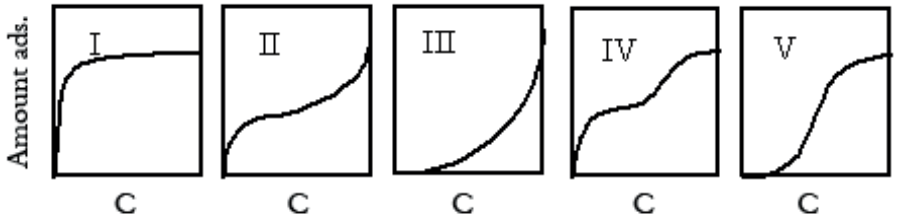

Figure 1. The five adsorption isotherm classes according to IUPAC [32].

To describe the different isotherms observed experimentally, several different models have been devised. The most common model is the Langmuir adsorption model which is a mathematical model describing type I isotherms, see equation 1. It was derived based on three assumptions: only monolayer adsorption is possible, the adsorption takes place at specific sites, and that all sites are equivalent [31, 32].

$$\theta = \frac{q}{q_o} = \frac{K \cdot C}{1 + K \cdot C} \qquad (1)$$

where the fractional loading, θ, is defined as the ratio between loading (q) or surface concentration at a particular concentration in the fluid bulk divided by the saturation loading (q_o) i.e. the surface concentration at monolayer coverage, K is the Langmuir adsorption parameter and C is the concentration of the adsorbate in the fluid bulk in equilibrium with the adsorbed phase.

Another adsorption model frequently encountered is the Freundlich adsorption model. Even though this model was based on the empirical application of equation 2 to experimental data, this model can also be derived with the assumption that the heat of adsorption varies exponentially with surface coverage [33]. However, the experimentally calculated parameters for this equation (2) normally only fit the adsorption data for a small concentration range [31].

$$q = k \cdot C^n \qquad (2)$$

where the parameters k and n in the equation are fitted constants, q is the loading and C is the concentration of the adsorbate in the fluid bulk in equilibrium with the adsorbed phase.

1.3.2 Column adsorption experiments

Packing an adsorbent in a fixed bed in a column is a widely used method for removing contaminants, such as arsenate, from water by adsorption. The feed solution, containing the contaminant is pumped through the adsorbent bed. The contaminant is removed from the solution by adsorption and as a consequence, the effluent out of the column is virtually free of the contaminant. As the adsorbent saturates, the concentration of the contaminant in the effluent stream will start to rise. At this stage the process is usually stopped and the adsorbent regenerated or replaced/disposed [32]. Moreover, the column is often simple and relatively inexpensive to build, while by keeping the adsorbent in a fixed position, erosion of the adsorbent is avoided.

In a column adsorption experiment, the mass transfer zone (MTZ) is the part of the bed where the adsorption reaction takes place. Assuming an upwards flow, below the MTZ the adsorbent particles would be at equilibrium with the solution and no further adsorption would take place. On the other hand, above the MTZ, the concentration of arsenate in solution would be negligible and no adsorption would take place [32]. At the beginning of the adsorption process the adsorption reaction takes place at the bottom of the bed, Figure 2 a. As adsorption reaches equilibrium, the MTZ moves upwards through the bed, Figure 2 b. While the MTZ is completely inside the fixed bed, the adsorbate concentration in the effluent is negligible. The concentration of the adsorbate in the effluent begins to increase as the MTZ reaches the top of the fixed bed column, Figure 2 c. The concentration of adsorbate in the effluent will hereafter increase, Figure 2 d. The time at which all of the adsorbent in the fixed bed is in equilibrium with the fluid, Figure 2 e, the concentration in the effluent equals the concentration of the adsorbate in the influent. A direct indication of the length of the MTZ is the sharpness of the breakthrough curves [32]. The narrower the curve, the smaller the MTZ, and consequently a sharp breakthrough curve is an indication of an efficient adsorption process.

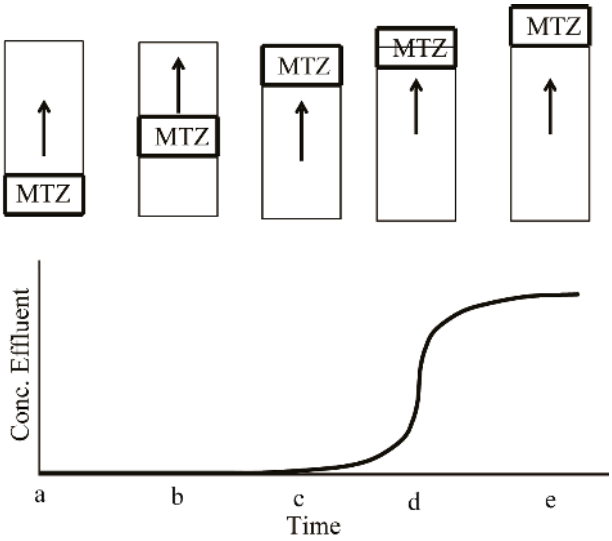

Figure 2. Schematic representation of the location of the MTZ in the adsorbent fixed bed column in relation to the breakthrough curve. The breakthrough curve is obtained by plotting the effluent concentration of the adsorbate vs. time.

The Thomas Model is widely used for modeling the adsorption in column breakthrough experiments [34 - 39]. This model assumes that there is a plug flow in the bed, that the adsorption equilibrium follows the Langmuir adsorption model and that the kinetics of adsorption follows a second-order reversible reaction [35]. The Thomas model is described by equation 3 [35].

$$\frac{C}{C_o} = \frac{1}{1+exp\left(\frac{K_{tho}}{Q}(q \cdot W - C_o \cdot V)\right)} \qquad (3)$$

where C is the concentration of the adsorbate in the effluent, C_o is the feed concentration, K_{tho} the Thomas rate constant, q the amount adsorbed in equilibrium with the concentration in the feed, W the mass of the adsorbent, V the throughput volume and Q the volumetric flow rate.

1.4 Adsorption of arsenate on iron oxides

1.4.1 Influence of pH

The adsorption of arsenate on iron oxides involves interactions between the adsorbate and the hydroxyl group of the iron oxide [27]. This phenomenon was clearly demonstrated when the adsorption of arsenate onto goethite was studied using IR spectroscopy [40]. The surface chemistry of the iron oxides varies with pH. At low pH, the hydroxyl groups at the surface of the iron oxide are doubly protonated ($\equiv FeOH_2^+$) and the surface charge of the iron oxide is thus positive. At a certain pH, the hydroxyl group is protonated with only one proton ($\equiv FeOH$) and thus the (net) surface charge of the iron oxide is neutral. This pH is called the point of zero charge and for iron oxides the point of zero charge (PZC) ranges between 5.5 and 9 [27]. At pH values above the PZC, the hydroxyl group is deprotonated ($\equiv FeO^-$), and consequently the iron oxide surface bears a negative charge. A maximum adsorption of arsenate has been observed at acidic pH values around 4 [41 - 42]. At these pH values, the electrostatic attraction between the negative oxoanion and the positive charge of the iron oxide surface favours adsorption [27]. At pH lower than 3, fully protonated arsenate (H_3AsO_4) species are present in solution and electrostatic attraction is no longer possible, resulting in a lower adsorption. At pH values above the point of zero charge, the iron oxide is negatively charged, and repels the negatively charged arsenate. Consequently adsorption is substantially lower at these pH-values.

1.4.2 Arsenate speciation at the iron oxide surface

Figure 3 shows the possible chemical structures which arsenate may form on the iron oxide surface upon chemical adsorption. The various alternatives have been extensively studied using Extended X-ray Absorption Fine Structure (EXAFS) and FTIR spectroscopy [42 - 46]. Bidentate binuclear complexes have traditionally been reported as the most thermodynamically stable complex formed and thus the most probable [42 - 45].

The conclusions in the literature are, however, contradictory regarding the formation of monodentate complexes. In a recent publication [46], based on EXAFS and FTIR measurements, it was concluded that the only complex formed on the goethite surface was the monodentate species. On the other hand, in other studies it has been concluded that the

formation of monodentate species only occurred at low surface coverage, whereas bidentate binuclear complexes formed at higher surface coverage [43 – 45]. Moreover, in another study it was concluded that the peak assigned to monodentate complex was instead due to the formation of a bidentate mononuclear complex [44]. In yet another publication [45], the conclusion was that the formation of monodentate and bidentate mononuclear complexes was not very likely since they are thermodynamically unstable and that the peak previously assigned to a bidentate mononuclear complex should be assigned to the As-O-O-As structure. Despite the many studies aiming at elucidating the structure of arsenate complexes adsorbed on iron oxide, the reported results are contradictory and there is still no consensus regarding the structure of the complex.

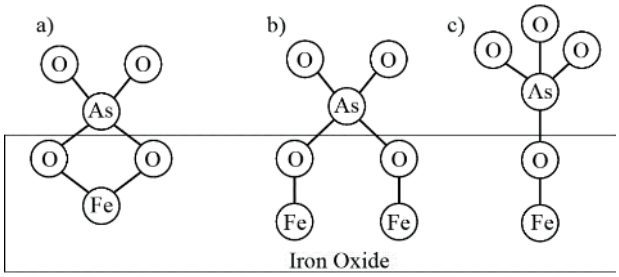

Figure 3. Schematic representation of different complexes that may form on the iron oxide surface. (a) bidentate mononuclear; (b) bidentate binuclear; (c) monodentate. Protons and charges are, of course, not considered in the sketch.

1.4.3 Kinetics of adsorption

The kinetics of adsorption of arsenate on iron oxides have been studied previously [47 – 48], and two distinct adsorption regimes were observed. In the first step, a fast adsorption was observed followed by a second step with significantly slower kinetics. It was proposed that arsenate was adsorbing as monodentate complex in the first relatively fast step, whereas in the second slower step, the monodentate complex reacted forming a bidentate complex [48]. On the other hand, in another study, two different adsorption sites were reported [47]. In that study, the fast adsorption was assigned to arsenate adsorption on more accessible adsorption sites whereas the subsequent slow adsorption process was due to arsenate adsorption on less accessible sites.

1.4.4 Influence of other inorganic anions

Phosphate and arsenate adsorption on iron oxides are very similar with regards to pH dependence, showing higher adsorption capacity at low pH [22, 24]. When arsenate was pre-adsorbed on iron oxides, the adsorption of phosphate was drastically reduced, but the reduction of arsenate adsorption was not as high in the experiment carried out under opposite conditions. Arsenate thus seemed to be more strongly adsorbed on iron oxides than phosphate [22].

The adsorption of phosphate on iron oxide has been studied using ATR (Attenuated Total Reflection) – FTIR spectroscopy [49 – 51]. Protonated binuclear bidentate complexes were predominantly adsorbed at pH values between 3 and 6. At pH > 7.5, however, non-protonated binuclear bidentate complexes were predominantly adsorbed.

The influence of carbonate on the adsorption of arsenate on iron oxide has also been studied [52-53]. Carbonate was reported to slightly enhance arsenate adsorption on hematite at pH 4 and pH 6 [52]. Although a non-straightforward explanation for the arsenate adsorption enhancement was suggested by the authors, the decrease in surface charge density upon carbonate adsorption in combination with arsenate occupying different adsorption sites than carbonate was suggested as a tentative explanation. At pH 8, the arsenate adsorption was reduced by the presence of carbonates [52, 54]. At this pH value, arsenate competes predominantly with bicarbonate for the adsorption sites.

Silicate could inhibit arsenate adsorption on an iron oxide adsorbent more effectively at pH 10 than at pH 7 [54]. Sulfate also decreased the arsenate adsorption on iron oxy-hydroxide from pH 4 to pH 7, while the adsorption of arsenate on zerovalent iron was not significantly decreased by the presence of sulphate [54].

1.4.5 Influence of Zn (II)

Gräfe et al. performed batch adsorption measurements and found that the adsorption of arsenate on goethite was enhanced by 30 % at pH 4 and by more than 500 % at pH 8 in the presence of Zn^{2+} [25]. Two mechanisms were proposed to explain the enhancement of

arsenate adsorption on iron oxide in the presence of Zn^{2+} [25]. At lower concentrations arsenate could form bridging complexes on iron and zinc sites. At higher concentrations a surface precipitate could be formed on the hydroxyl groups of the iron oxide.

Yang et al. performed batch adsorption measurements where the adsorption of arsenate on magnetite in the presence of Zn^{2+} showed an enhancement in the adsorption of arsenate on magnetite at pH 8, although no significant changes in the arsenate adsorption was observed at pH 4 [55]. The formation of a ternary zinc – arsenate - iron oxide complex was reported as the most plausible explanation for the enhanced arsenate adsorption on magnetite at pH 8 [55].

1.4.6 Iron-based adsorbents

Iron oxide minerals are quite abundant in nature, relatively inexpensive as well as shows high adsorption affinity for both arsenate and arsenite [56, 57]. Therefore, the use of iron oxides as adsorbents constitutes a very attractive alternative for removing arsenate from contaminated water [1, 27, 57]. For an adsorbent to show high adsorption capacity, a high specific surface area is necessary, and this is typically achieved by reducing the particle size to nanoparticles scale. However, the separation of nanoparticles from solution after the removal process may be difficult [1].

A strategy to produce an effective iron oxide based adsorbent that simultaneously shows high adsorption capacities (high specific surface areas) and facilitates a straightforward separation of the adsorbent from solution, is to coat an inert material by active iron oxide nanoparticles with high specific surface area. The iron oxide nanoparticle coating may, for instance, be prepared by fast precipitation from Fe (III) salts. Examples of these kind of adsorbents are: iron oxide coated sand [34, 58 - 59], iron oxide coated cement [60 - 61], Fe (III)-modified natural zeolite tuff [62], iron hydroxide–coated alumina [63], iron salt pre-heated activated carbon [1] or iron oxide coated glass fibers [64]. Another strategy to obtain an effective adsorbent that is easy to separate from the solution is to granulate the fine iron oxide powder with a high pressure process obtaining a so-called granular ferric hydroxide [34]. The use of zero valent iron as an adsorbent is another alternative providing good arsenic removal from water [1]. The formation of iron oxide nanoparticles upon oxidation of the zero valent iron is, nevertheless, required before any substantial arsenic adsorption would take place [15].

1.5 In situ ATR - FTIR spectroscopy

ATR - FTIR spectroscopy has proven to be a powerful tool for the studies of adsorption on synthetic and natural mineral surfaces [65 - 69].
In the ATR technique, the incident IR beam is totally reflected inside an ATR crystal, see Figure 4. At each reflection, the electric field of the IR radiation probes the vicinity of the crystal surface where the sample is placed. The intensity of the electric field (E) probing the sample decreases exponentially with the distance from the surface of the ATR crystal according to equation 4.

$$E = E_0 \exp\left(-\frac{2\pi}{\lambda_1} \left(\sin^2 \theta - n_{21}^2 \right)^{1/2} Z \right) \qquad (4)$$

where E_0 is the intensity of the electric field at the surface of the ATR crystal (at Z = 0), λ_1 is the wavelength of the infrared radiation in vacuum (λ) divided by the refractive index of the ATR crystal (n_1), n_{21} is the ratio of the refractive index of the sample medium (n_2) divided by the refractive index of the ATR crystal (n_1), θ is the angle of incidence, and Z is the distance perpendicular from the surface of the ATR crystal.

Total reflection of the IR beam in the ATR crystal occurs when the refractive index of the sample (n_2) is significantly lower than the refractive index of the ATR crystal (n_1) and when equation 5 is fulfilled [70].

$$\sin^2 \theta - n_{21}^2 \geq 0 \qquad (5)$$

The depth of penetration, d_p, is defined as the distance from the ATR crystal at which the intensity of the electric field has decreased to a value of e^{-1} (37 %) of the intensity at the surface of the ATR crystal [70], and accordingly, it is a rough measure of the distance sampled. For a two-layer system (ATR crystal and sample) the penetration depth is given by equation 6.

$$d_p = \frac{\lambda}{2\pi n_1 \left(\sin^2 \theta - n_{21}^2 \right)^{1/2}} \qquad (6)$$

As seen in equation 6, the depth of penetration depends on the refractive indices of both the ATR crystal and the sample as well as of the wavelength of the incident beam. Thus, the depth of penetration increases with decreasing wavenumber. In the present work, the depth of penetration in the frequency range 1000 – 800 cm^{-1} is about 1 μm.[3] Since the technique only probes the vicinity of the crystal, it is a powerful tool for studying the properties of thin films and their surface chemistry, e.g. study of adsorption on nanoparticles films [71]. The nanoparticles typically give sufficiently high surface area, i.e. adsorption capacity, to obtain well resolved FTIR spectra [71]. Currently, only a few publications are available on the use of in situ ATR – FTIR techniques for studying As (V) oxyanion sorption on iron oxides [7, 46, 69].

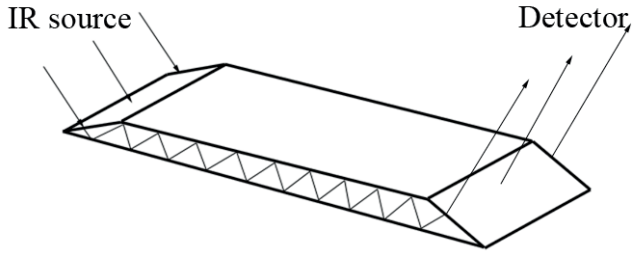

Figure 4. Schematic representation of the IR beams propagating through the ATR element.

1.6 Scope of the present work

The scope of the present work can be summarized in three main points:

1. Develop novel flow methods for real in situ studies of adsorption on iron oxide films by means of ATR – FTIR spectroscopy. Two different systems were studied by the developed methods: arsenate adsorption on ferrihydrite and the "unwanted" adsorption of a collector agent on hematite. The development and application of such techniques for these systems is novel.
2. Study systems relevant to stabilization of CCA contaminated soils by means of real in situ ATR – FTIR spectroscopy to provide new scientific insights. The two different systems studied were: the competitive adsorption of phosphate and arsenate on ferrihydrite and the effect of Zn (II) on the adsorption of arsenate onto ferrihydrite.
3. Develop an inexpensive method for preparing an effective adsorbent from an iron oxide raw material for arsenate removal from water.

2 Experimental

2.1 Synthesis of the materials

Hematite films (Paper I): Synthetic hematite nanoparticles were synthesized in accordance with the method described by Matijevic et al. 1985 [72]. The resulting hematite particles were centrifuged and redispersed in a 0.06 M acetic acid solution. Hematite films coating both sides of an ATR crystal (ZnSe; Crystan; trapezoidal 52 mm x 20 mm x 2 mm, 45 ° edge cut) were obtained by means of dip coating using a 2 (w) % hematite suspension in 6.27 M acetic acid solution, see paper I.

Ferrihydrite films (Paper II – IV): Ferrihydrite nanoparticles were synthesized in accordance with the method described by McComb et al. 2007 [73], see Paper II – IV. The obtained ferrihydrite particles were purified by dialysis against distilled water. A volume, 600 µl in the work described in Paper II or 500 µl in the work described in Paper III – IV, of the ferrihydrite suspension, diluted with 50 (w) % methanol, was spread on each side of the ATR crystal. A ferrihydrite film was thus formed on both sides of the waveguide crystal after the spread drop dried.

Iron oxide based Adsorbent (Paper V): Magnetite powder (Magnachem 10, Minelco, > 98.7 %) was heat-treated from 24 hours at 1200 °C. The solid body which was obtained as a result of the heat treatment was crushed and sieved to a size range -1.2 mm to +0.59 mm. The sieved particles were subsequently in contact with a 6 M hydrochloric acid solution for 3 h. The particles were thereafter repeatedly (5 times) rinsed with 12 M sodium hydroxide solution and dried at 50 °C and finally rinsed with generous amounts of distilled water.

2.2 Characterisation of the materials

Scanning electron microscopy (SEM): The hematite and ferrihydrite film morphology was investigated using scanning electron microscopy (SEM). A Phillips XL 30 microscope was used in the work described in Paper I and II to investigate gold coated samples. In the work

described in Paper III – V a FEI Magellan 400 microscope was used to investigate the ferrihydrite film and the adsorbent particles without gold coating.

X-Ray Diffraction (XRD): The crystallographic structure of the hematite film (Paper I) and the ferrihydrite freeze-dried powder (Paper II) were performed using a Siemens D5000 diffractometer running in Bragg-Brentano geometry. The crystallographic structure of the adsorbent particles (Paper V) was analysed using a PANalytical Empyrean instrument, equipped PIXcel3D detector and a Cu LFF HR X-ray tube.

Electrophoresis: The point of zero charge of the hematite and ferrihydrite films was determined using a ZetaCompact instrument, see Papers I and II. The electrophoretic mobility of the iron oxide particles in 0.01M KNO_3 aqueous solutions at pH values from about 2 to 11 was measured. The data was evaluated applying the Smoluchowski equation.

Nitrogen adsorption: The specific surface area of the hematite (Paper I), ferrihydrite (Paper II) and adsorbent particles (Paper V) was determined from N_2 adsorption data at liquid nitrogen temperature using a Micrometrics ASAP 2010 instrument.

2.3 In situ ATR – FTIR adsorption measurements

A Bruker IFS 66v/s FTIR-spectrometer equipped with either a liquid nitrogen cooled MCT (mercury cadmium telluride) detector (Paper I) or a DTGS (Deuterated TriGlycine Sulphate) detector (Paper II – IV) was used for recording infrared spectra.

Figure 5 shows a schematic of the experimental set-up. The pH value (Paper I) or the pD value (Paper II – IV) of the solutions were automatically controlled with a Mettler Toledo, T70 pH-stat instrument. Deuterium oxide (D_2O, Aldrich, 99 atom % D) was used as solvent in the work presented in Paper II – IV since ordinary water is interfering with the absorption bands from arsenic species. The liquid solution was pumped by a peristaltic pump from the solution vessel into the stainless steel flow cell mounted in the spectrometer. The flow cell comprised two liquid compartments of about 2.5 cm^3 each connected in series. After being in contact with both sides of the ATR crystal, the solution was recirculated back to the vessel.

A background spectrum, using the same solvent (H_2O/D_2O), ionic strength and pH/pD value as in the subsequent experiment, was recorded before each adsorption experiment after the solvent and the iron oxide films had stabilized for several hours. Thereafter, the solution containing the adsorbate was pumped through the system and spectra were periodically recorded during the adsorption experiment.

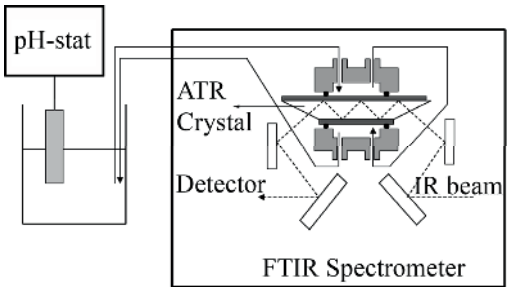

Figure 5. Schematic figure of the experimental set-up used to perform the in situ ATR-FTIR measurements.

2.4 Batch adsorption experiments.

Batch adsorption experiments of solutions/suspensions at pH 8 were performed at different arsenate and Zn (II) concentrations, see Table 2 in section 3 for details (Paper IV). The equilibration time for adsorption was 72 h, and the pH was controlled and adjusted every 24 h. The ferrihydrite nanoparticles were separated from the solution by filtration and the supernatant was subsequently analysed by means of Induced Coupled Plasma – Optical Emission Spectroscopy (ICP - OES, Perkin Elmer optima 2000 DV).

Different volumes of a 0.48 g[As]/l arsenate stock solution were added to 100 ml distilled water containing 3 g of the adsorbent (Paper V). The pH of the suspension was controlled and automatically adjusted to pH 5 using an automatic multi-titrator (TitroWico, Witenfeld and Cornelius). After 24 h of equilibration time, the iron oxide based adsorbent particles were separated from the suspension by filtration and the supernatant was analysed by means of ICP - OES.

2.5 Column adsorption experiments

A glass column (i.d. = 1.9 cm; H = 20 cm) was filled with 45 g adsorbent. The height of the bed of adsorbent was about 10 cm (Paper V). A 500 μg[As]/l arsenate solution in distilled water adjusted to pH 5 was pumped upwards through the column at three different flow rates: 3.5 ml/min, 12.5 ml/min and 21.7 ml/min using a peristaltic pump. The effluent solution from the column was transported through a propylene tube to a 2 ml open vessel from where small aliquots were automatically sampled for analysis by an arsenic online analyzer (Istran, EcaMon SaFIA, using a E-T Au electrode) with an analytical range from 5 μg[As]/l to 500 μg[As]/l.

Desorption experiments were performed after saturation of the adsorbent by flushing the column with water adjusted to pH 12 or pH 5 at a flow rate of 21.7 ml/min.

3 Results & Discussion

3.1 Method development for real in situ studies of adsorption on iron oxide films (Papers I, II)

3.1.1 Method to study the adsorption of collector agents on a hematite film in situ (Paper I)

Figure 6 shows a cross-sectional SEM image of a hematite film on top of a ZnSe ATR crystal. Samples like this were used for studies of the unwanted adsorption of collector agents by in situ ATR – FTIR experiments. The film is comprised of spherical particles with a diameter of about 130 nm. The particles formed a porous and even film on top of the crystal with an average thickness of about 1 μm. The crystal phase of the iron oxide particles in the film was determined to be hematite by means of XRD, see Paper I. The point of zero charge of the iron oxide was estimated by electrophoresis to be 4.8, see Paper I.

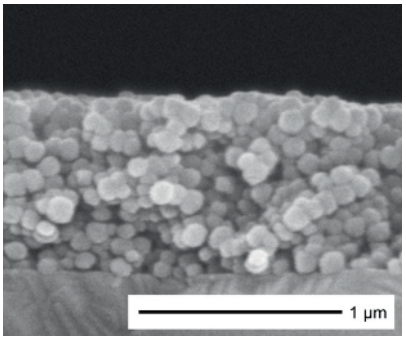

Figure 6. Cross-sectional SEM image of a hematite film on a ZnSe crystal.

A real in situ method to study the unwanted adsorption of Atrac 1563 (a commercial flotation collector), with the chemical structure shown in Figure 7 (a), on hematite at pH 8.5 was developed, as described in Paper I. Three model compounds were selected in order to better understand the adsorption mechanism of Atrac 1563 on hematite: ethyl oleate see Figure 7 (b), maleic acid see Figure 7 (c) and poly(ethylene glycol) monooleate (PEGMO) presented in figure 7 (d) .

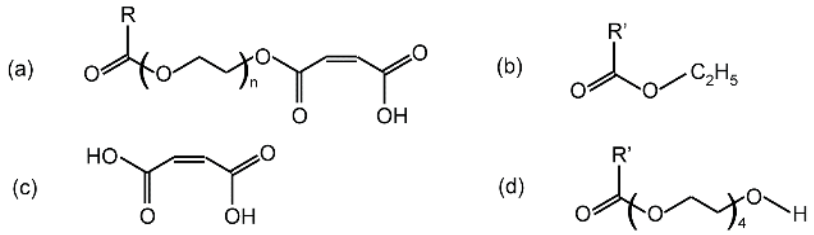

Figure 7. Chemical structures of (a) Atrac 1563, (b) ethyl oleate, (c) maleic acid (d) poly (ethylene glycol) monooleate (PEGMO). R represents a linear alkyl chain from fatty acids or a $C_{19}H_{29}$ chain in resin acids while R' represents $CH_3(CH_2)_7CH{=}CH(CH_2)_7$.

Figure 8 illustrates spectra recorded of pure Atrac 1563 and pure PEGMO spread on an uncoated ATR crystal and of 10 mg/l, Atrac 1563 and PEGMO, solutions in contact with a hematite film coated on an ATR-crystal. No signal arose from the surfactants (Atrac and PEGMO) when 10 mg/l solutions were in contact with uncoated ATR crystals, indicating that very little adsorption of reagent on the ATR crystal occurred. However, when the ATR crystal was coated with a hematite film several bands assigned to the surfactants appeared in the spectra, indicating a substantial adsorption of the surfactant on the hematite particles. The C=O bond of the free carboxylic acid was observed at 1709 cm^{-1} in the spectrum recorded of pure Atrac 1563 using an uncoated ATR crystal, Figure 8 (top-left). This band was not observed in the spectrum recorded of Atrac 1563 adsorbed on hematite, Figure 8 (bottom-left), however, two bands situated at 1568 cm^{-1} and 1456 cm^{-1} appeared in the spectrum, revealing that the carboxylic group of adsorbed Atrac 1563 was deprotonated at pH 8.5. No adsorption of maleic acid on hematite was observed at the pH studied. This result was explained by the electrostatic repulsion between the carboxylate ion and the negatively charged surface of hematite. Hence, the contribution of the free carboxylic group of Atrac 1563 on its adsorption on hematite was considered as minor at pH 8.5. A substantial shift of the ester carbonyl band of Atrac 1563, from 1736 cm^{-1} (pure Atrac; top-left image) to 1722 cm^{-1} (adsorbed Atrac, bottom-left image), was observed upon adsorption. This result suggests that other polar parts of the molecule apart from the carboxylic acid e.g. the ester- and ethoxy groups were mainly interacting with the iron oxide surface.

PEGMO adsorbed on the hematite film to a similar extent as Atrac 1563, Figures 8 and 11 in Paper I. The adsorption of PEGMO on hematite was suggested to occur via the poly (ethylene glycol) chain since shifts in the vibration frequencies of both the C-O group, from 1115 cm^{-1} (pure PEGMO, Figure 8, top-right image) to 1095 cm^{-1} (adsorbed PEGMO, Figure 8, top-

left), and the O-H group, from 1070 cm^{-1} to 1047 cm^{-1}, were observed upon adsorption. The adsorption of ethyl oleate on hematite was ca. 6 times lower than the extent of adsorption of PEGMO or Atrac 1563 (Figure 9 Paper I) probably because of the weak interaction between the ester group of ethyl oleate and the hematite surface.

Flushing experiments with distilled water at pH 8.5 and pH 10 (Fig. 13 in Paper I) showed that Atrac 1563 could only partially be desorbed from the hematite surface, which implies a relatively strong interaction between the surfactant and the iron oxide.

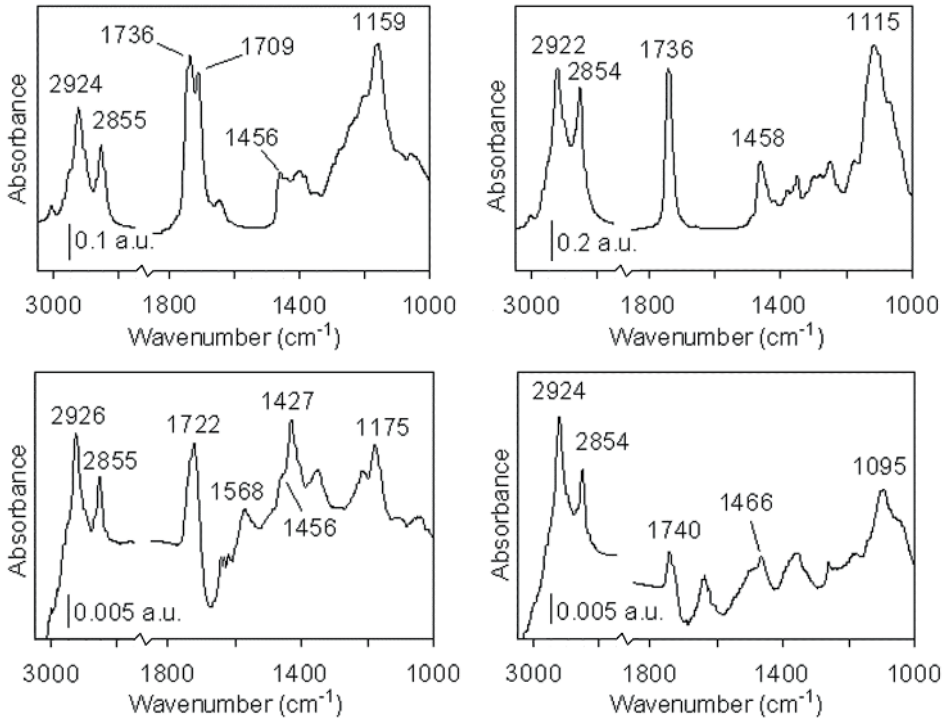

Figure 8: left: Infrared spectra of (top) Atrac 1563 on ZnSe and (bottom) Atrac adsorbed on hematite film from a 10 mg/l aqueous solution. **right:** Infrared spectra of (top) PEGMO on ZnSe and (bottom) PEGMO adsorbed on hematite film from a 10 mg/l aqueous solution.

To summarize, a mechanism for Atrac 1563 adsorption on hematite could be proposed as a result of the investigations on how the commercial collector as well as the model substances adsorbed on hematite using the developed method. It was also shown that an increase in the pH value, from 8.5 to 10, would prevent the unwanted adsorption of Atrac 1563 on hematite.

3.1.2. Method to study the adsorption of arsenate on a ferrihydrite film in situ (Paper II)

Figure 9 (left) shows an X-ray diffractrogram of the freeze dried ferrihydrite powder prepared in the present work. The peak positions were in good agreement with the reference pattern for 6-line-ferrihydrite. The peaks were very broad indicating that the crystal size of the iron oxide was very small as reported previously [27]. The Z-potential of the iron oxide surface in a 0.01 M KNO_3 background electrolyte was determined as a function of pH, see Figure 9. The point of zero proton charge was estimated to be between 7.5 and 8, which is in good agreement with the values reported in the literature [27]. Even though all the adsorption experiments were performed in D_2O as solvent and not in H_2O, it was assumed that the iron oxide surface behaves in a similar manner in both solvents, and thus the point of zero deuterion charge was assumed to be close to the point of zero proton charge.

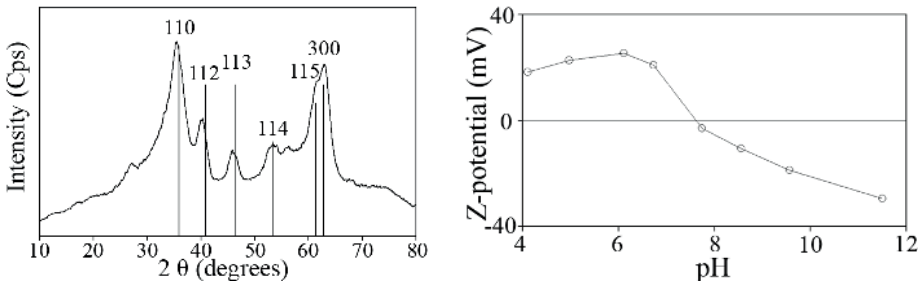

Figure 9. To the left: X-ray diffractogram of the freeze-dried iron oxide powder. The vertical bars indicate the peak positions with their relative intensities and the Miller indices of the planes from the reference pattern of 6-line-ferrihydrite. **To the right:** Z-potential of the iron oxide as a function of pH in a 0.01M KNO_3 background electrolyte

Figure 10 shows a cross-sectional SEM image of a 6-line ferrihydrite film on an ATR-crystal. Similar films were subsequently used in the ATR experiments. The film was comprised of very small and densely packed particles. The film thickness was about 200 nm. (Paper IV). Several images were recorded at different locations on the film and it was found that the film thickness was even for a single film. However, the films used in the measurements presented in Paper II showed a film thickness of 800 nm and the film used in Paper III showed a film thickness of about 400 nm. The difference in thickness between the films was mainly a result of different amounts and concentration of ferrihydrite suspension used when preparing the films. Figure 10 also shows a high magnification image of the ferrihydrite particles in the film showing that the diameter of the ferrihydrite particles was below 10 nm.

The surface area of the iron oxide freeze-dried powder was determined to be 190 m^2/g from N_2 adsorption data. From the specific surface area, and by assuming spherical, non-porous particles, and a particle density of ferrihydrite of 3.96 g/cm^3 [27], a particle size of 8 nm was calculated, which is in good agreement with the observation by SEM.

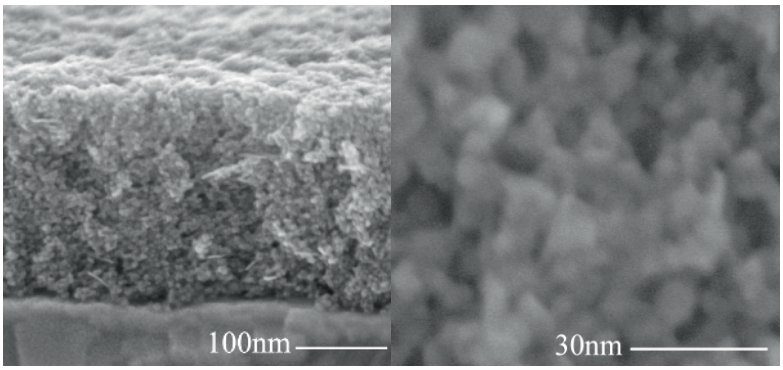

Figure 10. To the left: cross-sectional SEM images of 6-line ferrihydrite film (gold uncoated) (paper IV). **To the right:** High magnification SEM image of 6-line ferrihydrite particles (gold uncoated) comprising the film.

Figure 11 shows the spectra recorded from arsenate solutions (13 mM) using an uncoated ATR crystal at pD 4 (a), at pD 8.5 (b), and at pD 11.8 (c). Consequently the signal in these spectra only originates from arsenate species in solution. Three absorption bands viz. at 908 cm^{-1}, 875 cm^{-1} and 730 cm^{-1} appeared in the spectrum at pD 4. At this pD value, $D_2AsO_4^-$ is the predominant specie in solution (reaction 1 [1]). At pD 8.5, only one absorption band at 856 cm^{-1} appeared in the spectrum (Figure 11b). The predominant arsenate species in solution at this pD is $DAsO_4^{2-}$. At pD 11.8, both $DAsO_4^{2-}$ and AsO_4^{3-} species are present in solution (reaction 1). Therefore, the spectrum recorded at this pD (Figure 11c) shows an absorption band at 856 cm^{-1} assigned to the $DAsO_4^{2-}$ species in solution and another absorption band at 806 cm^{-1} originating from AsO_4^{3-}. It is thus possible to distinguish between the different arsenate species in solution using the ATR – FTIR technique. Figure 11 also shows the spectra recorded after 5 hours of arsenate adsorption on a ferrihydrite film from a 0.03 mM solution at pD 4 (d). As elaborated in Paper II, no signal from arsenate species in solution could be detected at concentrations below 1 mM, which indicates that the bands shown in this spectrum originated from arsenate adsorbed on ferrihydrite. The bands were situated at 875 cm^{-1} and 840 cm^{-1}, i.e. at different wavenumbers than the bands from the dominating arsenate species in solution at this pD, viz. $D_2AsO_4^-$ which had absorption bands at 908 cm^{-1}, 875 cm^{-1} and

730 cm^{-1}. Therefore, Figure 11 illustrates the ability of the technique to distinguish arsenate species adsorbed on an iron oxide film from arsenate species in solution.

$$H_3AsO_4 \xleftrightarrow{pKa1=2.1} H_2AsO_4^- + H^+ \xleftrightarrow{pKa2=6.7} HAsO_4^{2-} + 2H^+ \xleftrightarrow{pKa3=11.2} AsO_4^{3-} + 3H^+ \quad (1)$$

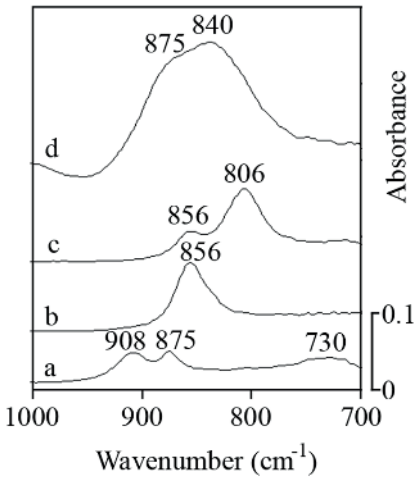

Figure 11. Spectra of a 13 mM arsenate solution recorded at a) pD 4, b) pD 8.5 and c) pD 11.8 using an uncoated ZnSe crystal. Spectrum d) was recorded from a 0.03 mM arsenate solution after 5 hours in contact with a feriydrite film.

To conclude, a method for studying the adsorption of arsenate on a ferrihydrite film was developed. It was shown that the different arsenate species in solution could be distinguished from arsenate species adsorbed on ferrihydrite by means of ATR – FTIR spectroscopy. At concentrations in solution below 1 mM, only species adsorbed on ferrihydrate could be detected (no signal from species in solution).

3.2 Adsorption of arsenate on ferrihydrite (Paper II – IV)

3.2.1 Influence of pD on arsenate adsorption on ferrihydrite (Paper II)

Figure 12 shows spectra of arsenate species adsorbed on a ferrihydrite film from a 0.03 mM arsenate solution at different pD values ranging from 4 to 12. Two bands, situated at 875 cm^{-1} and 840 cm^{-1} in the spectra recorded at pD 4 and 6, originated from adsorbed arsenate on ferrihydrite. The bands shifted to 855 cm^{-1} and 830 cm^{-1} in the spectrum recorded at pD 8. The observed shifts are probably due to de-deuteration of the adsorbed arsenate species, as elaborated in Paper II. Further, the absorption bands were more intense at lower pD, indicating that arsenate adsorbed to a larger extent at lower pD values. Spectra recorded at pD 10 only showed weak bands indicating very low adsorption of arsenate at this pD, and at pD 12, no bands from adsorbed arsenate could be observed in the spectrum. Notice here that the intensity of the absorption bands should be proportional to the amount of species adsorbed onto ferrihydrite [70]. This statement is true provided: that the infrared absorption from species in solution can be neglected, that the change of the refractive index of the sample with time can be neglected, and that the molar absorptivity of adsorbed arsenate was constant. The observed adsorption behaviour, with less adsorption at higher pD values, was expected since the iron oxide surface is more positively charged at lower pD values and the electrostatic attraction between the iron oxide surface and the negatively charged oxoanion would thus favour the adsorption at lower pD values. This result is in agreement with previous reports on the adsorption of arsenate on ferrihydrite [74]. At higher pD values, the surface of the iron oxide is negatively charged and thus the electrostatic repulsion between iron oxide surface and the negatively charged oxoanions would hamper the oxoanion adsorption.

Figure 13 shows the peak height of the band at 840 cm^{-1} originating from arsenate adsorbed on the ferrihydrite film from a 0.03 mM arsenate solution at pD 4 plotted versus the time of adsorption. After 300 minutes, the pD was changed to either 8.5 (Δ) or 12 (□) while keeping the arsenate concentration constant. As the pD was changed from 4 to 8.5, arsenate immediately desorbed from the iron oxide and after 5 hours approximately 20 % of the arsenate originally adsorbed had desorbed from the surface. However, when the pD was changed from 4 to 12, about 65 % of the arsenate had desorbed after the same time. At both values of pD, the desorption of arsenate was very fast within the first 40 min followed by a slower desorption process at longer times.

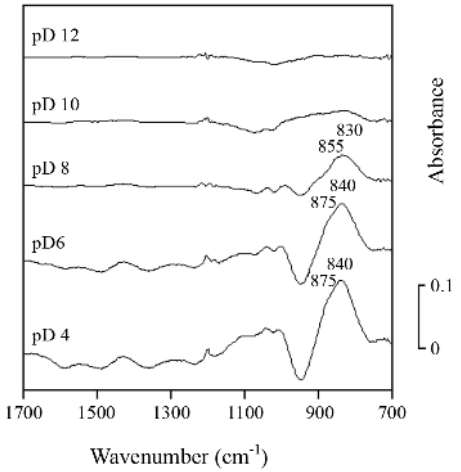

Figure 12. Spectra of arsenate adsorbed on iron oxide at different pD values after 70 min of adsorption from a 0.03 mM arsenate solution.

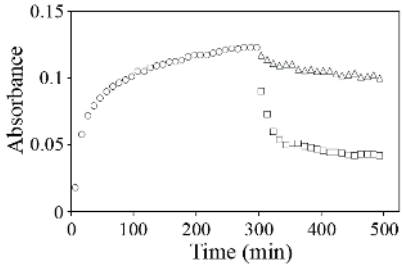

Figure 13. Adsorption and desorption kinetics followed by monitoring the 840 cm^{-1} absorption band of arsenate. The adsorption (○) was conducted at pD 4 at a concentration of 0.03mM. At t = 300 min, the pD was changed to either (Δ) 8.5 or (□) 12, while keeping the concentration of arsenate in the solution constant at 0.03 mM.

Rinsing experiments were designed to assess the stability of the arsenate complexes formed on the iron oxide film at different pD values. Figure 14 shows the spectra recorded at different times while pre-adsorbed arsenate was rinsed by pure D_2O adjusted to the same pD as in the pre-adsorption. At pD 4, Figure 14 (left), only a small fraction of arsenate desorbed from the iron oxide film during the duration of the rinsing experiment (200 minutes). About 90 % of the arsenate pre-adsorbed was still adsorbed after 200 minutes of the rinsing experiment. On the other hand, significant desorption of arsenate was observed in the rinsing experiment performed at pD 8.5, Figure 14 (right), with 60 % remaining after 200 minutes of rinsing. The percentage of the remaining arsenate adsorbed on the iron oxide surface after the rinsing experiment was calculated from the change in the peak height of the spectra. These experiments thus indicate that the arsenate complexes were more strongly bonded to the iron

oxide surface at pD 4 than at pD 8.5. The weaker adsorption at the latter pD may be explained by the decrease in the electrostatic attraction between arsenate species and iron oxide surface at pD 8.5 combined with the hypothesis that a higher fraction of D-bonded complexes were formed at the lower pD, see Paper II for more information.

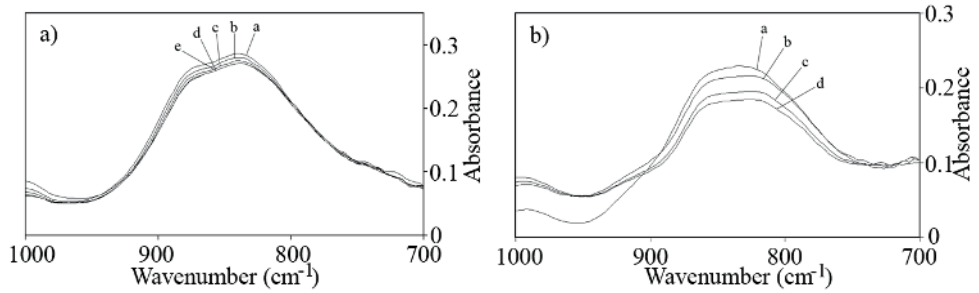

Figure 14. Spectra recorded at different desorption times, from 1.5 to 300 minutes (the times at which spectra were recorded follows a<b<c<d<e for the two figures) at pD 4, **left side**, and at pD 8.5, **right side**. Before desorption, the iron oxide film was equilibrated for 24 hours with a 0.03 mM arsenate solution at the same pD value.

3.2.2 Influence of phosphate on the adsorption of arsenate on ferrihydrite (Paper III)

Figure 15 shows spectra recorded from phosphate (60 mM) solution at pD 4 (a) and pD 8.5 (b) in contact with an uncoated ATR crystal. Three bands at 1180 cm^{-1}, 1084 cm^{-1} and 940 cm^{-1} appeared in the spectrum recorded at pD 4 where $D_2PO_4^-$ is the predominant phosphate species (reaction 2 [49]). Two absorption bands, at 1084 cm^{-1} and 988 cm^{-1} were observed in the spectrum recorded at pD 8.5, where DPO_4^{2-} is the predominant species in solution (reaction 2). Figure 15 also shows the spectrum recorded of phosphate adsorbed on a ferrihydrate film from a 0.03 mM phosphate solution at pD 4 (c) and at pD 8.5 (d). At pD 4, five absorption bands at 1124 cm^{-1}, 1084 cm^{-1}, 1035 cm^{-1}, 1014 cm^{-1}, 998 cm^{-1} assigned to adsorbed phosphate species were obtained. At pD 8.5, bands assigned to adsorbed phosphate appeared at 1064 cm^{-1} and 1021 cm^{-1}, see Paper II for information regarding band assignments. Figure 15 thus clearly illustrates that phosphate species in solution and phosphate species adsorbed on the iron oxide film may unambiguously be distinguished from each other using ATR-FTIR spectroscopy. The study of arsenate and phosphate adsorption on iron oxides could thus, in situ, be studied by the developed analytical method.

$$H_3PO_4 \xleftrightarrow{pKa1=2.16} H_2PO_4^- + H^+ \xleftrightarrow{pKa2=7.21} HPO_4^{2-} + 2H^+ \xleftrightarrow{pKa3=12.32} PO_4^{3-} + 3H^+ \quad (2)$$

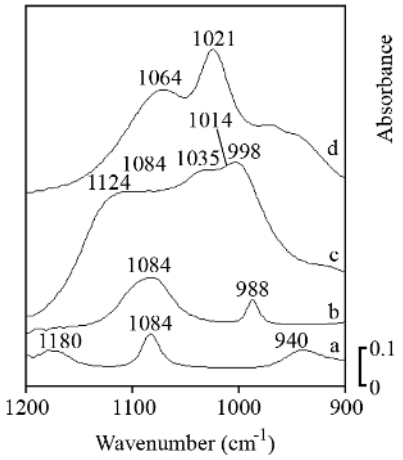

Figure 15. Spectra of phosphate (60 mM) recorded at a) pD 4, b) pD 8.5 using an uncoated ZnSe crystal. Spectra recorded of a 0.03 mM phosphate solution at c) pD 4 and d) pD 8.5 after 5 hours in contact with an iron oxide film.

An experiment in which arsenate was first pre-adsorbed from a 0.03 mM solution on the iron oxide film for 5 hours followed by addition of phosphate (either 0.03 mM or 0.15 mM) to the system was performed at pD 4 and 8.5. This experiment was chosen as a very simple simulation of a real application where arsenate contaminated soil is amended with iron oxide and where phosphates are subsequently added as plant nutrient. The kinetics of adsorption/desorption of arsenate on ferrihydrite was obtained by plotting the peak height of the band at about 840 cm^{-1} assigned to arsenate adsorbed on iron oxide plotted as a function of time. The kinetics of adsorption curves of arsenate at pD 4 and 8.5 followed by the desorption induced by the addition of phosphate at t = 300 min, while keeping the arsenate concentration constant, are shown in Figure 16 (left). Arsenate desorbed to a larger extent at the higher concentration of phosphate in the solution as might be expected. At pD 4, the final concentration of pre-adsorbed arsenate changed from 90 % of the maximum surface concentration at equimolar concentrations of phosphate (0.03 mM) and arsenate (0.03 mM) to 70 % of the maximum surface concentration when the phosphate concentration (0.15 mM) was five times the arsenate concentration (0.03 mM) in solution. The final concentration of adsorbed arsenate at pD 8.5 was about 80 % at equimolar concentrations of arsenate and phosphate, while the concentration of adsorbed arsenate decreased to about 50 % when the phosphate concentration added to the system was five times higher than the concentration of

arsenate. The substitution of arsenate by phosphates was greater at pD 8.5 than at pD 4 at both phosphate concentrations studied.

A very similar experiment was carried out albeit reversing the order of addition of arsenate and phosphate to the system. The integrated area of all bands assigned to phosphate adsorbed on ferrihydrite was plotted vs. time in order to obtain the kinetics of adsorption/desorption of phosphate. The kinetics of adsorption curves of phosphate at pD 4 and 8.5 followed by the desorption induced by the addition of equimolar concentration of arsenate at t = 300 min are shown in Figure 16 (right). The remaining amount of pre-adsorbed phosphate on the iron oxide after 300 minutes of desorption time was about 67 % at pD 4 and about 54 % at pD 8.5.

The substitution of phosphate upon arsenate addition was thus greater than the substitution of arsenate upon phosphate addition at the pD values and concentrations studied, as shown by these experiments.

In summary, the adsorption of arsenate on the iron oxide was relatively stable under the conditions studied. However, the adsorbed arsenate was less stable in the presence of higher phosphates concentrations and at higher pD. Therefore, parameters like pH and phosphate concentration in the soil must be controlled in order to apply chemical amendments that reduce the mobility of arsenate in arsenic contaminated soils.

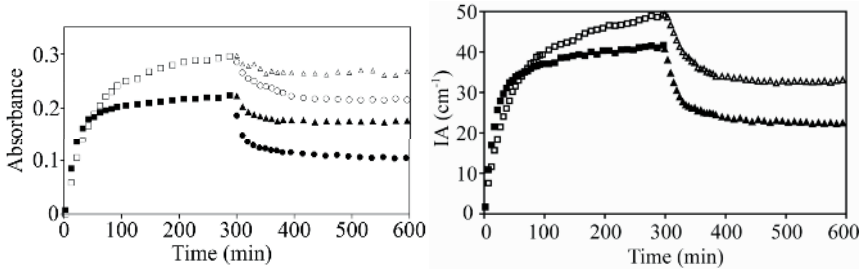

Figure 16. To the left: Peak height of the band at ~ 840 cm^{-1} assigned to arsenate adsorbed on iron oxide plotted as a function of time. The arsenate concentration was 0.03 mM and the pD was (■) 8.5 and (□) 4. At t = 300 min; phosphate was added in appropriate amounts while keeping the arsenate concentration constant at 0.03 mM. The arsenate desorption after phosphate addition was monitored at pD 4 (phosphate concentrations of (Δ) 0.03 mM and (○) 0.15 mM) and at pD 8.5 (phosphate concentration of (▲) 0.03 mM and (●)0.15 mM). **To the right:** Integrated absorbance (IA) of adsorbed phosphate vs. time. Adsorption took place from a 0.03 mM phosphate solution at (■) pD 8.5 and at (□) pD 4. At t = 300 min, 0.03 arsenate was added yielding a solution with equal (molar) concentration (0.03 mM) in phosphate and arsenate. The rate of the following phosphate desorption ((▲)pD 8.5 and (Δ) pD 4) was monitored for 5 h.

Figure 17 shows spectra (from a to e) recorded during the experiment in which phosphate was pre-adsorbed from a 0.03 mM solution at pD 4 on an iron oxide film for 5 hours. As stated earlier, five bands situated at 1124 cm^{-1}, 1084 cm^{-1}, 1035 cm^{-1}, 1014 cm^{-1}, 998 cm^{-1} appeared and became more intense with time, indicating increased adsorption of phosphate with time. The relative intensities of the most intense bands at 1124 cm^{-1}, 1035 cm^{-1} and 998 cm^{-1} were constant and were thus assigned to the same complex, viz. either the deuterated binuclear bidentate complex ($(\equiv FeO)_2(OD)PO$) or the monodentate doubly deuterated complex ($(\equiv FeO)(OD)_2PO$). On the other hand, the bands at 1084 cm^{-1} and 1014 cm^{-1} were assigned to de-deuterated complexes, viz. either the non-deuterated binuclear bidentate complex ($(\equiv FeO)_2PO_2^-$) or the mono-deuterated monodentate complex ($(\equiv FeO)(OH)PO_2^-$), see Paper III for details. Since the intensity of the bands assigned to the deuterated phosphate complex (at 1124 cm^{-1}, 1035 cm^{-1} and 998 cm^{-1}) was greater than the intensity of the bands caused by the de-deuterated complex (at 1084 cm^{-1} and 1014 cm^{-1}), the concentration of adsorbed deuterated complex appeared higher than the concentration of de-deuterated complex throughout the adsorption of phosphate. Again, the latter statement is based on the assumption that the molar absorptivities of the two complexes are the same.

After 50 minutes of adsorption (spectrum b), only the bands at 1124 cm^{-1}, 1035 cm^{-1} and 998 cm^{-1} were observed. Hence, the deuterated phosphate complex adsorbed mainly within the first hour of adsorption. On the other hand, spectrum e-b (shown in the lower part of Figure 17) which is the result of subtracting spectrum b (recorded after 50 minutes of adsorption) from spectrum e (recorded after 5 hours of adsorption), only showed bands evolving from species adsorbed between 50 minutes and 5 hours adsorption time. Only the two bands at 1084 cm^{-1} and 1014 cm^{-1} were observed in spectrum e-b, indicating that only the de-deuterated phosphate complex adsorbed after the first hour of adsorption, thus showing a significantly slower kinetics of adsorption than the deuterated phosphate complex.

After these first 5 hours, arsenate was added to the solution achieving equimolar concentration of the two oxoanions in solution, while keeping the pD constant during the whole experiment. Spectra in the central part of Figure 17 (from f to h) were recorded during this second stage of the experiment. Bands previously assigned to adsorbed arsenate, in the range 900 - 800 cm^{-1}, immediately appeared as arsenate was added to the solution and their intensity increased with time. Simultaneously, the bands originating from phosphate complexes (at 1200 - 950 cm^{-1}) decreased in intensity with time as a result of desorption of phosphate species from the iron oxide. Furthermore, the bands assigned to the deuterated phosphate

complex (at 1124 cm^{-1}, 1035 cm^{-1} and 998 cm^{-1}) were reduced very fast whereas the bands assigned to the de-deuterated complex (at 1084 cm^{-1} and 1014 cm^{-1}) remained almost unchanged, which indicates very different stability for the two types of phosphate – iron oxide complexes. Spectrum e-h (shown in the lower part of Figure 17), which is the result of subtracting spectrum h (recorded after 5 hours of phosphate desorption in the presence of arsenate in the system) from spectrum e (recorded after 5 hours of pure phosphate adsorption), highlights only the bands in which the intensity decreased during the competitive adsorption with arsenate. Only bands assigned to the deuterated complex (at 1124 cm^{-1}, 1035 cm^{-1} and 998 cm^{-1}) appeared in spectrum e-h, which indicates that only this complex desorbed when arsenate was introduced in the system, and the results further imply that the de-deuterated complex was very stable under these conditions.

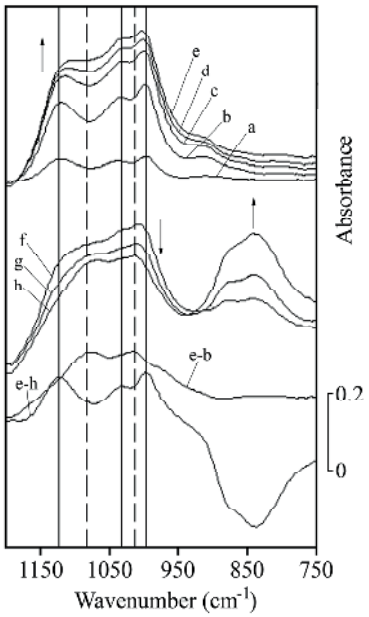

Figure 17. Spectra recorded as a 0.03 mM phosphate solution at pD 4 was flowing over a ferrihydrite film after (a) 7 min (b) 50 min (c) 122 min (d) 200 min and (e) 5 hours. After 5 hours, the solution was adjusted to be equimolar in phosphate and arsenate viz. 0.03 mM at pD 4 and spectra were recorded after (f) 320 min (g) 360 min and (h) 600 min (e-b) spectrum calculated from the subtraction of spectrum (b) from spectrum (e). The (e-h) spectrum was calculated by subtracting spectrum (h) from spectrum (e). The continuous vertical lines represent the wavenumbers 1124 cm^{-1}, 1035 cm^{-1} and 998 cm^{-1} whereas the discontinuous lines represent 1084 cm^{-1} and 1014 cm^{-1}.

In summary, two different phosphate complexes were found on the ferrihydrite surface at pD 4. The two complexes showed different adsorption kinetics and perhaps more importantly, the complexes showed different stabilities regarding their replacement by arsenate. To the best of our knowledge, this is the first report showing that the two phosphate complexes formed on ferrihydrate showed different stabilities.

3.2.3 Influence of zinc (II) on the adsorption of arsenate on ferrihydrite (Paper IV)

3.2.3.1 Adsorption at pH/pD 4

The influence of Zn (II) on the adsorption of arsenate on ferrihydrite was found to be negligible at pH/pD 4 as shown from both spectroscopic and batch adsorption studies. See paper IV to see the evidence leading to this conclusion.

3.2.3.2 Adsorption at pH/pD 8

3.2.3.2.1 Batch adsorption experiments

The presence of 1200 μM Zn (II) in the arsenate - ferrihydrite system considerably enhanced the removal of arsenate from solution at pH 8, with concentration of arsenate in the supernatant being reduced from 60 mM to 11.1 μM in the absence of Zn (II), and to 2.3 μM in the presence of Zn (II) (Table 2, batch experiments 1 and 3). The concentration of Zn (II) was also reduced from 1200 μM to 45.8 μM. The enhancement of arsenate removal in the presence of Zn (II) is in line with previous investigations performed at pH 7 and pH 8 [25, 55]. Those reports attributed the decrease in Zn (II) and arsenate in solution to enhanced adsorption of arsenate on iron oxide via the formation of ternary complexes of zinc, arsenate on the iron oxide surface. However, in the present work, a decrease of similar extent in the concentration of both arsenate and Zn (II) in solution was observed also in the absence of ferrihydrite (Table 2, batch experiment 3), implying that only the presence of Zn (II) at high concentrations could reduce the aqueous concentration of arsenate. This result thus suggests that the ternary zinc – arsenate - ferrihydrite complex may not be the only possible mechanism that would explain arsenate removal from solution. No significant arsenate removal was observed when the initial concentration of Zn (II) was reduced to 60 μM (Table 2, experiment 4), although the Zn (II) concentration in solution decreased to 22.7 μM.

The concentration of Zn (II) in solution (without arsenate and ferrihydrite) decreased at pH 8 at both Zn (II) concentrations studied, 1200 μM and 60 μM, see Table 2, batch experiment 5 and 6. The reduction in Zn (II) was attributed to precipitation of zinc hydroxide carbonate and zinc oxide as shown by a combination of experimental data obtained by means of XRD, FTIR, SEM and thermodynamic simulations, see Paper IV for more details.

The influence of Zn (II) precipitates, $Zn_x(CO_3)_y(OH)_z$ (650 mg/l) and ZnO (650 mg/l), on the arsenate removal from solution was therefore assessed by means of batch adsorption experiments. The results of these experiments are presented in Table 2 (experiments 7 and 8). The experiments showed that the arsenate concentration in the aqueous solution decreased in the presence of the Zn (II) precipitates. These results indicate that the interaction of arsenate with zinc precipitates may explain the arsenate removal by Zn (II) at pH 8. However, other mechanisms, such as the presence of surface complexes of zinc, arsenate and iron oxide [25, 55] and/or the precipitation of zinc arsenate, could not be dismissed.

Table 2. Summary of experimental conditions and final ion concentration for the batch adsorption experiments conducted at pH 8.

Experimental conditions (initial concentrations)						**Final concentrations**	
Batch experime	**As μM**	**Zn μM**	**Ferrihydrite mg/l**	**$Zn_x(CO_3)_y(OH)_z$ mg/l**	**ZnO mg/l**	**As μM**	**Zn μM**
1	60	–	56	–	–	11.1	< 0.03
2	60	1200	56	–	–	2.3	45.8
3	60	1200	–	–	–	7.0	41.2
4	60	60	–	–	–	55.7	22.7
5	–	1200	–	–	–	< 0.01	34.5
6	–	60	–	–	–	< 0.01	29.6
7	60	–	–	650	–	5.6	0.09
8	60	–	–	–	650	35.6	0.5

3.2.3.2.2 In situ ATR – FTIR measurements

A 0.03 mM arsenate solution was in contact with a ferrihydrite film for 5 hours at pD 8, at this time spectrum (a) in Figure 18 was recorded. Two broad absorption bands at about 855 cm^{-1} and 830 cm^{-1} originating from adsorbed arsenate species on ferrihydrite were observed in the spectrum. After 5 hours of adsorption, Zn (II) (1.2 mM) was added to the solution while

keeping the pD and the arsenate concentration in solution constants. Spectrum (b) was recorded 5 hours after the addition of Zn (II). The addition of Zn (II) to the system induced a slight desorption of arsenate from the ferrihydrite as indicated by the slight decrease in the intensity of the bands assigned to arsenate adsorbed on ferrihydrite. As shown by the batch adsorption experiments (Table 2 experiment 3), the addition of 1.2 mM Zn (II) led to a decrease in the arsenate concentration in solution. The decrease in arsenate concentration in the solution might also have induced the desorption of arsenate from the ferrihydrite film as already described in subsection 3.2.1.

The reversed order of addition of zinc and arsenate was also investigated. Spectrum (c) was recorded 5 hours after the addition of arsenate (0.03 mM) when the ferrihydrite film had been in contact with a 0.03 mM Zn (II) solution prior to the arsenate addition. The spectrum shows two bands assigned to arsenate adsorbed on ferrihydrite. The peak height of the bands were slightly lower than the intensity of the bands observed in the spectra (a and b) recorded when arsenate was added to the system prior to the addition of Zn (II). Small differences in the spectral features, regarding band broadening and relative intensity of the bands, were observed between spectrum (c) as compared to spectrum (a) and (b). The differences suggested that, although most of arsenate adsorbed via similar mechanisms independently of the presence or absence of Zn (II) in the system, a small fraction of the arsenate possibly may have adsorbed via co-precipitation/complexation with Zn (II) at the ferrihydrite surface when Zn (II) was added prior to arsenate adsorption. Spectrum (d) was recorded 5 hours after the addition of arsenate (0.03 mM) when the ferrihydrite film had previously been exposed to a 1.2 mM Zn (II) solution. The spectrum does not show any bands in the 900 - 800 cm^{-1} region of the spectrum which implies that arsenate did not adsorb on ferrihydrite. This indicates that a high concentration of Zn (II) prevented adsorption of arsenate on ferrihydrite, presumably due to the formation of a precipitate containing zinc in solution involving arsenate ions as discussed above. Therefore the adsorption of arsenate on $Zn_x(CO_3)_y(OH)_z$ and ZnO films was assessed by means of in situ ATR - FTIR spectroscopy.

Spectrum (e) was recorded after 5 hours of adsorption of a 0.03 mM arsenate solution at pD 8 in contact with a $Zn_x(CO_3)_y(OH)_z$ film. Negative IR absorption bands appeared at 950 cm^{-1} and 833 cm^{-1} originating from re-dispersion and/or dissolution of $Zn_x(CO_3)_y(OH)_z$, as shown in Paper IV. Broad bands located between 900 cm^{-1} to 750 cm^{-1} were clearly distinguished in the spectrum. Since the intensity of the bands increased with time (not shown) and the

contribution from arsenate in solution may be neglected at these concentrations (0.03 mM, see subsection 3.1.2), the bands were assigned to arsenate adsorbed on $Zn_x(CO_3)_y(OH)_z$. The adsorption mechanism of arsenate on the Zn (II) precipitate was proposed to occur via the hydroxyl group of the precipitate, see Paper IV. This experiment showed that adsorption of arsenate on zinc hydroxide carbonate may be one reason why the adsorption of arsenate on ferrihydrite was prevented by pre-addition of Zn (II) to the system. However, other mechanisms like precipitation of zinc arsenate cannot be completely dismissed.

Spectrum (f) was recorded after 5 hours of adsorption of a 0.03 mM arsenate solution at pD 8 and a ZnO film. No bands in the spectral range between 900 cm^{-1} and 800 cm^{-1} could be observed indicating that arsenate did not adsorb on the ZnO particles in detectable levels. This result appeared to contradict the result obtained by means of batch adsorption experiments in which the arsenate concentration in solution was reduced in a ZnO suspension. A possible explanation for these results might be that the specific surface area, as measured by nitrogen adsorption, of the commercial ZnO was low, i.e. 4.7 m^2/g and the adsorption of arsenate on ZnO could therefore not be detected by infrared spectroscopy.

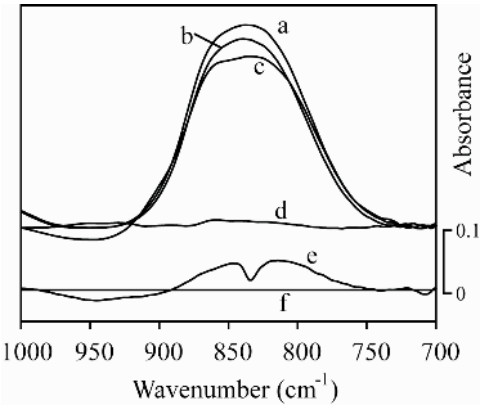

Figure 18. a) Spectrum of arsenate adsorbed on the ferrihydrite film from a 0.03 mM solution at pD 8 after 5h. Thereafter, 1.2 mM Zn (II) were added, and a spectrum b) was recorded 5 h after the addition of Zn (II). Spectra c) and d) were recorded after 5 hours of arsenate adsorption from a solution of 0.03 mM at pD 8 when the film first had previously been equilibrated for 5 hours with 0.03 mM and with 1.2 mM Zn (II), respectively. ATR spectra recorded after 5 hours of contact between a 0.03 mM arsenate solution at pD 8 and e) a $Zn_x(CO_3)_y(OH)_z$ film, f) a ZnO film.

Batch adsorption experiments showed that adding Zn (II) (1.2mM) increased arsenate removal from solution at pH 8. On the other hand, the order of addition of the two contaminants,

Zn (II) and As (V), to the system played an important role in the adsorption of arsenate onto ferrihydrite. Pre-adsorbed arsenate species on ferrihydrite did not easily desorb from the ferrihydrite surface upon addition of Zn (II), whereas pre-addition of a high concentration of Zn (II) (1.2 mM) to the system resulted in that no arsenate adsorbed on ferrihydrite. This seemingly contradicts the results obtained from batch adsorption experiments. However, the formation of a Zn (II) precipitate, followed by the adsorption of arsenate on the precipitate was proposed to be the most likely cause.

The results presented here are important if an arsenic contaminated soil is to be remediated by the addition of ferrihydrite based adsorbents. The speciation and concentration of zinc in the soil prior to the remediation may be one of the factors leading to the success or failure of the subsequent remediation.

3.3 Development of an iron oxide based adsorbent for arsenate removal from water (Paper V)

3.3.1 Characterisation of the adsorbent

Figure 19 shows an SEM image of the fine magnetite used as a raw material (left). The powder consisted of irregular-shaped particles, with a varying size up to ca. 50 nm. Figure 19 (right) shows a SEM image of the iron oxide particles after heat treatment at 1200 ºC for 24 h. The image shows that the original magnetite particles sintered upon heat treatment. Apart from sintering, the magnetite transformed to hematite upon heat treatment as confirmed by XRD data, see Paper V. Phase transformation from magnetite to hematite as well as the sintering of hematite and magnetite at 1200 ºC have previously been reported [30].

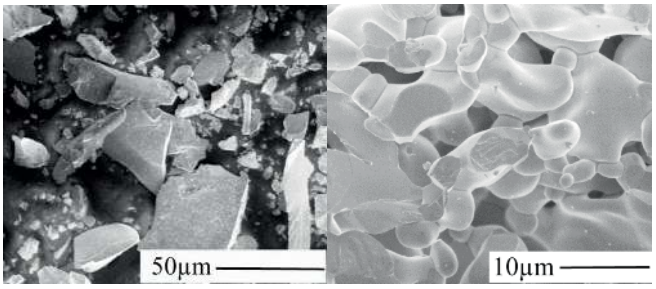

Figure 19. SEM image of magnetite raw material **(left)**, hematite particles formed after heat treatment at 1200 ºC for 24 h **(right)**.

Figure 20 shows SEM images of the adsorbent particles. The outside of the sintered hematite particles were completely covered by nanoparticles as can be observed in Figure 20 (top-left image). Figure 20 (top-middle image) shows a cross-section image of a fractured adsorbent particle. The image clearly shows that nanoparticles cover the walls of the pores. Figure 20 (top-right image) shows a film of about 20 nm thickness coating the hematite particles. However, the thickness of this film varied in the different spots analysed (ranging from 10 nm up to 150 nm at some locations).

Figure 20 (bottom-left image) shows very small crystals, with a particle size of about 8 nm and spherical crystal habit. Small crystal size (from 1 – 10 nm) and spherical habit has previously been reported for ferrihydrite ($Fe_5O_8H \cdot H_2O$) [see Paper II – IV, 27]. Figure 20 (botom-middle image) shows particles with acicular habit of about 35 nm length and about 13 nm diameter. Goethite (α-FeOOH) or akaganéite (β-FeOOH) (prepared in atmospheres rich in Cl^-) often shows acicular habit [27]. These two images were recorded at very specific locations where the two habits were found segregated. However, the two crystal habits were, in general, found coexisting together, as shown in Figure 20 (bottom-right and top-right image).

The specific surface area of the hematite particles significantly increased after the coating, from 0.5 m^2/g to 3.75 m^2/g, as determined by N_2 adsorption measurements. Moreover, the percentage of nanoparticles covering the hematite particles was estimated to be about 1 (w) %. This value was calculated from the N_2 adsorption data and thermogravimetric data by the application of two simple models, see Paper V for further details.

The crystallographic phase of the nanoparticles could not be obtained by means of XRD, DRIFT or Raman measurements due to the small amount of nanoparticles present in the adsorbent.

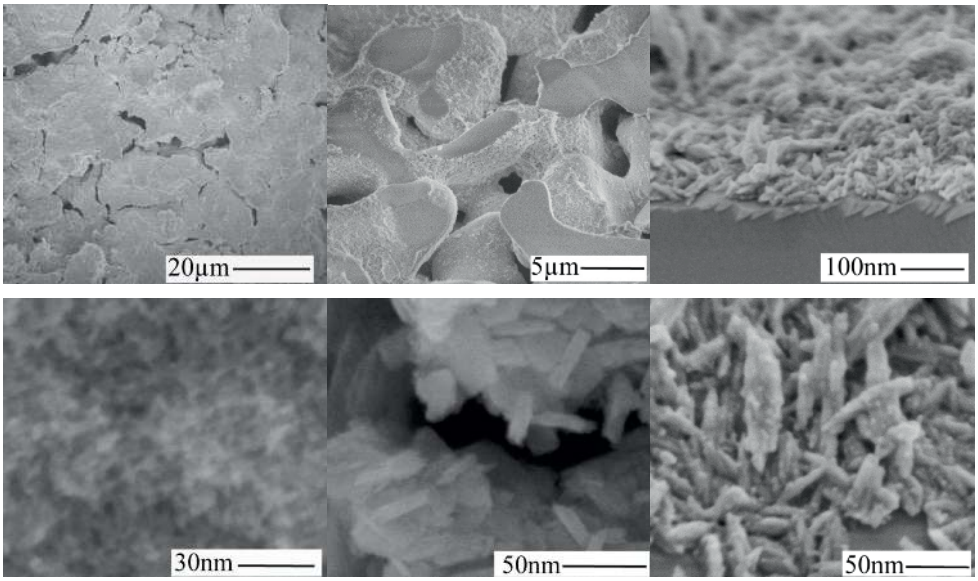

Figure 20. **top:** SEM image of the outside surface of the sintered particles after the acid treatment (left), cross section image of the half-cut sintered particles, showing the inside of the pores in the sintered particles after acid treatment (middle), SEM image of the nanoparticles film coating the sintered hematite particles (right). **bottom:** high magnification images of 8 nm spherical habit crystals (left), acicular habit crystals (middle), combined acicular and spherical habit crystals (right).

3.3.2 Adsorption measurements

No removal of arsenate from solution was observed when the sintered hematite particles (before coating with the nanoparticle film) were used as adsorbents in batch adsorption experiments or in column breakthrough experiments. The low specific surface area (0.5 m^2/g) of the sintered hematite particles may explain the low adsorption capacity.

3.3.2.1 Batch adsorption experiments

Figure 21 shows the adsorption isotherm data of arsenate adsorbed on the adsorbent particles at pH 5. The adsorption isotherm curve (Figure 21 image to the left) appeared to follow the Langmuir adsorption model. Therefore, a linear regression of the experimental data points to the linearized equation of the Langmuir Adsorption model, equation 7, was used in order to determine K and q_o from the experimental adsorption data.

$$\frac{C}{q} = \frac{1}{q_o} \cdot C + \frac{1}{q_o \cdot K} \qquad (7)$$

In equation 7, q is the equilibrium concentration adsorbed on the adsorbent (mg/g); K is the Langmuir adsorption constant (l/mg[As]); q_o is the monolayer capacity (mg/g) and C is the adsorbate (arsenate) concentration in solution (mg/l).

Figure 21 (on the right) shows the plot of the linearized Langmuir adsorption data. The experimental data fitted the Langmuir adsorption model very well with a regression coefficient (R^2) of 0.9998. The monolayer adsorption capacity, q_o, was estimated to be 0.65 mg[As]/g while the Langmuir adsorption constant, K, was 15.0 l/mg[As]. The adsorption capacity of 0.65 mg[As]/g appeared to be reasonably good as compared with reported adsorbents, see Paper V.

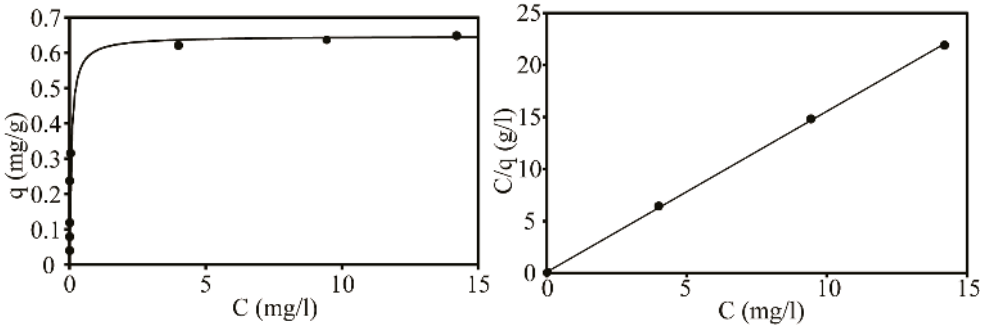

Figure 21. Adsorption isotherm of arsenate on the adsorbent at pH 5. **To the left**, the isotherm is plotted as amount adsorbed in equilibrium, q_e (mg/g) vs. concentration of As in solution, C_e. **To the right** plotted as C_e/q_e vs C_e which represents the linearized Langmuir model equation. Filled circles are the experimental data points whereas the lines denote the fitted Langmuir model.

3.3.2.2 Column adsorption experiments

Figure 22 shows the breakthrough curves obtained when a 500 μg[As]/l arsenate solution at pH 5 was pumped at three different flow rates through the adsorbent bed. The breakthrough curves showed a characteristic S-shape as expected for this kind of experiment. Since the arsenic guideline concentration for drinking water is 10 μg/l [1] (2 % of the influent concentration, C/C_0=0.02), C/C_0=0.02 was defined as the breakthrough point. Table 3 shows that the adsorption capacity at the 2 % breakthrough point (usable adsorption capacity) increased as the flow rate increased. Although the change in the flow rate from 3.5 ml/min to

21.7 ml/min decreased the usable adsorption capacity ($q_{b2\%}$) by 50 %, the time required to complete the usable adsorption capacity of the bed ($t_{b2\%}$) decreased by about 90 %. Table 3 also reports the total adsorption capacity (q_b), as calculated from the integration of the whole breakthrough curve. The total adsorption capacity was about the same, 0.50 – 0.54 mg[As]/g for the three flow rates.

Table 3. Summary of data from experimental breakthrough data.

Flow rate (ml/min)	$V_{b2\%}$ (L)	$t_{b2\%}$ (min)	$q_{b2\%}$ (mg[As]/g)	$V_{b50\%}$ (L)	$t_{b50\%}$ (min)	q_b (mg[As]/g)	$V_{b90\%}$ (L)
3.5	41.5	11739	0.42	53.6	15157	0.54	58.8
12.5	27.9	2236	0.28	54.1	4330	0.54	70.05
21.7	19.3	889	0.19	50.1	2337	0.50	84.7

The linearized equation of the Thomas Model (subsection 1.3), the so-called Yoon-Nelson equation, described by equation 8, was used in order to determine the q and K_{YN} from the breakthrough adsorption data by linear regression [39].

$$Ln\left(\frac{C_o}{C} - 1\right) = -K_{YN} \cdot (t - \tau) \qquad (8)$$

In this equation, C is the effluent concentration of the adsorbate (μg/l), C_o is the concentration of the adsorbate in the feed (μg/l), τ (qW/QC_o) is the time required to reach 50% of the feed concentration in the effluent (C/C_o=0.5) and K_{YN} ($K_{tho}C$) is the Yoon-Nelson rate constant (min^{-1}).

The continuous lines in Figure 22 represent the Thomas Model (eq. 8) fitted to the experimental data. As can be seen, the model fits the experimental data well ($R^2 \geq 0.898$, see table 4). The values of τ and K_{YN} were obtained from the fitting, values reported in Table 4. K_{YN} increased linearly with flow rate (R^2=1). This tendency possibly indicates that the adsorption process was controlled by diffusion of arsenate through the liquid film surrounding the particles. The adsorption capacity of the adsorbent could be calculated from the parameter τ (q_oW/QC_o), see Table 4.

The estimated adsorption capacity from the column experiments, 0.50 – 0.54 mg[As]/g (experimental data) or 0.6 mg[As]/g (Thomas Model) agreed well with estimations from the

batch experiments: i.e. the loading of the adsorbent, at a concentration in solution of 500 μg[As]/l, can be calculated to be 0.571 mg[As]/g using the Langmuir model.

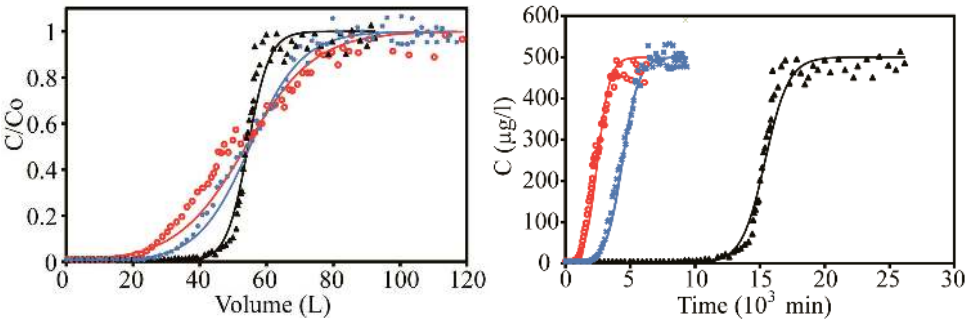

Figure 22. Breakthrough adsorption curves obtained for 500 μg[As]/l arsenate concentration at pH 5 pumped through 45 g of the adsorbent bed at a flow rate of 21.7 ml/min (red), 12.5 ml/min (blue) and 3.5 ml/min (black). **To the left**, the breakthrough curves are plotted in a normalized fashion, the ratio between the effluent and the influent arsenic concentration (C/C_o) vs. the throughput volume. **To the right** the curves are represented by plotting the influent arsenic concentration vs. time. The dots represent the experimental data, while the lines represent the Thomas Model equation fitted to the experimental data.

Table 4. Parameters obtained by fitting the Thomas Model to the experimental data.

Flow rate (ml/min)	τ (min)	K_{YN} (min^{-1})	q (mg[As]/g)	R^2
3.5	15402	0.0021	0.60	0.898
12.5	4402	0.0016	0.61	0.979
21.7	2477	0.0011	0.60	0.947

Figure 23 shows the desorption curves, relevant for regeneration of the adsorbent, obtained when a saturated adsorbent bed (saturated with a 500 μg[As]/l arsenate solution at pH 5 at a flow rate of 21.7 ml/min) was flushed with distilled water at pH 12 (filled triangles) and distilled water at pH 5 (open squares), at a flow rate of 21.7 ml/min. Arsenate could easily be desorbed when the adsorbent was flushed at pH 12, as indicated from the high arsenate concentration in the effluent, 12000 μg/l, at the beginning of the desorption experiment (Figure 23 to the left). When the flushing started 27 mg[As] was adsorbed on the adsorbent bed, 25 mg[As] (93 % of the pre-adsorbed arsenate) was desorbed during the desorption experiment from which about 17 mg[As] (60 %) were desorbed within the first 5 liters of rinsing. On the other hand, when the saturated adsorbent bed was flushed with distilled water at pH 5 the concentrations in the effluent were much lower. At this pH, the total arsenic

desorbed during the desorption experiment was about 3 mg[As] (11 % of the previously adsorbed arsenic), a value which is in line with the value of about 10 % of arsenate desorbed from synthetic ferrihydrite after 200 min of flushing with D_2O at pD 4, see subsection 3.2.1.

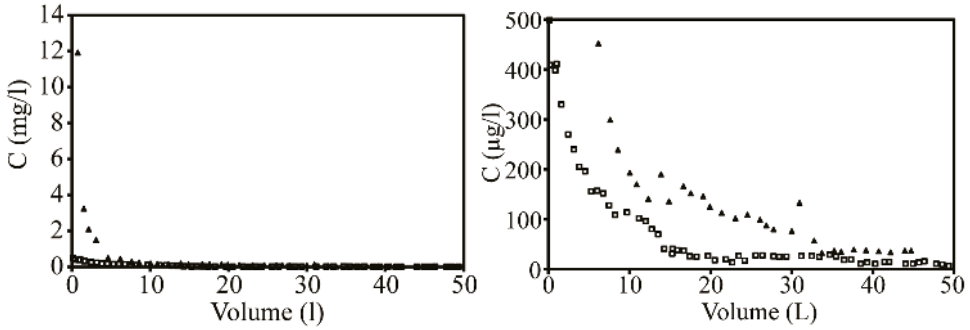

Figure 23. Desorption curves obtained from distilled water pumped, at 21.5 ml/min, through the adsorption bed at pH 5 (non-filled squares) and at pH 12 (filled triangles). Prior to the desorption, the adsorbent bed was saturated by pumping a 500 µg[As]/l arsenate solution at pH 5 at a flow rate of 21.5 ml/min. The desorption curve is plotted in the concentration range 0 – 14 m/l **(to the left)** and in the concentration range 0 – 500 µg/l **(to the right)**.

To conclude, the adsorption capacity of coarse hematite was significantly increased, from negligible to 0.65 mg[As]/g, by treating the hematite using the developed method. Results regarding adsorption performance and regeneration of the adsorbent were very promising. Therefore, the presented results open the possibility to straightforwardly and inexpensively prepare an adsorbent from materials containing coarse iron oxide minerals, such as waste from mining companies.

4 Conclusions

The new in situ ATR – FTIR spectroscopy flow method developed in this work was proven to be very useful for studying the adsorption and desorption of different species, such as collector agents, arsenate or phosphate, on synthetic iron oxide films used as model systems. Both single component and binary systems could be studied in situ.

By using the new in situ flow method previously reported findings could be confirmed:

• The adsorption of arsenate and phosphate on iron oxide was highly pD dependent with higher adsorption capacities at lower pD in the range studied.

• Adsorption/desorption experiments suggested that the stability of the arsenate complexes formed on the ferrihydrite surface was higher at pD 4 than at pD 8.5.

• Arsenate showed stronger adsorption than phosphate on iron oxide under similar conditions.

• Two different phosphate complexes adsorbed on iron oxide at pD 4, one deuterated and one de-deuterated.

• Although the formed arsenate complexes were relatively stable under the conditions studied, the results clearly indicate that when applying iron oxides as a soil amendment, care should be taken to control pH and the phosphate content in the amended soil so as to minimize leaching of arsenate to the environment.

The experimental work also lead to new findings:

• The two phosphate complexes formed on ferrihydrite surface at pD 4 showed distinct differences in their stabilities. The deuterated complex was easily desorbed due to competitive adsorption with arsenate species whereas the de-deuterated phosphate complex was more difficult replaced by arsenate species.

• Presence of Zn(II) increased the arsenate removal in a ferrihydrite containing suspension at pH 8, but in situ ATR – FTIR spectroscopy showed that no adsorption of arsenate on a ferrihydrite film occurred at pD 8 in the presence of a high concentration of Zn(II). This seemingly contradictory data could be explained by the precipitation of zinc hydroxide carbonate which was found to play a crucial role in the arsenate removal from a solution in the presence of Zn(II) at pH/pD 8.

• Pre-adsorbed arsenate species on ferrihydrite did not easily desorb from the ferrihydrite surface upon addition of Zn (II).

• A method for preparing an adsorbent from iron oxide was developed. The adsorbent is comprised of hematite particles covered by a thin film of iron oxide nanoparticles. The adsorbent was evaluated as an arsenate adsorbent with both batch and breakthrough column experiments. The adsorbent worked very well and was proven to be an effective adsorbent for arsenate with an adsorption capacity of about 0.6 mg[As]/g.

5 Future Work

Further studies on the influence of redox potential as well as the influence of other compounds such as sulphate, chromate, carbonates, silicates, Al, Cu and humic acids on the adsorption of arsenate on iron oxides is recommended.

EXAFS measurements on the system studied might help in identifying which complexes were formed on the iron oxide.

The exploitation of the good adsorption properties of the iron oxides to develop efficient adsorbent material is recommended. A further study of the long term stability of the iron (oxy-hydroxide) nanoparticles of the adsorbent would be required.

6 References

[1] Mohan, D.; Pittman, C.U., Arsenic removal from water/wastewater using adsorbents-a critical review. *J. Hazard. Mater.* 142, (1-2) **(2007)** 1-53.

[2] Galetovic Carabantes, A.;de Fernicola N.A.G.G., G., Arsénico en el agua de bebida: un problema de salud pública. *Revista brasileira de ciências farmacêuticas*, 39, (4) **(2003)** 365-372.

[3] Thirunavukkasaru, O.S; Viraghavan T.; Subraimanian KS.; Removal of arsenic in drinking water by iron oxide-coated sand and ferrihydrite-batch studies. Water Qual. Res. J. Canada 36 **(2001)** 55-70.

[4] Andreae, M.O; Andreae T.W.; Dissolved arsenic species in the schelde estuary and watershed, Belgium. Estuarine, coastal and shelf science 29, 5 **(1989)** 421-433.

[5] Seyler, P.; Martin, J.M.; Distribution of arsenite and total dissolved arsenic in major french estuaries- dependence on biogeochemical processes and anthropogenic inputs. Mar. Chem. 29 2-3 **(1990)** 277-294.

[6] Petine, M.; Camusso, M.; Martinotti, W.; Dissolved and particulate transport of arsenic and chromium in the Po river (Italy). Sci. Tot. Environ. 119 **(1992)** 253-280.

[7] McAuley, B.; Cabaniss, S.E., Quantitative detection of aqueous arsenic and other oxoanions using attenuated total reflectance infrared spectroscopy utilizing iron oxide coated internal reflection elements to enhance the limits of detection. *Anal. Chim. Acta*, 581, (2) **(2007)** 309-317.

[8] Cullen, W.R.; Reimer, K.J.; Arsenic speciation in the invironment. Chemical Reviews. 89, 4 **(1989)** 713-764.

[9] Smedley, P.L.; Zhang, M.; Zhang, G., Luo, Z.; Mobilisation of arsenic and other trace elements in fluviolacrustine aquifers of the Huhhot Basin, Inner Mongolia. App. Geochem. 18, 9 **(2003)** 1453-1477.

[10] Chuah, T.G.; Robiah, Y.; Gregory Koay, F.L.; Azni, I., Arsenic toxicity, health hazards and removal techniques from water: an overview. *Desalination* 217, (1-3) **(2007)** 139-166.

[11] Jurate, K., Assesment of Trace Element Stabilization in Soil. Doctoral Thesis, Luleå University of technology, **2005**:38, ISSN:1402-1544.

[12] Magalhães, M. C. F., Arsenic. An environmental problem limited by solubility. *Pure Appl. Chem.*, 74, (10) **(2002)** 1843-1850.

[13] Boisson, J.; Ruttens, A.; Mench, M.; Vangronsveld, J., Evaluation of hydroxyapatite as a metal immobilizing soil additive for the remediation of polluted soils. Part 1. influence of hydroxyapatite on metal exchangeability in soil, plant growth and plant metal accumulation. *Environ. Pollution* 104 **(1999)** 225-233.

[14] Cao, X.; Ma, L.Q., Effects of compost and phosphate on plant arsenic accumulation from soils near pressure-treated wood. *Environ. Pollution* 132 **(2004)** 435-442.

[15] Kumpiene, J., Ore, S., Renella, G., Mench, M., Lagerkvist, A., Maurice, C., Assessment of zerovalent iron for stabilization of chromium, copper, and arsenic in soil. *Environ. Pollution* 144 **(2006)** 62-69.

[16] Mench, M., Vangronsveld, J., Beckx, C., Ruttens, A., Progress in assisted natural remediation of an arsenic contaminated agricultural soil. *Environ. Pollution* 144 **(2006)** 51-61.

[17] Shiralipour, A.; Ma, L.Q.; Cao, R.X. 2002. Effects of compost on arsenic leachability in soils and arsenic uptake by a fern; University of Florida; Gainesville, FL; Report #02-04.

[18] Zhang, J. S.; Stanforth, R.; Pehkonen, S.O., Irreversible adsorption of methyl arsenic, arsenate, and phosphate onto goethite in arsenic and phosphate binary systems. *J. Colloid Interface Sci.*, 317, (1) **(2008)** 35-43.

[19] Zeng, H.; Fisher, B.; Giammar, D.E., Individual and competitive adsorption of arsenate and phosphate to a high-surface-area iron oxide-based sorbent. *Environ. Sci. Technol.*, 42, (1) **(2008)** 147-152.

[20] Violante, A.; Pigna, M., Competitive sorption of arsenate and phosphate on different clay minerals and soils. *Soil Sci. Soc. Am. J.*, 66, (6) **(2002)** 1788-1796.

[21] Vetterlein, D.; Szegedi, K.; Ackermann, J., Competitive mobilization of phosphate and arsenate associated with goethite by root activity, *J. Environ Qual.*, 36, (6) **(2007)** 1811-1820.

[22] Liu, F.; De Cristofaro, A.; Violante, A., Effect of pH, phosphate and oxalate on the adsorption/desorption of arsenate on/from goethite. *Soil Sci.*, 166, (3) **(2001)** 197-208.

[23] Frau, F.; Biddau, R.; Fanfani, L., Effect of major anions on arsenate desorption from ferrihydrite-bearing natural samples. *Appl. Geochem.*, 23, (6) **(2008)** 1451-1466.

[24] Antelo, J.; Avena, M.; Fiol, S.; Lopez, R.; Arce, F., Effects of pH and ionic strength on the adsorption of phosphate and arsenate at the goethite-water interface. *J. Colloid Interface Sci.*, 285, (2) **(2005)** 476-486.

[25] Gräfe, M.; Nachtegaal, M.; Sparks, D.L.; Fprmation of Metal-Arsenate Precipitates at the goethite-water interface. Environ. Sci. Technol. 38 **(12004)** 6561-6570.

[26] Battacharya, P.; Mukherjee, A.B.; Jacks, G., Nordqvist, S.; Metal contamination a a wood preservative site: characterisation and experimental studies on remediation. Sci. Tot. Environ. 290 **(2002)** 165-180.

[27] Cornell, R.M.; Schwertmann, U., The iron oxides: structure, properties, reactions, ocurrences and uses, VCH, Weinheim, **(1996)**.

[28] Castaño, J.G.; Arroyave, C., La funcionalidad de los óxidos de hierro. *Rev. Metal. Madrid*, 34, (3) **(1998)** 274-280.

[29] Potapova, E.; Grahn, M.; Holmgren, A., Hedlund, J.; The effect of calcium ions and sodium silicate on he adsorption of anionic flotation collector on magnetite studied by ATR-FTIR spectroscopy. J. Coll. Interf. Sci. 345 **(2010)** 96-102.

[30] Forsmo,S.P.E.; Samskog, P-O.; Björkman, B.M.T.; A study on plasticity and compression strength in wet iron ore green pellets related to real process variation in raw material fineness. Powder technology 181 **(2008)** 321-330.

[31] Masel, R.I.; Principles of adsorption and reaction on solid surfaces, John Wiley and sons, **(1996)**.

[32] Crittenden, B.; Thomas, W.J.; Adsorption Technology and Design, Butterworth-Heinemann, 1st edition. 1998.

[33] Shaw, D.J., Introduction to colloid and surface chemistry, Butterworth-Heinemann **(1992)**.

[34] Thirunavukkarasu, O.S.; Viraraghavan, T.; Subramiam, K.S.; Arsenic removal from drinking water using iron oxide-coated sand. *Wat. Air Soil Pol.* **(2003)** 142, 95-111.

[35] Lezehari, M.; Baudu, M.; Bouras, O.; Basly, J.P.; Fixed-bed column studies of pentachlorophenol removal by use of alginate-en-capsulated pillared clay microbeads. *J. Coll. Interf. Sci.* **(2012)** 379 (1), 101-106.

[36] Yahaya, N.K.E.M; Abusta, I.; Latiff, M.F.P.M.; Bello, O.S.; Ahmad, M.A.; Fixed-bed column study for Cu(II) removal from aqueous solutions using rice husk based activated carbon. *Int. J. Eng. Tech.* **(2011)** 11 (1), 248-252.

[37] Suksabye, P.; Thirvetyan, P.; Nakbanpote, W.; Column study of Chromium (VI) adsorption from electroplating industry by coconut coir pith. *J. Hazard Tech.* **(2008)** 160, 56-62.

[38] Sansalone, J.; Asce, M.; Ma, J.; Parametric Analysis and Breakthrough Modeling of Phosphorous from Al-Oxide Filter Media. *J. Environ. Eng.* **(2011)** 137 (2), 108-118.

[39] Luo, W.; Wei, P.; Chen, H.; Fan, L.; Huang, L.; Huang, L.; Huang, J.; Xu, Z.; Cen, P.;Kinetics and optimization of L-tryptophan separation with io-exchange chromatography. *Korean J. Chem. Eng.* **(2011)** 28 (5), 1280-1285.

[40] Lumsdon, D.G.; Fraser, A.R.; Russel, J.D.; Livesey, N.T., New infrared bands assignments for the arsenate ion adsorbed on synthetic goethite (α-FeOOH), *Soil Sci.* 35 **(1984)** 381-386.

[41] Gimenez, J.; Martinez, M.; De pablo, J.; Rovira, M.; Duro, L., Arsenic sorption onto natural hematite, magnetite, and goethite, *J. Hazard. Mater.* 141(3) **(2007)** 575-580.

[42] Sherman, D.M.; Randall, S.R., Surface complexation od arsenic(V) to iron(III) (hydr)oxides: structural mechanism from ab initio molecular geometries and EXAFS spectroscopy, *Geochim. Cosmochim. Acta* 67 (22) **(2003)** 575-580.

[43] Fendorf, S.; Eick, M.J.; Grossl, P.; Sparks, D.L., Arsenate and chromate retention mechanisms on goethite.1. Surface structure, *Environ. Tecnol.* 31 (2) **(1997)** 315-320.

[44] Manceau, A., The mechanism of anion adsorption on iron-oxides- evidence for the bonding of arsenate tetrahedra on free Fe(O,OH)(6) edges, *Geochim. Cosmochim. Acta* 59 (17) **(1995)** 3647-3653.

[45] Waychunas, G.; Rea, B.A.; Fuller, C.C., Surface-chemistry of ferrihydrite.1. EXAFS studies of the geometry of coprecipitated and adsorbed arsenate, *Geochim. Cosmochim. Acta* 57 (10) **(1993)** 2251-2269.

[46] Loring, J.S.; Sandström, M.H.; Norén, K.; Persson, P., Rethinking Arsenate coordination at the surface of goethite. *Chem. Eur. J.*, 15 **(2009)** 5063-5072.

[47] Luengo, C.; Brigante, M.; Avena, M., Adsorption kinetics of phosphate and arsenate on goethite. A comparative study, *J. Colloid Interface Sci.,* 311 (2) **(2007)** 354-360.

[48] Grossl, P.R; Eick, M.; Sparks, D.L.; Goldberg, S.; Ainsworth, C.C, Arsenate and chromate retention mechanisms on goethite.2.Kinetics evaluation using a pressure-jump relaxation technique, *Environ. Tecnol.* 31 (2) **(1997)** 321-326.

[49] Tejedor-Tejedor, M.I.; Anderson, M.A, Protonation of phosphate on the surface of goethite as studied by CTIR-FTIR and electrophoretic mobility. *Langmuir*, 6, (3) **(1990)** 602-611.

[50] Luengo, C.; Brigante, M.; Antelo, J.; Avena, M., Kinetics of phosphate adsorption on goethite: comparing batch adsorption and ATR-IR measurements. J. *Colloid Interface Sci.*, 300 **(2006)** 511-518.

[51] Arai, Y.; Sparks, D.L., ATR-FTIR spectroscopic investigation on phosphate adsorption mechanism at the ferrihydrite-water interface. *J Colloid Interface Sci.*, 241 **(2001)** 317-326.

[52] Arai, Y.; Sparks, D.L.; Davis, J.A., Effects of dissolved carbonate on arsenate adsorption and surface speciation at the hematite-water interface, *Environ. Technol.* 38 (3) **(2004)** 817-824.

[53] Stollenwerk, K.; Breit, G.N.; Welch, A.H.; Yount, J.C.; Whitney, J.W.; Foster, A.L.; Uddin, M.N.; Majumder, R.K.; Ahmed, N., Arsenic attenuation by oxidazed aquifer sediments in Bangladesh, *Sci. Total Environ.* 379 (2-3) **(2007)** 133-150.

[54] Su, C. Puls, R.W.; Arsenate and Arsenite Removal by Zerovalent Iron: Effects of Phosphate, Silicate, Carbonate, Borate, Sulfate, Chromate, Molbdate, and Nitrate, relative to Chloride. *Environ. Sci. Environ.* 35 **(2001)** 4562-4568.

[55] Yang, W.; Kan, A.T., Chen, W., Tomson, M.B.; pH-dependent effect of zinc on arsenic adsorption to magnetite nanoparticles. *Water Res.* 44 **(2008)** 5693-5701.

[56] Khan M.A.; Ho Y-S; Arsenic in Drinking Water: A Review on Toxicological Effects, Mechanism of Accumulation and Remediation, Asian Journal of Chemistry, Vol. 23, No 5 **(2011)** 1889-1901.

[57] Aredes S.; Klein B.; Pawlik M.; The removal of arsenic from water using natural iron oxide minerals. *J. Cle. Prod.* 2012 29-30, 208-213.

[58] Joshi, A.; Chaudhuri, M; Removal of Arsenic from ground water by iron oxide-coated sand. *J. Environ. Eng.* **(1996)** 122 (8), 769-771.

[59] Vaishya, R.C.; Gupta, S.K.; Arsenic removal by sulfate modified iron oxide coated sand (SMIOCS) in Fixed Bed Column. *Water Qual. Res. J. Canada.* **(2006)** 41 (2) 157-163.

[60] Kundu, S.; Gupta. A.K.; Adsorptive removal of As(III) from aqueous solution using Iron Oxide Coated Cement (IOCC): Evaluation of Kinetic, equilibrium and thermodynamic models. *Separation and Purification Technology*. **(2006)** 51, 165–172.

[61] Kundu, S.; Gupta. A.K.; Arsenic adsorption onto iron oxide coated cement (IOCC): regression analysis of equilibrium data with several isotherm models and their optimization. *Chemical Engineering Journal.* **(2006)** 122, 93–106.

[62] Stanić, T.; Daković, A.; Živanović, A.; Tomašević-Čanović, M.; Dondur, V.; Milićević, S.; Adsorption o arsenic (V) by iron (III)-modified natural zeolite tuff. Environ. Chem. Lett. **(2009)** 7, 161-166.

[63] Hlavay, J.; Polyák, K.; Determination of surface properties of iron hydroxide-coated alumina adsorbent prepared for removal of arsenic from drinking water. *J. Coll. Interf. Sci.* **(2005)** 284 , 71-77.

[64] Kumar, A.; Gurian, P.L.; Bucciarelli-Tieger, R.H.; Mitchell-Blackwood, J.; Iron oxide-coated fibrous sorbents for arsenic removal. *Am. Water Works Ass. J.* **(2008)** 100 (4), 151-164.

[65] Axe, K.; Vejgarden, M.; Persson, P., An ATR_FTIR spectroscopic study of the competitive adsorption between oxalate and malonate at the water-goethite interface, *J. Colloid Interface Sci.* 294 (1) **(2006)** 31-37.

[66] Fredriksson, A.; Holmgren, A., An in situ ATR-FTIR study of the adsorption kinetics of xanthate on germanium, *Colloid Surf. A-Physicochem. Eng. Asp.* 302 **(2007)** 96-101.

[67] Grahn, M.; Lobanova, A.; Holmgren, A.; Hedlund, J., Orientational analysis of adsorbates in molecular sieves by FTIR/ATR spectroscopy, *Chem. Mater.* 20 (19) **(2008)** 6270-6276.

[68] Larsson, M.L.; Fredriksson, A.; Holmgren, A. Direct observation of a self-assembled monolayer of heptyl xanthate at the germanium/water interface: a polarized FTIR study, *J. Colloid Interface Sci.* 273 **(2004)** 345-349.

[69] Roddick-Lanzilota, A.; McQuillan, A.J.; Craw, D., Infrared spectroscopic characterisation of arsenic (V) ion adsorption from mine waters, Macraes mone, New Zealand, Appl. Geochem. 17 (4) **(2002)** 445-454.

[70] Mirabella, F.M., Internal Reflection Spectroscopy: theory and applications, Marcel Dekker, **(1993)**

[71] McQuillan, J.A.; Probing Solid-Solution Interfacial Chemistry with ATR-FIR spectroscopy of Particle Films. *Adv. Mater.* **(2001)** 13, 12-13, 1034-1038.

[72] Matijevic, E.; Production of monodispersed colloidal particles. Annu. Rev. Mater. Sci. 15 **(1985)** 483-516.

[73] McComb, K.; Craw, D.; McQuillan, A.J.; ATR-IR spectroscopic study of antimoniate adsorption to iron oxide. Langmuir. **(2007)** 23, 24, 12125-12130.

[74] Raven, K.P.; Jain, A.; Loeppert, R.H., Arsenite and Arsenate Adsorption on Ferihydrite: Kinetics, Equilibrium, and adsorption envelopes. Environ. Sci. Technol. **(1998)** 32, 344-349.

Paper I

Studies of Collector Adsorption on Iron Oxides by in Situ ATR-FTIR spectroscopy

E. Potapova, I. Carabante, M. Grahn, A. Holmgren, J. Hedlund

Industrial & Engineering Chemistry Research, 49 (2010) 1493-1502

Studies of Collector Adsorption on Iron Oxides by in Situ ATR-FTIR Spectroscopy

E. Potapova,* I. Carabante, M. Grahn, A. Holmgren, and J. Hedlund

Division of Chemical Engineering, Luleå University of Technology, SE-971 87 Luleå, Sweden

In this work, the adsorption of three model collectors, viz., poly(ethylene glycol) monooleate (PEGMO), ethyl oleate, and maleic acid, as well as the commercial fatty-acid-type collector Atrac 1563, was studied in situ on synthetic hematite using attenuated total reflectance Fourier transform infrared (ATR-FTIR) spectroscopy. The adsorption behavior of the studied compounds on hematite was determined to a large extent by the polar headgroup. Adsorption of Atrac and PEGMO as a function of concentration showed good agreement with the Freundlich adsorption model, suggesting energetically heterogeneous adsorption. In situ desorption experiments revealed that a large fraction of the Atrac was weakly attached to the hematite surface, as it was partially removed by flushing with water at pH 8.5 and 10. These results suggest that a separate washing unit after the flotation step could be beneficial in reducing the contamination of iron ore by flotation chemicals.

Introduction

Iron ore pellets are an important refined product used as a raw material in the manufacturing of steel. The production of iron ore pellets comprises several stages: grinding and upgrading of the iron ore; balling of wet, so-called, green pellets; and drying, sintering, and oxidation of the green pellets to the final product, to be transported to iron or steel plants.

LKAB is a Swedish mining company whose pelletizing plants utilize magnetite iron ore from two deposits located in northern Sweden: Kiruna and Malmberget. The Kiruna ore is a mixture of magnetite and apatite having a phosphorus content of ca. 1 wt %. To reduce the phosphorus content to an acceptable level for the blast furnace process[1] (i.e., to less than 0.025%), the ore is subjected to reverse flotation with an anionic fatty-acid-type collector reagent (Atrac 1563) with methyl isobutyl carbinol (MIBC) used as a frother. To increase flotation selectivity and phosphorus recovery, sodium silicate is added to the system. The sodium silicate is used in fairly small amounts (300−500 g t^{-1}) and thus acts primarily as a dispersant, and it has not been found to prevent collector adsorption on the magnetite surface to any great extent.[2,3]

Ideally, the collector should adsorb only on the apatite gangue, rendering it hydrophobic and thus easily floated from the magnetite. However, unwanted adsorption of the flotation reagents on magnetite also occurs. It has been estimated that the amount of Atrac adsorbed on the magnetite fed to balling circuits is 10−30 g t^{-1}.[4] Once the collector is adsorbed on the surface of magnetite, it is difficult to eliminate.[5] Therefore, the collector should be added in sufficiently small amounts so that the apatite surface is rendered hydrophobic whereas the adsorption on magnetite is minimized. However, in the real process, the Atrac dosage is adjusted based on the phosphorus content in the pellet feed, and there is a slight degree of overdosage to ensure that the desired phosphate levels are achieved. Typically, the dosage varies in the range of 30−70 g per tonne of magnetite concentrate.[6]

After the flotation step, the pulp passes through magnetic separation and filtration steps where it is subjected to repeated dilutions and thickenings that can have a mild washing effect on the ore, partly removing the flotation reagents from the magnetite surface. However, no separate washing unit is used for the purification of magnetite from the flotation chemicals at LKAB.

It has been found that adsorption of the flotation collector agent on the iron ore has a negative effect on the balling process, as the collector adsorbed on the surface of magnetite makes the particles more hydrophobic, which can lead to the attachment of air bubbles onto the surface of the iron ore particles.[6] The air bubbles incorporated into green pellets decrease the green pellet strength in both the wet and dry states. A low wet strength tends to cause a wide size distribution of the green pellets leaving the balling drums. The undersize fraction is recirculated back to the balling drum, thus leading to increased energy consumption and decreased capacity of the pelletizing plant. Breakage of the pellets at the stage of drying and induration causes dust formation and decreased pellet bed permeability, resulting in lower production volumes and aggravated pellet quality.[7]

To minimize the influence of the collector on the pelletizing process, it is important to understand the mechanism by which the collector interacts with the iron oxide. For instance, it has been shown that the presence of Ca^{2+} ions in the process water increases the adsorption of flotation collector reagent on magnetite.[8] In that work, the adsorption of the collector OS 130 on magnetite was studied in the batch experiments by measuring the residual concentration of the collector in solution after adsorption using the method of Gregory.[9] According to the suggested[8] mechanism, positively charged calcium ions adsorb at negatively charged surface sites on the magnetite surface, which results in a more positively charged surface, rendering it more favorable for the adsorption of negatively charged collector species.

Spectroscopic techniques have been used extensively for studying the adsorption of fatty-acid-based collectors onto mineral surfaces.[10−12] Fourier transform infrared (FTIR) spectroscopy is widely applied because it provides the possibility of identifying complexes formed at the surface.[13] Ex situ FTIR techniques, such as diffuse reflectance infrared Fourier transform (DRIFT) spectroscopy and reflection absorption infrared spec-

* To whom correspondence should be addressed. E-mail: elisaveta.potapova@ltu.se. Tel.: +46 920 491 776.

10.1021/ie901343f
Published on Web 01/07/2010

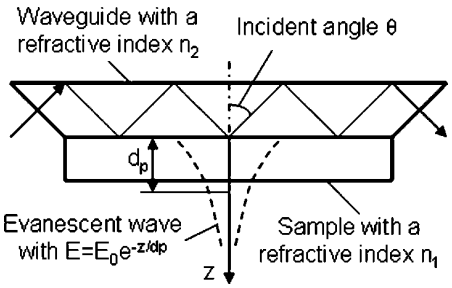

Figure 1. Schematic image of an ATR waveguide illustrating the ATR phenomenon. For the sake of clarity, the thickness of the sample (in this case, iron oxide film) and the penetration depth d_p are enlarged.

troscopy (RAIRS), imply drying of the sample after adsorption, which can affect surface complexes and, hence, the validity of the results. On the contrary, FTIR attenuated total reflectance (FTIR-ATR) spectroscopy facilitates in situ studies of both adsorption kinetics[14] and complexes formed on the surface in the presence of water.[13,15] In the ATR technique (Figure 1), a sample with a certain refractive index, n_1, is placed in a close contact with a waveguide characterized by a high refractive index, n_2. The IR beam is passed through the waveguide at a certain incident angle θ. In the case when sin θ is larger than the ratio n_1/n_2, the beam is totally reflected inside the waveguide, forming a perpendicular evanescent wave of the IR radiation at each point of reflection. This wave propagates through the sample in the vicinity of the waveguide and interacts with the sample, causing partial absorption of the radiation by the sample material and thus a reduction of the intensity of the totally reflected beam. The penetration depth, d_p, is defined as the distance from the interface at which the electric field of the wave is equal to E_0e^{-1} (see Figure 1), where E_0 is the electric field of the wave at the interface. Typical values of the penetration depth are from some hundred nanometers to a few micrometers, depending on the refractive indices of both the waveguide and the sample, as well as on the wavelength and incident angle of the radiation. Such a range of penetration depths makes FTIR-ATR spectroscopy a very surface-sensitive technique, providing the possibility for in situ studies of surfaces in contact with aqueous solutions.

During the past decade, the FTIR-ATR technique has been developing, and new applications in surface chemistry have evolved, for example, as a tool for studying adsorption[13,16−19] and diffusion[20−24] in thin films or at interfaces. This technique has also been used in studies of catalytic reactions,[25,26] as well as in sensor applications.[27,28] FTIR-ATR spectroscopy has also been applied for studying the adsorption of surfactants at mineral surfaces, both qualitatively[29,30] and quantitatively.[14,31−33] Our group has developed the ATR technique for studies of adsorption in zeolite films[17,27,34−37] and on mineral surfaces.[14,18,38−41] The studies have been both qualitative[35−38,40,41] and quantitative,[14,17,18,27,34,39] and even the molecular orientations of adsorbates have been determined.[17,18,35,38,41]

Although magnetite (Fe_3O_4) is the main iron-containing mineral in the ore utilized by LKAB, it was found to become partly oxidized during storage in air, forming first maghemite (γ-Fe_2O_3), which has the same crystal structure but mostly Fe^{3+} on the surface, and then hematite (α-Fe_2O_3), which has a different crystal structure than magnetite and maghemite.[42] This phenomenon was described earlier for submicrometer-sized magnetite particles by both Haneda and Morrish[43] and Gedikoglu.[44] In solution, the oxidation of magnetite was also observed and explained by the leaching of Fe^{2+} ions from the surface.[45] Thus, when magnetite ore is subjected to grinding and flotation, apparent oxidation of the surface can occur both in water and in air.

In this work, the adsorption of flotation collector reagents on iron oxide was studied in situ using FTIR-ATR spectroscopy for the purpose of obtaining essential information about the interaction between the flotation collector reagents and the iron oxide surface in the presence of water. This information is crucial for the improvement of the pelletizing process, as it could suggest possibilities to reduce the unwanted collector adsorption on the iron ore surface and improve green-pellet strength. Hematite was chosen as the adsorbent because it was reported to be the final product of the surface oxidation of magnetite. In addition, reports on the adsorption properties of collector-type molecules on hematite were found to be very scant in the literature.

Materials and Methods

Materials. Hematite crystals were synthesized from an $FeCl_3$ solution according to the method described by Matijević.[46] The obtained hematite crystals were purified by repeated (five times) centrifugation at 20000 rpm for 30 min and redispersion in a 0.06 M aqueous solution of acetic acid (glacial, >99.7%, Alfa Aesar). The crystals were stored as a 2 wt % suspension in a 0.06 M aqueous solution of acetic acid at pH 3. For powder X-ray diffraction analysis, the suspension was freeze-dried, yielding a fine hematite powder.

The flotation collector reagent, Atrac 1563 (Akzo Nobel, Sweden), was provided by LKAB. Atrac 1563 is a yellow viscous liquid with a complex chemical composition: 50−100% ethoxylated tall oil ester of maleic acid and 1−5% maleic anhydride (Akzo Nobel material safety data sheet). Tall oil is a byproduct of the Kraft pulp manufacturing process and is a mixture of mainly fatty acids (e.g., oleic acid) and resin acids (e.g., abietic acid). A similar collector for the froth flotation of oxide and salt-type minerals that is a combination of a monoester of a dicarboxylic acid and a monocarboxylic acid is described in a patent.[47] As described in the patent, the first component is an aliphatic monocarboxylic acid containing 8−22 carbon atoms bonded to a dicarboxylic acid containing 4−8 carbon atoms through an alkylene oxide group with 2−4 carbon atoms, thus resulting in a molecule with two ester carbonyls and one free carboxylic group at the end of the molecule. Monocarboxylic acid with 6−24 carbon atoms is added to increase the selectivity and/or yield of the monoester.

Poly(ethylene glycol) monooleate (PEGMO) with a typical number-average molecular weight (M_n) of 460 (Aldrich), maleic acid (Fluka, ≥ 99%), and ethyl oleate (Aldrich, 98%) were used as model collector reagents. From the average molar mass, the length of the poly(ethylene glycol) chain in the PEGMO model collector reagent was estimated to be about four ethylene glycol units. Oleic acid esters were chosen because oleic acid is one of the main components of tall oil. Ethoxylated tall oil could thus be modeled by using PEGMO, which has the same structure as ethoxylated oleic acid. Maleic acid was chosen as one of the model compounds because it is the tail group of the molecules in Atrac. Ethyl oleate was used as the third model compound to study the effect of the poly(ethylene glycol) chain on the adsorption properties of oleate.

Working solutions of Atrac and the model collector reagents were prepared in the following way: First, a 0.1 g L^{-1} stock solution of the compound in distilled water was prepared. In

the next step, the required amount of the stock solution was mixed in distilled water to give final solutions of the desired concentration (1−25 mg L^{-1}).

All aqueous solutions were prepared using distilled water. The distilled water used for the spectroscopic measurements was first boiled for 1 h, and then argon was bubbled through the water to minimize the amount of dissolved carbon dioxide.

The pH was controlled during the experiments by a Mettler Toledo T70 titrator using a 0.05 M aqueous solution of sodium hydroxide (per analysis, Merck).

Dip-Coating. Hematite films were deposited on ZnSe substrates using a Nima DC-multi 8 dip-coater. Prior to deposition, the substrates were washed in acetone (≥99.5%, VWR), ethanol (99.7%, Solveco Chemicals AB), and distilled water (10 min in each). A 2 wt % hematite suspension was prepared by dispersing the hematite crystals in a 6.27 M aqueous solution of acetic acid. The substrates were immersed in the suspension and withdrawn at a speed of 5 mm min^{-1}, and the film thickness was controlled by the number of dips. To prepare a film with a thickness of ca. 1 μm, eight dips were needed.

Scanning Electron Microscopy (SEM). SEM images of the hematite film on a ZnSe substrate were obtained using a Philips XL 30 microscope with a LaB_6 filament. The samples were mounted on alumina stubs using carbon glue and subsequently sputtered with a thin layer (ca. 10 nm) of gold to provide conductivity.

X-ray Diffraction. X-ray diffraction patterns of both hematite powder and film were collected with a Siemens D5000 diffractometer running in Bragg−Brentano geometry using Cu K_α radiation. To analyze the film, the hematite-covered ZnSe substrate was mounted with carbon glue onto a custom-made alumina holder.

Zeta-Potential Measurements. The point of zero charge (PZC) of the hematite crystals used in this work was determined by electrophoresis using a ZetaCompact instrument equipped with a charge-coupled device (CCD) tracking camera. The obtained electrophoretic mobility data were further processed by the Zeta4 software applying the Smoluchowski equation. The samples were prepared in the following way: One drop of the hematite suspension was dispersed in 1 L of 0.01 M potassium nitrate. The pH of the samples (10 samples, 100 mL each) was adjusted using potassium hydroxide and nitric acid. The samples spanned the pH range from 2 to 11. For each sample, the measurement was repeated three times, and the final PZC was calculated as an average of the obtained values.

FTIR-ATR Spectroscopy. Infrared spectra were recorded using a Bruker IFS 66v/S spectrometer equipped with a liquid-nitrogen-cooled mercury cadmium telluride (MCT) detector. ZnSe ATR crystals (Crystran Ltd.) in the form of a trapeze with 45° cut edges and dimensions of 50 × 20 × 2 mm were used in this study. Measurements of adsorption on the hematite-coated ATR crystals were performed in situ in a cell with a flow pumped through on both sides of the ATR crystal; see Figure 2. The incidence angle of the infrared beam was set to 45°.

All adsorption experiments on hematite were performed at room temperature using water solutions of model collectors or Atrac at pH 8.5 (the pH used in the flotation process at LKAB) pumped continuously through the cell at a flow rate of 10 mL min^{-1} with recirculation. Prior to the adsorption measurements, the hematite film was flushed with a weakly alkaline solution (pH 8.5) for 2 h to remove the residues of acetic acid and carbonate species from the surface. A background spectrum was recorded afterward with water at pH 8.5 in contact with a hematite-coated ZnSe substrate. Spectra of the model collectors and Atrac in pure form were recorded in argon atmosphere using a bare ZnSe substrate with a droplet of a collector spread over its surface. ZnSe in argon atmosphere was recorded as a single-beam background spectrum. All background and sample spectra were obtained by averaging 500 scans at a resolution of 4 cm^{-1}. Data processing was performed using Bruker Opus 4.2 software.

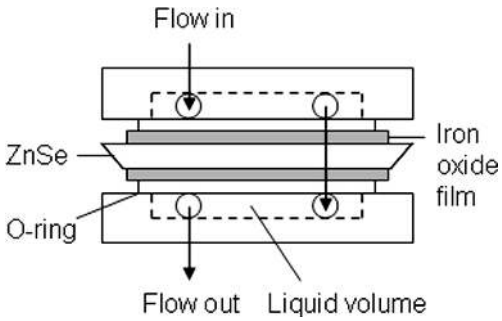

Figure 2. Schematic image of the FTIR-ATR flow cell. For the sake of clarity, the thickness of the iron oxide film is enlarged.

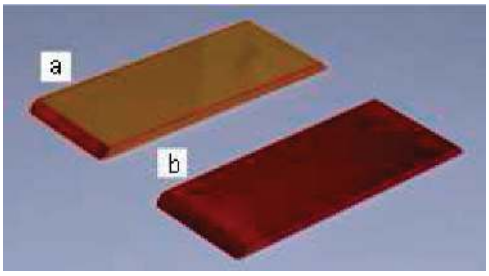

Figure 3. Images of (a) uncoated and (b) hematite-coated ZnSe ATR crystals.

Results and Discussion

Film and Powder Characterization. Figure 3 shows a photograph of ZnSe crystals before and after being coated with a hematite film. As is evident from the uniform red color of the coated ATR crystal, the obtained film appeared to be quite uniform, continuous, and even along the crystal surface and stable under the conditions used for the in situ experiments, because the visual appearance of the coated crystal did not change after the experiments.

SEM images (Figure 4) showed that the hematite crystals had a uniform spherical habit with a diameter of ca. 130 nm and that the crystals were distributed evenly over the ATR crystal surface, forming a porous film with an average thickness of ca. 1 μm.

Figure 5 shows XRD patterns of freeze-dried synthetic hematite powder and a hematite film on a ZnSe crystal. The XRD pattern of the powder shows that the synthesized material contained pure, randomly oriented hematite crystals without any other iron oxide phase present in amounts detectable by XRD. By comparing the relative reflection intensities in the powder and in the film, it can be concluded that the crystals in the film were also randomly oriented.

Figure 6 shows the ζ-potential of the synthetic hematite crystals used in this work as a function of pH. The point of

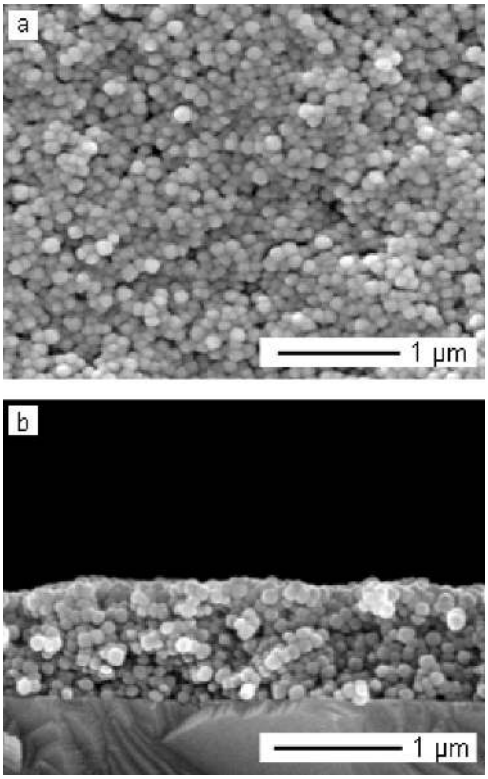

Figure 4. (a) Top- and (b) side-view SEM images of a hematite film on a ZnSe crystal.

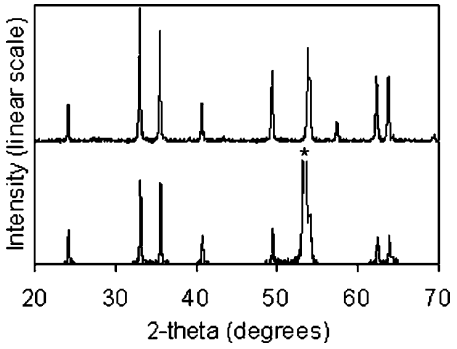

Figure 5. XRD patterns of hematite powder (top) and hematite film on a ZnSe crystal (bottom). The peak labeled with an asterisk (*) emanates from the ZnSe substrate.

zero charge (PZC) is at about pH 4.8. According to data compiled by Fuerstenau[48] and Cromieres,[49] the PZC of hematite has been reported to occur within a broad range of pH values, viz., from 4.8 to 10.3. Factors that can influence the value of the PZC are[1] the technique used to determine the ζ-potential, impurities (especially in the case of minerals), sample preparation procedure, and species adsorbed on the surface (e.g., carbonates).[50,51]

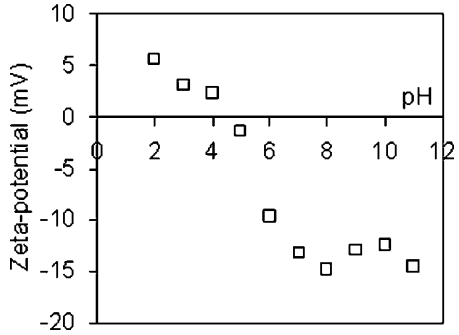

Figure 6. ζ-potential of the hematite crystals as a function of pH.

In the present study, the PZC of hematite was probably affected by the carbonate species adsorbed on the surface, which are known to lower the PZCs of iron oxides by ca. 1 pH unit.[52]

The presence of the carbonate species was confirmed by spectra (not shown) recorded during flushing of the hematite film with distilled water at pH 8.5 prior to the adsorption experiments. Weak negative bands at ca. 1490 and 1340 cm^{-1} originating from the outer-sphere carbonate species[52] were observed in the spectra, indicating the desorption of carbonates from the hematite surface. Desorption of carbonates had ceased already after 30 min of flushing, suggesting that carbonate species in solution and on the surface were in equilibrium.

Adsorption of Model Compounds. To better understand the adsorption mechanism of Atrac on hematite, three model compounds of Atrac were studied. As it is known that Atrac contains maleic acid esterified with an ethoxylated tall oil (Akzo Nobel material safety data sheet), poly(ethylene glycol) monooleate (PEGMO) and maleic acid were chosen as model compounds. From the number-average molecular weight, M_n = 460, it was estimated that an average poly(ethylene glycol) chain in PEGMO contained four repeated ethoxy units ($-CH_2-O-CH_2-$). Ethyl oleate was used as an additional model compound to study the effect of the poly(ethylene glycol) chain on the adsorption properties of oleate.

PEGMO is a nonionic surfactant[53] characterized by a higher solubility in water than the corresponding fatty acid because of the poly(ethylene glycol) chain. PEGMO can be expected to interact with the iron oxide surface in three different ways, viz., through the ester carbonyl, the ether oxygen linkages, or the tail hydroxyl group. Figure 7 shows spectra of a droplet of pure PEGMO on ZnSe and PEGMO adsorbed on hematite from aqueous solution.

Strong absorption bands at 2922 and 2854 cm^{-1} in Figure 7a originate from asymmetric and symmetric stretching vibrations of the C−H bonds (ν_{as} and ν_s).[54] Long-chain carboxylic acids (e.g., oleic acid) contain significantly more methylene groups than methyl groups and are thus characterized by much stronger absorption bands corresponding to the CH_2 groups compared to the CH_3 groups. The latter can be observed only as shoulders. C−H deformation in methyl and methylene groups is found around 1458 cm^{-1}.[55] The absorption band observed in pure PEGMO at 1736 cm^{-1} (Figure 7a) is associated with stretching vibrations of the C═O ester bond.[56] It is only slightly shifted upon adsorption on hematite (Figure 7b), indicating that no significant interaction occurs between the ester carbonyl and the surface. The absence of bands around 1570 and 1430 cm^{-1}, corresponding, respectively, to asymmetric and symmetric

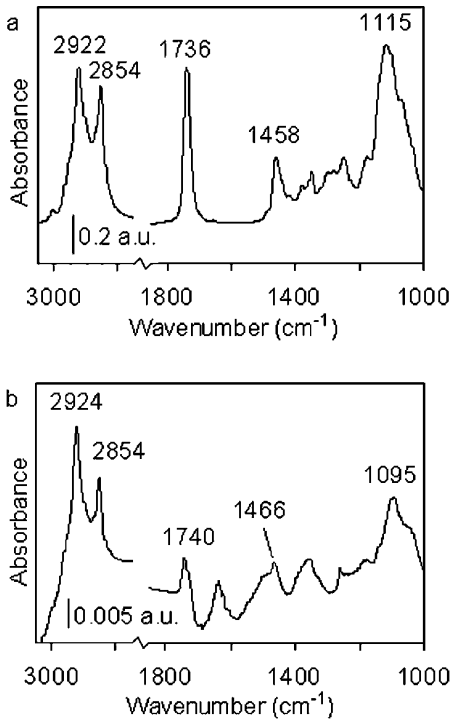

Figure 7. Infrared spectra of (a) a droplet of pure PEGMO on ZnSe and (b) PEGMO adsorbed on a hematite film in situ from a 10 mg L^{-1} aqueous solution. Note that a.u. represents arbitrary units here and elsewhere.

stretching of a carboxylate group,[12,57] suggests that the ester bond in PEGMO does not break upon adsorption on hematite.

The intense band at 1115 cm^{-1} (Figure 7a) emanates from the C−O−C stretching vibration in the poly(ethylene glycol) chain.[58] It has a shoulder on its low-frequency side at ca. 1070 cm^{-1} probably emanating from the stretching of the C−O bond between the hydroxyl group and the CH_2 group at the end of the poly(ethylene glycol) chain.[59] Both the peak frequency and the shoulder frequency are shifted to lower wavenumbers when PEGMO is adsorbed on hematite (see Figure 7b; 1115 → 1095 cm^{-1} and 1070 → 1047 cm^{-1}, respectively), suggesting that the poly(ethylene glycol) chain is involved in the bonding to the surface.

Figure 8 shows the change in absorbance (measured as peak height) of the 2854 cm^{-1} band during the adsorption of PEGMO on hematite at different concentrations after 1 h of adsorption at each concentration. The experiment was started at the lowest concentration of 1 mg L^{-1}; thereafter, the concentration in solution was increased, and the measurement was continued.

Figure 8 shows that the intensity of the band originating from the symmetric stretching vibration (ν_s) of the C−H bond increased with increasing concentration in solution, suggesting an increase of the adsorption of PEGMO on hematite. The experimental data exhibited a poor fit with the Langmuir model of adsorption, with a coefficient of determination (R^2) of 0.87. Plotting the data on a logarithmic scale yielded a straight line with $R^2 = 0.99$, indicating that the obtained data were in good agreement with the Freundlich model of adsorption, which implies that the surface of adsorption is heterogeneous, for

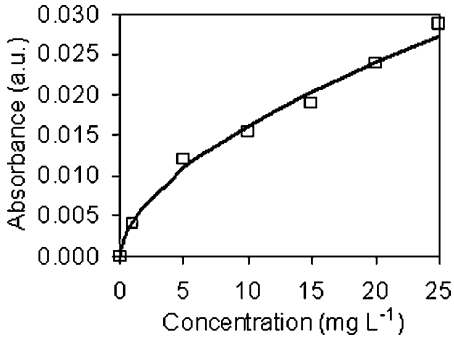

Figure 8. Intensity of the band originating from the symmetric stretching vibration (ν_s) of the C−H bond as a function of concentration of PEGMO in solution (□). The solid line represents the fitted Freundlich adsorption model.

instance, with different adsorption sites grouped patchwise based on their adsorption energies, as suggested earlier.[60] A desorption experiment (not shown) showed that the intensity of the band originating from the symmetric stretching vibration (ν_s) of the C−H bond in PEGMO was reduced only by 5% upon flushing the cell with water at pH 8.5 for 1 h, indicating that most of the PEGMO was strongly adsorbed to the hematite surface.

Maleic acid was the second model compound studied. The ability of maleic acid to form intramolecular hydrogen bonds makes it easily soluble in water. In aqueous solution at pH 8.5, it is expected to be fully deprotonated.[61]

From the spectroscopic measurements it was concluded that maleic acid did not adsorb on hematite to any considerable extent at pH 8.5 in the concentration range studied, viz., 1−25 mg L^{-1}. This could be explained by the fact that, at pH 8.5, the hematite surface is negatively charged and thus repels maleic acid, which, at this pH, contains two negatively charged carboxylate ions. Hwang and Lenhart[60] studied the adsorption of maleic acid on hematite at various pH values and concluded that the adsorption was controlled by the surface charge of hematite, suggesting that electrostatic interaction is the predominant force of adsorption of maleic acid on hematite, which agrees well with our observations.

Ethyl oleate was the third model compound of Atrac used in the experiments. It is almost insoluble in water due to the fact that, instead of a hydrophilic poly(ethylene glycol) chain, it has a hydrophobic ethyl group bonded to the carboxylate. This change in chemical composition, of course, also affects the adsorption properties of the molecule. The change in absorbance of the 2852 cm^{-1} band during the adsorption of ethyl oleate on hematite at different concentrations is shown in Figure 9. The measurements were performed in the same way as for PEGMO. Equilibrium was achieved at each concentration within 2 h.

Figure 9 shows that the absorbance of the band originating from the symmetric stretching vibration (ν_s) of the C−H bond is about a factor of 6 lower at all concentrations of ethyl oleate than the absorbance of the same band at corresponding concentrations of PEGMO. This indicates that about 6 times less ethyl oleate is adsorbed compared to PEGMO at the corresponding concentrations. The interaction between ethyl oleate and the surface was probably very weak, as no significant band shifts were observed in the spectrum of ethyl oleate on hematite (not shown) compared to the spectrum of pure ethyl oleate.

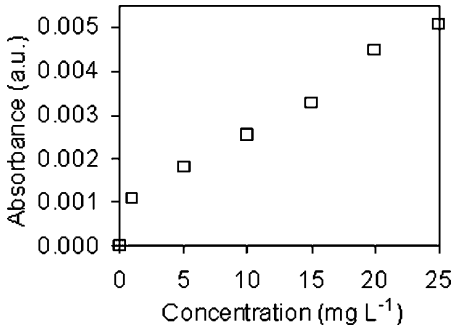

Figure 9. Intensity of the band originating from the symmetric stretching vibration (ν_s) of the C−H bond as a function of the concentration of ethyl oleate in solution.

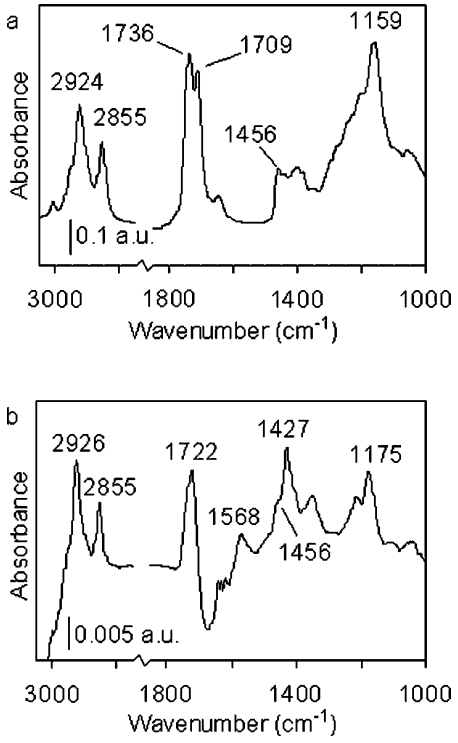

Figure 10. Infrared spectra of (a) a droplet of pure Atrac on ZnSe and (b) Atrac adsorbed on a hematite film in situ from a 10 mg L^{-1} aqueous solution.

Atrac Adsorption. Anionic fatty-acid surfactants are believed to interact with iron oxides electrostatically, that is, to adsorb on the positively charged iron oxide surface below its point of zero charge (PZC).[1] Nevertheless, oleate species are also known to chemisorb on hematite at several pH units above the PZC, forming iron oleate.[12,62] Despite the fact that, at pH 8.5, the hematite surface is charged negatively (see Figure 6), adsorption of Atrac on hematite at this pH was still observed. Figure 10 shows the infrared spectra of a droplet of pure Atrac on ZnSe and Atrac adsorbed on hematite from an aqueous solution.

Table 1. Assignment of Absorption Bands Originating from Pure Atrac Spread over ZnSe and Atrac Adsorbed on Hematite in Situ from a 10 mg L^{-1} Aqueous Solution

pure Atrac on ZnSe	Atrac adsorbed on hematite	peak assignment
2924	2926	ν_{as} (CH_2)[54]
2855	2855	ν_s (CH_2)[54]
1736	1722	ν(C═O) in ester[56]
1709		ν(C═O) in acid[65]
	1568	ν_{as} (COO^-)[66]
	1427	ν_s (COO^-)[66]
1456	1456	δ (CH_2 and CH_3)[55]
1159	1175	ν (C−O) in esters[63]

Being a multicomponent system, Atrac presents a rather complicated infrared spectrum with several absorption bands in the 1000 and 3000 cm^{-1} regions (Figure 10). Several bands in the spectrum of pure Atrac (see Figure 10a) are similar to those observed in the spectrum of pure PEGMO (see Figure 7a), including CH_2 stretching vibrations at 2924 and 2855 cm^{-1} and CH_2 deformation at 1456 cm^{-1}. The absorption bands observed in pure Atrac at 1736 and 1159 cm^{-1} (see Figure 10a) are associated with stretching vibrations of the C═O[55] and C−O[63] bonds in esters, respectively. Upon complexation of the ester group with a metal ion, ν(C═O) shifts to lower frequency, and ν(C−O) shifts to higher frequency.[64] These shifts are observed in the case of adsorption of Atrac on hematite, with ν(C═O) and ν(C−O) shifting by 14 and 16 cm^{-1}, respectively (see Figure 10b), suggesting rather strong interaction between the ester carbonyls in Atrac and the hematite surface.

The stretching vibration of the C═O bond of free carboxylic acids is observed in pure Atrac at 1709 cm^{-1} (see Figure 10a).[65] Upon deprotonation of the carboxylic group in solution this band disappears, and two new bands are observed at 1568 and 1427 cm^{-1} in the spectra of Atrac adsorbed on hematite (ν_{as} and ν_s, respectively; see Figure 10b).[66] As discussed above, adsorption of maleic acid on hematite was not observed under the experimental conditions used because of the electrostatic repulsion of the carboxylate anion and negatively charged hematite surface, suggesting that the adsorption of Atrac on hematite through carboxylate ions is unlikely and that the most probable interaction is through ester carbonyls connected by an ethoxy group. However, the carboxylate ions in the adsorbed molecules of Atrac are situated in the vicinity of the surface, and the bands originating from them can thus be found in the spectra of Atrac adsorbed on hematite. For band assignments, see Table 1.

As one of the main components of Atrac is known to be ethoxylated tall oil, stretching vibrations of the C−O−C group in the ethoxy chain were expected to be observed around 1100 cm^{-1}.[58] However, rather weak absorption bands were found in that wavenumber range in the spectra of both pure Atrac and Atrac adsorbed on hematite (see Figure 10), indicating that the degree of ethoxylation of the tall oil is quite low. This is further supported by the information found in the patent[47] indicating that only one ethoxy group derived from an alkylene oxide with two to four carbon atoms is found in the collector. A shorter poly(ethylene glycol) chain and the possible presence of highly nonpolar resin acids in Atrac result in a lower solubility of Atrac as compared to that of PEGMO.

Prior to studying the adsorption of Atrac as a function of concentration on hematite, the adsorption as a function of concentration on an uncoated ZnSe crystal was investigated. In Figure 11, the intensity of the 2855 cm^{-1} band is plotted as a function of Atrac concentration in solution. The measurements were carried out in a similar way as for PEGMO. At each concentration, steady state was reached within 1 h.

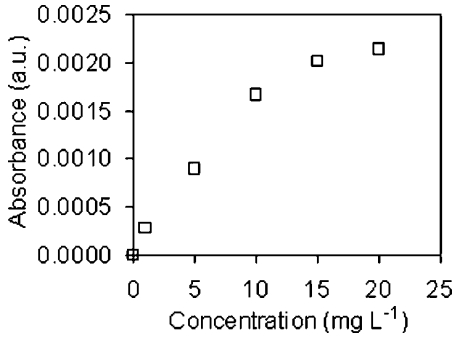

Figure 11. Intensity of the band originating from the symmetric stretching vibration (ν_s) of the C−H bond as a function of the concentration of Atrac in solution.

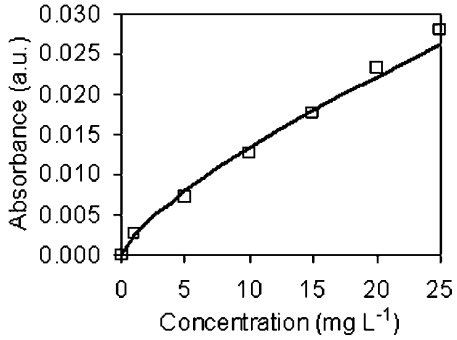

Figure 12. Intensity of the band originating from the symmetric stretching vibration (ν_s) of the C−H bond as a function of the concentration of Atrac in solution (□). The solid line represents the Freundlich adsorption model fitted to the experimental data.

Figure 11 illustrates that the absorbance increases with increasing concentration, but not linearly, suggesting that the recorded signal corresponds not to the bulk concentration but to the amount of Atrac adsorbed on ZnSe. The measured absorption intensities are quite low, as expected for a polished ZnSe surface with a very low surface area. Atrac was detected on the crystal even after the cell had been flushed with water for 1 h and the crystal had been dried in air, indicating a rather strong affinity for the ZnSe surface.

Figure 12 shows the change in the intensity of the band originating from the symmetric stretching vibration (ν_s) of the C−H bond during the adsorption of Atrac on hematite as a function of concentration. The measurements were performed in the same way as for PEGMO. Adsorption equilibrium was achieved at each concentration within 3−5 h.

Figure 12 demonstrates that the adsorption of Atrac on the hematite surface increased with increasing concentration in solution. A poor fit of the experimental data was observed for the Langmuir model of adsorption with a coefficient of determination (R^2) of 0.66. When plotted on a logarithmic scale, the experimental data resulted in a straight line with $R^2 = 0.99$, suggesting that the Freundlich adsorption model fitted the experimental data quite well.

Desorption of Atrac from hematite with time was studied in situ by flushing the cell with distilled water at two different pH values; see Figure 13. Prior to desorption, adsorption of Atrac

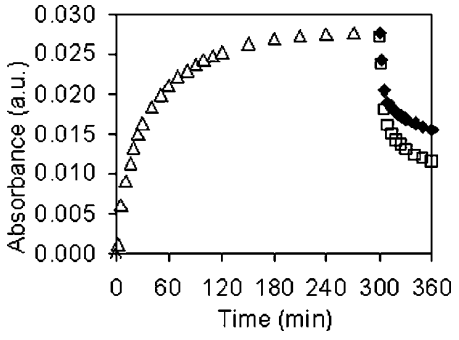

Figure 13. Intensity of the band originating from the symmetric stretching vibration (ν_s) of the C−H bond in Atrac as a function of time during the in situ adsorption of Atrac onto hematite from a 25 mg L^{-1} solution at pH 8.5 (Δ) and desorption by flushing with water at pH 8.5 (♦) and pH 10 (□).

on hematite was performed in situ from a 25 mg L^{-1} solution at room temperature and pH 8.5 until adsorption equilibrium was reached. After the first desorption experiment at pH 8.5, Atrac was adsorbed again on the same hematite film from the same solution until adsorption equilibrium was reached. After that, desorption at pH 10 was performed. As the two adsorption curves leveled out at approximately the same absorbance values, the second adsorption curve is not shown.

As illustrated by Figure 13, the absorbance was reduced rather rapidly, even when the sample was flushed with distilled water at pH 8.5 (i.e., the same pH as used during the adsorption), indicating that Atrac desorbed rather rapidly. However, the data indicate that, after 1 h of flushing, more than 50% of the Atrac still remained on the surface, suggesting that some amount of Atrac was strongly attached to the hematite surface. When the sample was flushed with distilled water at pH 10, the data indicate that Atrac desorbed more rapidly, probably because of the electrostatic repulsion between the carboxylic groups and the, at that pH, highly negatively charged hematite surface. Nevertheless, after 1 h of flushing, the data indicate that still about 40% of the originally adsorbed Atrac remained on the hematite surface. These results suggest that mild washing of the iron ore during magnetic separation and filtration in LKAB's process is not sufficient to completely remove the adsorbed flotation collector from the iron ore, especially if the pH of the water at these steps is below the flotation pH. At LKAB, the yearly average pH of water in the clarifying pond, which provides 80% of the process water, is reported to have varied in the range from 7.8 to 8.1 during the period of time from 1992 to 2004.[67] However, the seasonal variation of pH is much higher and covers the pH range from 7.2 to 9.2, with lower values during the period of snowmelt. A decrease of pH during washing as compared to that during flotation (8.5) could lead to further adsorption of the flotation reagent on the surface of iron ore. A separate washing unit operating at a pH higher than the flotation pH before the pelletization plant could be helpful in reducing the amount of Atrac adsorbed on the magnetite surface and possibly improving green-pellet strength.

Adsorption Mechanisms of Atrac and Model Compounds. As shown above, the mode of adsorption of carboxylic acids and their derivatives is determined by the tail group of the molecule and its polarity. Maleic acid did not adsorb on hematite at the pH of the experiments likely because of the electrostatic repulsion between the carboxylate anion and the negatively charged surface. Ethyl oleate showed a very weak interaction

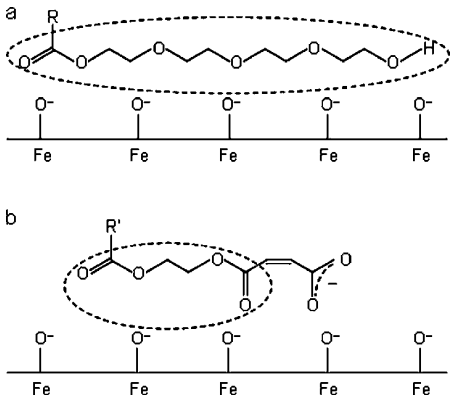

Figure 14. Proposed adsorption geometries of (a) PEGMO and (b) Atrac on hematite from aqueous solutions at pH 8.5. R represents alkyl radical in oleic acid [$CH_3(CH_2)_7CH{=}CH(CH_2)_7$], and R′ represents alkyl radical in fatty acids (including oleic acid). Dashed ovals indicate the groups involved in adsorption. These groups are polar without negative ionic entities and should interact with the polar and negatively charged Fe−O surface.

with hematite because of the nonpolar ester group. Both PEGMO and Atrac were found to adsorb on hematite at the experimental conditions. Based on the interpretation of the spectroscopic data, PEGMO and Atrac are proposed to adsorb as illustrated in Figure 14.

PEGMO showed rather strong absorption intensities in the IR spectra when adsorbed on hematite, with significant shifts of the bands originating from the ethoxy and hydroxyl groups, which indicate that the adsorption of PEGMO probably occurs through the long ethoxy chain and the tail hydroxyl group (Figure 14a), where the latter is not likely to be deprotonated at the pH used in this work.

Being a combination of ethoxylated fatty acids and maleic acid, Atrac contains ester carbonyls, ethoxy groups, and a free carboxylic group. The free carboxylic group is deprotonated in solution at pH 8.5 and is not likely to adsorb on the negatively charged hematite surface, whereas the ester carbonyls exhibited rather strong interactions with the hematite surface, as indicated by considerable shifts of the band originating from ester carbonyls in the IR spectra. Thus, the suggested mode of adsorption of Atrac on hematite is probably through ester carbonyls and the short ethoxy chain, as illustrated in Figure 14b.

Conclusions

Continuous and evenly distributed hematite films of controllable thickness were deposited on ATR crystals by dip-coating. It was shown that the adsorptions of both a flotation agent and the selected model compounds on such films could be monitored in situ by FTIR spectroscopy.

Maleic acid does not adsorb on hematite at pH 8.5 because of the repulsion between the negatively charged hematite surface and two carboxylate anions present in maleic acid at this pH, suggesting that electrostatic interactions affect the adsorption of maleic acid on hematite. No breakage of the ester bond was observed in either the model compounds or Atrac at the experimental conditions used in this work. Ethyl oleate showed very low adsorption on hematite, suggesting that the ester carbonyl does not form strong complexes with the hematite surface. For PEGMO, the adsorption on hematite likely took place through the tail hydroxyl group accompanied by the interaction of the poly(ethylene glycol) chain with the surface. Based on the adsorption behavior of maleic acid, it was concluded that Atrac could not adsorb on hematite through deprotonated carboxylic group at the chosen experimental conditions. The most probable mode of adsorption of Atrac on the hematite surface is through the ester carbonyls and the ethoxy group. Adsorption isotherms for both Atrac and PEGMO were in good agreement with the Freundlich model of adsorption describing adsorption on energetically heterogeneous surfaces.

Based on the desorption experiments, it was concluded that the strength of adsorption of Atrac on the surface of hematite varied for different species. Some of them, probably those attached directly to the surface, were strongly adsorbed and remained on the surface even when the sample was flushed with water at increased pH compared to the pH of adsorption. Other Atrac species showed rather weak interaction and could be removed from the surface by flushing with water at pH 8.5 (i.e., the same pH as during the adsorption). For PEGMO, the intensity of the band originating from the symmetric stretching vibration (ν_s) of the C−H bond in PEGMO was reduced by only 5% upon flushing of the cell with water at pH 8.5 for 1 h, suggesting a stronger interaction with hematite as compared with Atrac, probably because of the longer ethoxy chain and the presence of the tail hydroxyl group, which is not likely to be deprotonated at pH 8.5 and is thus not causing electrostatic repulsion of the molecule from the surface.

Further, the results of the desorption experiments suggested that a separate washing unit after the flotation step could be beneficial in reducing the contamination of iron ore by the flotation collector and possibly improving green-pellet strength.

The method developed here will be used in future works in which the effects of ionic strength, calcium ions, and silicates on the adsorption of Atrac and selected model compounds will be studied in detail.

Acknowledgment

The Hjalmar Lundbohm Research Center (HLRC) is gratefully acknowledged for financial support of this work.

Literature Cited

(1) Rao, K. H.; Forssberg, K. S. E. In Froth Flotation: a Century of Innovation; Fuerstenau, M. C., Jameson, G., Yoon, R.-H., Eds.; Society for Mining, Metallurgy, and Exploration, Inc.: Littleton, CO, 2007; p 498.

(2) Fuerstenau, M. C.; Gutierrez, G.; Elgilliani, D. A. The influence of sodium silicate in non-metallic flotation systems. *Trans. AIME* **1968**, *241*, 319.

(3) Gong, W.-Q. Selective flotation of Mt Weld phosphate: Methods and principles. Ph.D. Thesis, University of Western Australia, Perth, Australia, 1989.

(4) Gustafsson J.-O.; Adolfsson G. Adsorption of carboxylate collectors on magnetite and their influence on the pelletizing process. In *Proceedings of the XX International Mineral Processing Congress: 21-26 September 1997, Aachen, Germany*; Hoberg, H., von Blottnitz, H., Eds.; Gesellschaft für Bergbau, Metallurgie, Rohstoff-, und Umwelttechnik (GMDB): Clausthal-Zellerfeld, Germany, 1997, Vol. 3, p 377.

(5) Su, F. Dephosphorization of magnetite fines. Ph.D. Thesis, Luleå University of Technology, Luleå, Sweden, 1998.

(6) Forsmo, S. P. E.; Forsmo, S.-E.; Björkman, B. M. T.; Samskog, P.-O. Studies on the influence of a flotation collector reagent on iron ore green pellet properties. *Powder Technol.* **2008**, *182*, 444.

(7) Forsmo, S. P. E.; Samskog, P.-O.; Björkman, B. M. T. A study on plasticity and compression strength in wet iron ore green pellets related to real process variations in raw material fineness. *Powder Technol.* **2008**, *181*, 321.

(8) Rao, K. H.; Samskog, P.-O.; Forssberg, K. S. E. Pulp chemistry of flotation of phosphate gangue from magnetite fines. *Trans. Inst. Min. Metall. C* **1990**, *99*, 147.

(9) Gregory, G. R. E. C. The determination of residual anionic surface-active reagents in mineral flotation liquors. *Analyst* **1966**, *91*, 251.

(10) Giesekke, E. W. A review of spectroscopic techniques applied to the study of interactions between minerals and reagents in flotation systems. *Int. J. Miner. Process.* **1983**, *11*, 19.

(11) Mielczarski, J. A.; Cases, J. M.; Bouquet, E.; Barres, O.; Delon, J. F. Nature and structure of adsorption layer on apatite contacted with oleate solution. 1. Adsorption and fourier transform infrared reflection studies. *Langmuir* **1993**, *9*, 2370.

(12) Gong, W. Q.; Parentich, A.; Little, L. H.; Warren, L. J. Diffuse reflectance infrared Fourier transform spectroscopic study of the adsorption mechanism of oleate on hematite. *Colloids Surf.* **1991**, *60*, 325.

(13) Kirwan, L. J.; Fawell, P. D.; van Bronswijk, W. In situ FTIR-ATR examination of poly(acrylic acid) adsorbed onto hematite at low pH. *Langmuir* **2003**, *19*, 5208.

(14) Fredriksson, A.; Holmgren, A.; Forsling, W. Kinetics of collector adsorption on mineral surfaces. *Miner. Eng.* **2006**, *19*, 784.

(15) Norén, K. Coordination chemistry of monocarboxylate and aminocarboxylate complexes at the water/goethite interface. Ph.D. Thesis, Umeå University, Umeå, Sweden, 2007.

(16) Depalma, S.; Cowen, S.; Hoang, T.; Al-Abadleh, H. A. Adsorption thermodynamics of p-arsanilic acid on iron (oxyhydr)oxides: In-situ ATR-FTIR studies. *Environ. Sci. Technol.* **2008**, *42*, 1922.

(17) Grahn, M.; Lobanova, A.; Holmgren, A.; Hedlund, J. Orientational Analysis of Adsorbates in Molecular Sieves by FTIR/ATR Spectroscopy. *Chem. Mater.* **2008**, *20* (19), 6270.

(18) Fredriksson, A.; Larsson, M. L.; Holmgren, A. *n*-Heptyl xanthate adsorption on a ZnS layer synthesized on germanium: An in situ attenuated total reflection IR study. *J. Colloid Interface Sci.* **2005**, *286*, 1.

(19) Sukhishvili, S. A.; Granick, S. Kinetic regimes of polyelectrolyte exchange between the adsorbed state and free solution. *J. Chem. Phys.* **1998**, *1* (09), 6861.

(20) Vlasak, R.; Klueppel, I.; Grundmeier, G. Combined EIS and FTIR-ATR study of water uptake and diffusion in polymer films on semiconducting electrodes. *Electrochim. Acta* **2007**, *52*, 8075.

(21) Hallinan, D. T., Jr.; Elabd, Y. A. Diffusion and sorption of methanol and water in nafion using time-resolved fourier transform infrared-attenuated total reflectance spectroscopy. *J. Phys. Chem. B* **2007**, *111*, 13221.

(22) Sammon, C.; Yarwood, J.; Everall, N. A FTIR-ATR study of liquid diffusion processes in PET films: Comparison of water with simple alcohols. *Polymer* **2000**, *41*, 2521.

(23) Hanh, B. D.; Neubert, R. H. H.; Wartewig, S.; Christ, A.; Hentzsch, C. Drug penetration as studied by noninvasive methods: Fourier transform infrared-attenuated total reflection, Fourier transform infrared, and ultraviolet photoacoustic spectroscopy. *J. Pharm. Sci.* **2000**, *89*, 1106.

(24) Fieldson, G. T.; Barbari, T. A. Analysis of diffusion in polymers using evanescent field spectroscopy. *AIChE J.* **1995**, *41*, 795.

(25) Pintar, A.; Malacea, R.; Pinel, C.; Besson, M. Catalytic three-phase diastereoselective hydrogenation of *o*-toluic and 2-methyl nicotinic acid derivatives: In situ FTIR/ATR investigation. *Vib. Spectrosc.* **2007**, *45*, 18.

(26) Hamminga, G. M.; Mul, G.; Moulijn, J. A. Reaction kinetics and intermediate determination of solid acid catalysed liquid-phase hydrolysis reactions: A real-time in situ ATR FT-IR study. *Catal. Lett.* **2006**, *109*, 199.

(27) Grahn, M.; Wang, Z.; Larsson, M. L.; Holmgren, A.; Hedlund, J.; Sterte, J. Silicalite-1 coated ATR elements as sensitive chemical sensor probes. *Microporous Mesoporous Mater.* **2005**, *81*, 357.

(28) Aamouche, A.; Goormaghtigh, E. FTIR-ATR biosensor based on self-assembled phospholipids surface: Haemophilia factor VIII diagnosis. *Spectroscopy* **2008**, *22*, 223.

(29) Lu, Y.; Miller, J. D. Carboxyl stretching vibrations of spontaneously adsorbed and LB-transferred calcium carboxylates as determined by FTIR internal reflection spectroscopy. *J. Colloid Interface Sci.* **2002**, *256*, 41.

(30) Free, M. L.; Miller, J. D. The significance of collector colloid adsorption phenomena in the fluorite/oleate flotation system as revealed by FTIR/IRS and solution chemistry analysis. *Int. J. Miner. Process.* **1996**, *48*, 197.

(31) Sperline, R. P.; Muralidharan, S.; Freiser, H. In situ determination of species adsorbed at a solid−liquid interface by quantitative infared attenuated total reflectance spectrophotometry. *Langmuir* **1987**, *3*, 198.

(32) Jang, W. H.; Miller, J. D. Verification of the internal reflection spectroscopy adsorption density equation by fourier transform infrared spectroscopy analysis of transferred Langmuir−Blodgett films. *Langmuir* **1993**, *9*, 3159.

(33) Kellar, J. J.; Cross, W. M.; Miller, J. D. Adsorption density calculations from in situ FT-IR/IRS data at dilute surfactant concentrations. *Appl. Spectrosc.* **1989**, *43*, 1456.

(34) Grahn, M.; Holmgren, A.; Hedlund, J. Adsorption of *n*-hexane and *p*-xylene in thin silicalite-1 films studied by FTIR/ATR spectroscopy. *J. Phys. Chem. C* **2008**, *112*, 7717.

(35) Grahn, M.; Lobanova, A.; Holmgren, A.; Hedlund, J. A novel experimental technique for estimation of molecular orientation in zeolite. *Stud. Surf. Sci. Catal.* **2007**, *170*, 724.

(36) Wang, Z.; Grahn, M.; Larsson, M. L.; Holmgren, A.; Sterte, J.; Hedlund, J. Zeolite coated ATR crystal probes. *Sens. Actuators B: Chem.* **2006**, *115*, 685.

(37) Wang, Z.; Larsson, M. L.; Grahn, M.; Holmgren, A.; Hedlund, J. Zeolite coated ATR crystals for new applications in FTIR-ATR spectroscopy. *Chem. Commun.* **2004**, *24*, 2888.

(38) Fredriksson, A.; Holmgren, A. An in situ ATR-FTIR investigation of adsorption and orientation of heptyl xanthate at the lead sulphide/aqueous solution interface. *Miner. Eng.* **2008**, *21*, 1000.

(39) Fredriksson, A.; Holmgren, A. An in situ ATR-FTIR study of the adsorption kinetics of xanthate on germanium. *Colloids Surf. A: Physicochem. Eng. Aspects* **2007**, *302*, 96.

(40) Fredriksson, A.; Hellström, P.; öberg, S.; Holmgren, A. Comparison between in situ total internal reflection vibrational spectroscopy of an adsorbed collector and spectra calculated by ab initio density functional theory methods. *J. Phys. Chem. C* **2007**, *111*, 9299.

(41) Larsson, M. L.; Fredriksson, A.; Holmgren, A. Direct observation of a self-assembled monolayer of heptyl xanthate at the germanium/water interface: A polarized FTIR study. *J. Colloid Interface Sci.* **2004**, *273*, 345.

(42) Forsmo, S. P. E. Oxidation of magnetite concentrate powders during storage and drying. *Int. J. Miner. Process.* **2005**, *75*, 135.

(43) Haneda, K.; Morrish, A. H. Magnetite to maghemite transformation in ultrafine particles. *J. Phys. (Paris)* **1977**, *38* (C1), 321.

(44) Gedikoglu, A. Mössbauer study of low-temperature oxidation in natural magnetite. *Scr. Metall.* **1983**, *17*, 45.

(45) Wesolowski, D. J.; Machesky, M. L.; Palmer, D. A.; Anovitz, L. M. Magnetite surface charge studies to 290°C from in situ pH titrations. *Chem. Geol.* **2000**, *167*, 193.

(46) Matijević, E. Production of monodispersed colloidal particles. *Annu. Rev. Mater. Sci.* **1985**, *15*, 483.

(47) Swiatowski, P.; Andersen, A.; Askenbom, A. Process for the froth flotation of oxide and salt type minerals and composition. U.S. Patent 5,130,037, 1992.

(48) Fuerstenau, M. C.; Elgillani, D. A.; Miller, J. D. Adsorption mechanisms in nonmetallic activation systems. *Trans. AIME* **1970**, *247*, 11.

(49) Cromieres, L.; Moulin, V.; Fourest, B.; Giffaut, E. Physico-chemical characterization of the colloidal hematite/water interface: Experimentation and modeling. *Colloids Surf. A* **2002**, *202*, 101.

(50) Su, C.; Suarez, D. L. In situ infrared speciation of adsorbed carbonate on aluminum and iron oxides. *Clays Clay Miner.* **1997**, *45*, 814.

(51) Zeltner, W. A.; Anderson, M. A. Surface charge development at the goethite/aqueous solution interface: Effects of CO_2 adsorption. *Łangmuir* **1988**, *4*, 469.

(52) Bargar, J. R.; Kubicki, J. D.; Reitmeyer, R.; Davis, J. A. ATR-FTIR spectroscopic characterization of coexisting carbonate surface complexes on hematite. *Geochim. Cosmochim. Acta* **2005**, *69* (6), 1527.

(53) Schmitt, T. M. *Analysis of Surfactants*, 2nd ed.; Marcel Dekker, Inc.: New York, 2001.

(54) Fox, J. J.; Martin, A. E. Investigations of infra-red spectra. Absorption of the CH_2 group in the region of 3μ. *Proc. R. Soc. Ser. A* **1938**, *167*, 257.

(55) McMurry, H. L.; Thornton, V. Correlation of infrared spectra: Paraffins, olefins, and aromatics with structural groups. *Anal. Chem.* **1952**, *24*, 318.

(56) Hartwell, E. J.; Richards, R. E.; Thompson, H. W. The vibration frequency of the carbonyl linkage. *J. Chem. Soc. London* **1948**, 1436.

(57) Cameron, D. G.; Umemura, J.; Wong, P. T. T.; Mantsch, H. H. A Fourier transform infrared study of the coagel to micelle transitions of sodium laurate and sodium oleate. *Colloids Surf.* **1982**, *4*, 131.

(58) Beentjes, P. C. J.; Van Den Brand, J.; De Wit, J. H. W. Interaction of ester and acid groups containing organic compounds with iron oxide surfaces. *J. Adhesion Sci. Technol.* **2006**, *20*, 1.

(59) Zeiss, H.; Tsutsui, M. The carbon-oxygen absorption band in the infrared spectra of alcohols. *J. Am. Chem. Soc.* **1953**, *75*, 897.

(60) Do, D. D. *Adsorption Analysis: Equilibria and Kinetics*; Imperial College Press: London, 1998.

(61) Hwang, Y. S.; Lenhart, J. J. Adsorption of C4-dicarboxylic acids at the hematite/water interface. *Langmuir* **2008**, *24*, 13934.

(62) Kulkarni, R. D.; Somasundaran, P. Flotation chemistry of hematite/oleate system. *Colloids Surf.* **1980**, *1*, 387.

(63) Fowler, R. G.; Smith, R. M. Similarities in the infrared spectra of homologous compounds. *J. Opt. Soc. Am.* **1953**, *43*, 1054.

(64) Driessen, W. L.; Groeneveld, W. L.; Van der Wey, F. W. Complexes with ligands containing the carbonyl group. Part II. Metal(II) methyl formate, ethyl acetate and diethyl malonate solvates. *Recl. Trav. Chim. Pays-Bas* **1970**, *89*, 353.

(65) Colthup, N. B.; Daly, L. H.; Wiberley, S. E. *Introduction to Infrared and Raman Spectroscopy*, 3rd ed.; Academic Press: London, 1990.

(66) Dobson, K. D.; McQuillan, A. J. In situ infrared spectroscopic analysis of the adsorption of aliphatic carboxylic acids to TiO_2, ZrO_2, Al_2O_3, and Ta_2O_5 from aqueous solutions. *Spectrochim. Acta A* **1999**, *55*, 1395.

(67) Westerstrand, M. Process water geochemistry at the Kiirunavaara iron mine, northern Sweden. Ph.D. Thesis, Luleå University of Technology, Luleå, Sweden, 2009.

Received for review August 27, 2009
Revised manuscript received December 3, 2009
Accepted December 19, 2009

IE901343F

Paper II

Adsorption of As(V) on iron oxide nanoparticle films studied by in situ ATR-FTIR spectroscopy

I. Carabante, J. Kumpiene, M. Grahn, A. Holmgren, J. Hedlund

Colloids and Surfaces A. Physicochemical and Engineering Aspects, 346, 1-3 (2009) 106-113

Colloids and Surfaces A: Physicochem. Eng. Aspects 346 (2009) 106–113

Contents lists available at ScienceDirect

Colloids and Surfaces A: Physicochemical and Engineering Aspects

journal homepage: www.elsevier.com/locate/colsurfa

Adsorption of As (V) on iron oxide nanoparticle films studied by in situ ATR-FTIR spectroscopy

Ivan Carabante[a,*], Mattias Grahn[a], Allan Holmgren[a], Jurate Kumpiene[b], Jonas Hedlund[a]

[a] Division of Chemical Engineering, Luleå University of Technology, SE-97187, Luleå, Sweden
[b] Division of Waste Science and Technology, Luleå University of Technology, SE-97187, Luleå, Sweden

ARTICLE INFO

Article history:
Received 11 March 2009
Received in revised form 20 May 2009
Accepted 29 May 2009
Available online 11 June 2009

Keywords:
Ferrihydrite
Iron oxide film
In situ
ATR-FTIR
Arsenic (V)
Adsorption

ABSTRACT

Stabilization of arsenic contaminated soils by iron oxides has been proposed as a remediation technique to prevent leaching of arsenate into the environment. Fundamental studies are needed to establish under which conditions the complexes formed are stable. In the present work, a powerful technique, viz. ATR-FTIR spectroscopy, is adapted to the studies of adsorption of arsenate species on iron oxides. This technique facilitates acquisition of both quantitative and qualitative in situ adsorption data.

In the present work, about 800 nm thick films of 6-lineferrihydrite were deposited on ZnSe ATR crystals. Arsenate adsorption on the ferrihydrite film was studied at pD values ranging from 4 to 12 and at an arsenate concentration of 0.03 mM in D_2O solution. The amount of adsorbed arsenate decreased with increasing pD as a result of the more negatively charged iron oxide surface at higher pD values. The adsorption and desorption kinetics were also studied. Arsenate showed a higher adsorption rate within the first 70 min and a much lower adsorption rate from 70 to 300 min. The low adsorption rate at longer reaction times was partly due to a low desorption rate of already adsorbed carbonate species adsorbed at the surface. The desorption of carbonate species was evidenced by the appearance of negative absorption bands. The desorption of adsorbed arsenate complexes was examined by flushing with D_2O at pD 4 and 8.5 and it was found that the complexes were very stable at pD 4 suggesting formation of mostly inner-sphere complexes whereas a fraction of the complexes at pD 8.5 were less stable than at pD 4, possibly due to the formation of outer-sphere complexes.

In summary, the ATR technique was shown to provide in situ information about the adsorption rate, desorption rate and the speciation of the complexes formed within a single experiment, which is very difficult to obtain using other techniques.

1. Introduction

1.1. Background

Arsenic is an element known to cause several severe complications to the health. Long term exposure to low concentration may lead to cancer and skin diseases, whereas exposure to higher concentrations is lethal [1]. Still, arsenic is the 20th most abundant element in natural systems, the 14th most abundant element in seawater and the 12th in the human body. [1] Arsenic can be found in two different oxidation states, As(V) which dominates under oxidizing conditions, and As(III), which is the predominant species in reducing environments. The latter is considered more toxic and also presents a higher mobility than As(V) in natural systems.[1,2]

Bangladesh and the West Bengal in India are the two areas in the world that shows the most severe arsenic ground water contamination. [1] However, there are contaminated areas all over the world: China, Chile, Argentina, Poland and Sweden are a few examples. The arsenic contamination occurs naturally in the environment, but it can also be a result of human activities like mining, coal combustion, and the use of arsenic based pesticides. [2] CCA wood preservative was used for timber treatment since the 1930s and is a mixture of copper, chromium, and arsenic oxides or salts. The wood was preserved from decomposition by fungi, insects, and marine borers. The preservative also improved weather-resistance and paint adherence. As a consequence of deficient industrial practice, most of the wood impregnation sites have become contaminated with high concentrations of arsenic, chromium and copper.

Remediation of contaminated sites by removing the soil is expensive and environmentally disruptive. The risk of a contaminated site for the environment and human health, however, can be minimized by reducing the mobility and bioavailability of trace elements in soil. This can be achieved by amending soils with contaminant-immobilizing additives, i.e. stabilize the soil chemically. [3] Arsenic has been shown to be strongly adsorbed onto iron oxides. [4,5] Thus, stabilization of arsenic contaminated soil

* Corresponding author. Tel.: +46 0911 72791; fax: +46 920 491199.
E-mail address: ivan.carabante@ltu.se (I. Carabante).

0927-7757/$ – see front matter © 2009 Elsevier B.V. All rights reserved.
doi:10.1016/j.colsurfa.2009.05.032

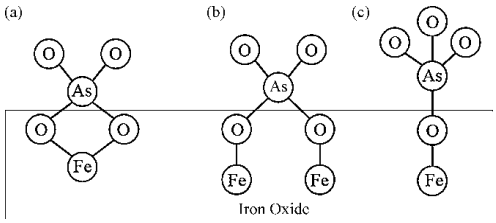

Fig. 1. Schematic representation of different complexes that may form on the iron oxide surface. (a) bidentate mononuclear; (b) bidentate binuclear; (c) monodentate.

by adsorption of iron oxide has been studied as a promising remediation technique. [3,6–8] Nevertheless, the technique is still under development and several factors e.g. pH, redox potential and presence of other ions may affect the adsorption and the stability of adsorbed arsenic species and further evaluation of these parameters are needed in order to develop a more reliable stabilization method.

The structure of arsenic (V) complexes adsorbed on iron oxide have been studied using the Extended X-ray Absorption Fine Structure (EXAFS) technique. [4,9–11] In all these studies, it is concluded that the bidentate binuclear inner-sphere complexes, see Fig. 1(b)), are the most thermodynamically favored and thus the most abundant species found on the iron oxide surface. However, there are some contradictions in the conclusions regarding the formation of bidentate mononuclear and monodentate complexes, see Fig. 1(a) and (c) respectively, demonstrating that the adsorption of arsenate on iron oxides is not fully understood.

The formation of the bidentate binuclear complex has also been studied by Fourier Transform Infrared Spectroscopy (FTIR) on dry samples [12,13] and it was demonstrated that the arsenic complexes were formed via the hydroxyl groups at the iron oxide surface.

The kinetics of arsenate adsorption on goethite was studied using the Pressure-Jump Relaxation technique. [14] Two distinct adsorption regimes could be distinguished, first an adsorption regime with high adsorption rate followed by a second regime with low adsorption rate. The proposed mechanism consists of two steps, formation of an inner-sphere monodentate surface complex with a high rate of adsorption followed by a slow ligand exchange leading to the formation of inner-sphere bidentate complexes. The kinetics of adsorption of arsenate on goethite was also studied through batch experiments. [15] In this study, again two kinetic regimes were observed. The authors concluded that the first high adsorption rate corresponds to the adsorption of arsenate on the more accessible sites on external surface of the iron oxide, whereas the low second adsorption rate is related to the slow diffusion of arsenate into the pores of the iron oxide particles and the subsequent adsorption on the internal surface.

The adsorption of carbonate species on metal oxide films like hematite [16] or zirconium dioxide [17] has been studied using in situ ATR-FTIR spectroscopy providing detailed information on the infrared absorbtion bands for the C—O bond in these species and describing their adsorption behavior. The effects of carbonate species in the adsorption of arsenic on iron oxides have also been studied, ex situ, using ICP-AES and ICP-MS as a quantitative method in batch adsorption experiments. [18,19] It was found that the final amount of arsenic adsorbed was not affected by the presence of carbonate species. Nevertheless the presence of carbonates reduced the adsorption rate during the early stage of the adsorption at pH 8, whereas it enhanced the rate at pHs 4 and 6. [18]

Currently, only very few publications are available on the use of the ATR-FTIR technique for studying As(V) oxyanion sorption on iron oxides. [2,20,21] In these studies, the technique was used in order to: decrease the Limit of Detection of arsenate in water, study the H_2O_2 catalyzed reduction of arsenic (V) adsorbed on ferrihydrite and the adsorption of As(V) on a natural soil sample.

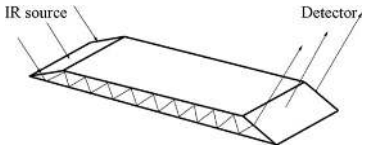

Fig. 2. Schematic representation of the IR beam propagating in the ATR element.

In the present work, the focus was on arsenate adsorption on synthetic iron oxide and to further develop the ATR method. The use of D_2O instead of H_2O increased considerably the signal to noise ratio in the region of the spectra where the As—O stretching bands appear and thus the detectability of the As(V) species adsorbed on iron oxide.

1.2. The ATR-FTIR technique

ATR-FTIR (Attenuated Total Reflection—Fourier Transform Infrared) spectroscopy [22] has proved to be a powerful tool for adsorption studies [23] including adsorption on metal oxides,[20,24–27] transition metals,[28–30] metal sulphides [31–33] and zeolites.[34,35] The technique may give both quantitative and qualitative information on the adsorption i.e. it can give information from which kinetics and thermodynamics of adsorption can be inferred and in addition it may be used for identification of the complexes formed. In the ATR technique, the incident IR beam is totally reflected inside an ATR crystal, see Fig. 2. At each reflection the electric field of the IR radiation probes the vicinity of the crystal surface where the sample is placed. The depth of penetration (d_p) which is a rough measure on the distance sampled by the electric field, depends on the refractive indices of both the ATR crystal and the sample as well as of the wavelength of the incident beam. Thus, the depth of penetration is increasing with decreasing wavenumber. In the present work, the depth of penetration in the frequency range 1000–800 cm^{-1} is ~1 μm. Since the technique only probes the vicinity of the crystal, it is a powerful tool for studying the properties of thin films and their surface chemistry.

As mentioned above, the focus here is on the development of the in situ ATR-FTIR method and its ability to reveal information about the stability in the adsorption of As(V) oxyanions on synthetic iron oxide films.

2. Experimental

2.1. Iron oxide synthesis and film preparation

An iron oxide suspension was synthesized following the method described by McQuillan. [26] 1 ml. of a 0.7 M iron (III) chloride ($FeCl_3 \cdot 6H_2O$; Riedel-de Haën, p.a. 99%) solution in distilled water was added drop-wise to 50 ml of boiling distilled water. The obtained solution was kept under vigorous stirring and boiling for 5 min. Subsequently, the dark brown-red suspension formed was retained and dialysed for approximately 24 h using a dialysis membrane (MWCO 12-14000; Spectra/Por Dialysis membrane; Spectrum laboratories). The suspension was dialyzed against distilled water. Throughout the dialysis, the distilled water on the opposite side of the dialysis membrane was changed several times in order to eliminate all the ions (ferric and chloride) originating from the initial iron chloride solution. As a result of the dialysis, the pH of the suspension changed from approximately 1.5 to 5.

The dialyzed iron oxide suspension was subsequently diluted by mixing the sample suspension with equal weights of methanol (CH_3OH; Kebo lab, >99.8%) in order to obtain better wetting properties in the following step. A volume of 600 μl of the suspension was spread, with the help of a pipette's tip, on the ATR crystal so that it covered about 5 cm^2 of the crystal. The volume of the suspension was dried in room air thus forming an even film. After drying, an identical film was prepared on the other side of the ATR crystal.

2.2. Characterization by scanning electron microscopy, X-ray diffraction, nitrogen adsorption and zeta potential measurements

The topography and thickness of the film was investigated using a scanning electron microscope (SEM, Phillips XL 30) equipped with a LaB_6 filament as the electron source.

The zeta potential of dilute iron oxide suspensions in 0.01 M KNO_3 at pH values from 4 to 11.5, was measured by electrophoresis (ZetaCompact) using the Smoluchowski equation.

A powder was obtained by freeze drying the iron oxide suspension after dialysis. The powder was characterized with X-ray Diffraction (XRD, Siemens D5000) using Bragg–Brentano geometry at a step size of 0.02 degrees. Nitrogen adsorption at liquid nitrogen temperature was measured using a Micrometrics ASAP 2010 instrument. The sample was degassed at a temperature of 140 °C for about 24 h prior to the measurements. The sample was degassed at this temperature in order to avoid phase transformation of the ferrihydrite to hematite. It has been reported that ferrihydrite powder was stable up to 170° after outgassing for 6 h whereas it transformed to hematite after 1 h exposed to an air atmosphere. [36]

2.3. ATR-FTIR measurements

A Bruker IFS 66 v/s equipped with a DTGS (Deuterated TriGlycine Sulphate) detector was used for the ATR-FTIR measurements. All spectra were recorded at a resolution of 4 cm^{-1} by co-adding 200 scans. A stainless steel flow cell with two compartments for liquid of about 2.5 cm^3 on each side of the ATR crystal, was used in the experiments. A trapezoidal ZnSe ATR crystal (Crystan) with a size of 52 mm × 20 mm × 2 mm and 45° cut edges was used and the cell/crystal interfaces were sealed by Viton gaskets. The arsenate solutions were prepared from sodium hydrogen–arsenate heptahydrate ($Na_2AsO_4{\cdot}7H_2O$; Fluka; p.a. 98,5%) in deuterium oxide (D_2O, Aldrich, 99 atom % D). The solutions were fed to both compartments of the flow cell, which were connected in series.

The solution was pumped through the flow cell and recirculated to a vessel using a peristaltic pump (Fig. 3b).

The pD in the vessel was controlled by adding solutions of either deuterium chloride (DCl; Aldrich; 99 atom % D) or sodium deuteroxide (NaOD; Aldrich; 99+ atom % D) in D_2O and argon gas (AGA, 99%) was bubbled through the liquid in the vessel to minimize the dissolution of atmospheric CO_2 into the solution. A single beam background spectrum of D_2O with the same pD value as used during the subsequent experiment was recorded before each experiment unless stated otherwise.

The total volume of the liquid in the system was about 50 ml and this solution thus contained about 1.5×10^{-6} mol As (V) species. The concentration of the iron oxide suspension was 10.75 g/l and as 1.2 μl of the iron oxide suspension was used to prepare the film, the weight of the iron oxide film was 1.3×10^{-5} g. The adsorption capacity of As (V) on ferrihydrite is about 650 mmol(As(V))/kg (ferrihydrite) [37] and the film thus had an adsorption capacity of about 8.4×10^{-9} mol As(V) species, i.e. there was about 180 times more As (V) species in solution compared to the adsorption capacity and the concentration in the solution will be constant during adsorption. The arsenate concentration was still analyzed before and after the experiment using Inductively Coupled Plasma—Optical Emission Spectroscopy (ICP-OES, PerkinElmer optima 2000 DV) in order to verify a negligible concentration change of the arsenates in solution during the adsorption process.

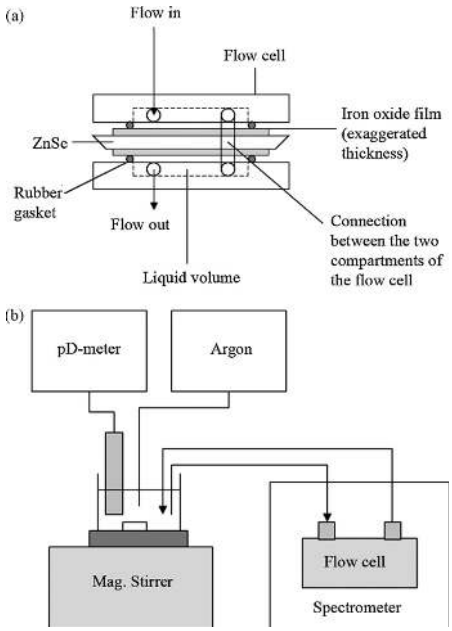

Fig. 3. Schematic figure of the ATR-FTIR flow cell (a) and of the experimental set-up (b).

3. Results and discussion

3.1. Characterization of the iron oxide powder

The XRD pattern recorded from the freeze dried iron oxide powder showed very broad reflections, which indicates small crystal size as expected for ferrihydrite, see Fig. 4. The peak positions and relative intensities agreed well with those reported for 6-lineferrihydrite. [36]

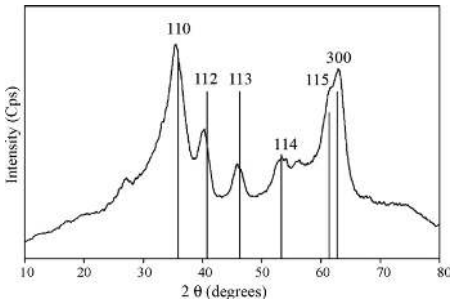

Fig. 4. X-ray diffractogram of the freeze dried iron oxide powder. The vertical bars indicate the peak position with their relative intensities and the Miller indexes of the planes from the reference pattern of 6-lineferrihydrite.[36].

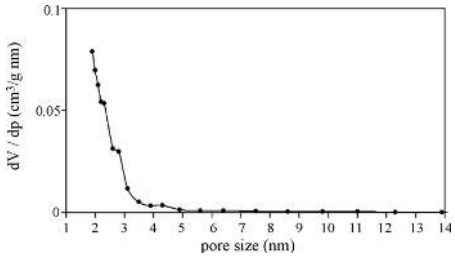

Fig. 5. BJH pore size distribution curve derived from the N_2 adsorption data on the 6-lineferrihydrite powder.

The surface area of the iron oxide powder, calculated by applying the BET equation on the nitrogen adsorption data, was 190 m^2/g and from the BJH analysis, pores ranging between 2 and 10 nm was observed, see Fig. 5. These pores likely originate from inter-particle voids in the powder sample and it is probable that the inter-particle pore size distribution was similar in the film.

Another XRD pattern of the iron oxide powder was recorded after degassing at 140 °C for 24 h in order to confirm that no phase transformation occurred during the degassing. The obtained XRD pattern was identical to the one recoded before heating showing that the heating associated with the degassing did not cause any phase transformation.

The zeta potential as a function of pH was measured from pH 4 to 12 and the point of zero proton charge was estimated to about 7.5–8. These results are in line with previous reports for 6-lineferrihydrite. [36] The point of zero D^+ charge is not known but was assumed not to be far from the point of zero proton charge and therefore the dominating surface sites at different pD values may be illustrated as follows:

$$\equiv Fe\text{–}OD_2^+ \quad (\text{dominatingatpD4}) \tag{I}$$

$$\equiv Fe\text{–}OD \quad (\text{dominatingatpD8}) \tag{II}$$

$$\equiv Fe\text{–}O^- \quad (\text{dominatingatpD} > 10) \tag{III}$$

Fig. 6a shows a top view SEM image of the film, which illustrates that the film appears to be comprised of spherical grains with a diameter smaller than 30 nm. The sample was coated with a thin (ca 10 nm) gold layer prior to recording the SEM images to avoid sample charging, however, this also results in that the particles appear larger than in reality. Fig. 6b shows a SEM image of the cross-section of the iron oxide film on a ZnSe crystal. Cross-sectional images recorded at numerous other locations were very similar and illustrated that the thickness of the film was about 700–900 nm throughout the entire sample. Further it can again be seen that the film consists of small, densely packed particles.

3.2. Absorption bands for As (V) species in solution and for adsorbed species on iron oxide

Fig. 7 shows the infrared spectra recorded with FTIR-ATR spectroscopy using an uncoated ZnSe crystal in contact with a 13 mM arsenate solution (in D_2O), at different pD's. All spectra were recorded using the same solution, only the pD was adjusted in steps from pD 4 to 12. Each time the pD was changed, the corresponding changes in the spectra were very rapid reflecting the time to pump the solution from the beaker to the cell. After the initial pD induced change, the spectra did not change during the following 60 min showing that the species formed were stable. Subsequently, the reverse experiment was performed i.e. the pD of the solution was adjusted in steps from pD 12 to pD 4, and the process was proved

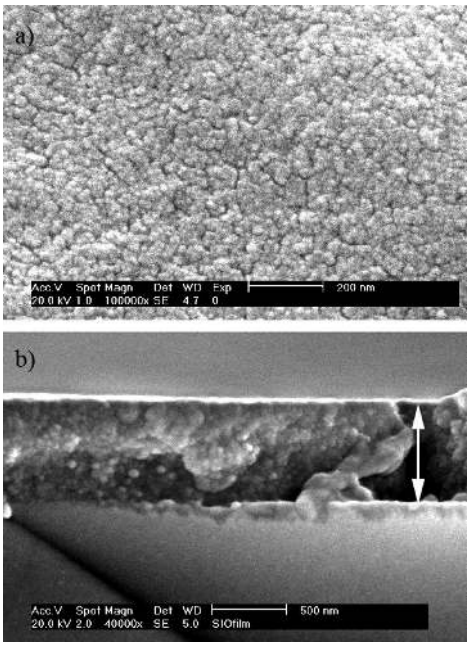

Fig. 6. (a) Top view SEM image of the iron oxide film. (b) Side image of the iron oxide film on top of a ZnSe crystal, the thickness of the iron oxide film is represented by a white arrow.

to be completely reversible (not shown). Moreover, the intensity of the bands from spectra recorded at different arsenate concentrations fits into a straight line passing through the origin (not shown). Therefore, we concluded that the signal mostly emanates from species in the solution and not from species adsorbed on the surface of the uncoated ATR crystal. The pK_a values of the arsenate species are 2.2, 6.7 and 11.2 for pK_{a1}, pK_{a2} and pK_{a3}, respectively. [1] Therefore the predominant specie at pD 4 is $H_2AsO_4^-$, whereas $HAsO_4^{2-}$ is dominating at pD 8.5 and AsO_4^{3-} together with $HAsO_4^{2-}$ at pD 11.8. Upon changing pD, the corresponding changes in spectra were immediate and did not change with time. Thus, the absorption bands illustrated in Fig. 7 originate from the different arsenate species present in solution. Consequently, the different species of arsenate in D_2O solution can be distinguished. From the spectrum at

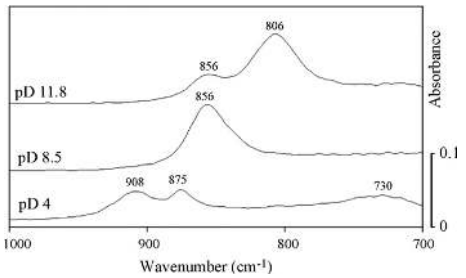

Fig. 7. Spectra of arsenate (13 mM) in D_2O solution recorded at different pD's using an uncoated ZnSe crystal.

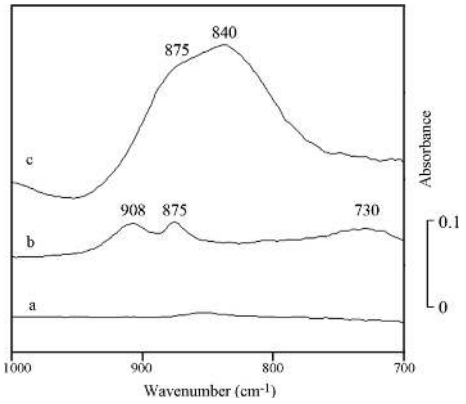

Fig. 8. Spectra recorded with an uncoated ATR crystal in (a) a 1 mM and (b) a 13 mM arsenate solution in D_2O at pD 4. Spectrum (c) was recorded using an ATR crystal coated with an iron oxide film in contact with a 0.03 mM arsenate solution in D_2O at pD 4 after 5 h of adsorption.

pD 4, the bands appearing at 908, 875 and 730 cm^{-1} originate from $H_2AsO_4^-$ in D_2O. The spectrum recorded at pD 8.5 shows only one band in the As—O stretching area. This absorbance band is located at 856 cm^{-1} and stems from the As—O stretching vibration of the $HAsO_4^{2-}$ entity. [20] The spectrum recorded at pD 11.8 shows both the $HAsO_4^{2-}$ band at 856 cm^{-1} and a band at 806 cm^{-1} originating from AsO_4^{3-}.

Fig. 8 illustrates spectra obtained with an uncoated ATR crystal and with an ATR crystal coated with an iron oxide film. The spectra shown in Fig. 8 were all recorded during different experiments. Spectrum (a) was recorded when a 1 mM arsenate solution in D_2O at pD 4 was flowing over an uncoated ZnSe crystal. D_2O at pD 4 flowing on a ZnSe crystal was used as a background spectrum. At this concentration, no significant signal from arsenate in solution was detected. However, if the concentration in solution is increased to 13 mM, absorption bands are observed, as illustrated in (b) and discussed earlier. Again, a background spectrum of D_2O at pD 4 flowing on a ZnSe crystal was used as when recording spectrum (a). Spectrum (c) was recorded after flowing a 0.03 mM arsenate solution at pD 4 for 300 min over a ZnSe crystal coated with an iron oxide film. Two intense bands at 875 and 840 cm^{-1} originating from arsenate adsorbed on the iron oxide film were observed in the spectrum. By comparing the spectra, the concentrating effect exerted by the film is evident. The concentration used to record spectrum (c) was approximately 30 times lower than the concentration used for spectrum (a). This demonstrates that the technique is promising for sensor applications for detecting low concentrations of arsenate in solution. The bands in spectrum (c) are approximately 6 times more intense than the bands observed in spectrum (b). And still, the arsenate concentration used when recording spectrum (b) was approximately 400 times higher than the arsenate concentration used when recording spectrum (c) again showing the concentrating power of the iron oxide coated element. These comparisons are of course built on the assumption that the molar absorptivity of the adsorbed arsenate species is similar to the molar absorptivity of the arsenate species in solution, which is not necessarily true. However, the data clearly illustrates that when using ATR crystals coated with iron oxide in dilute solutions (0.03 mM) of arsenate species, the entire signal detected from stems from species adsorbed on the iron oxide film and not from species in solution.

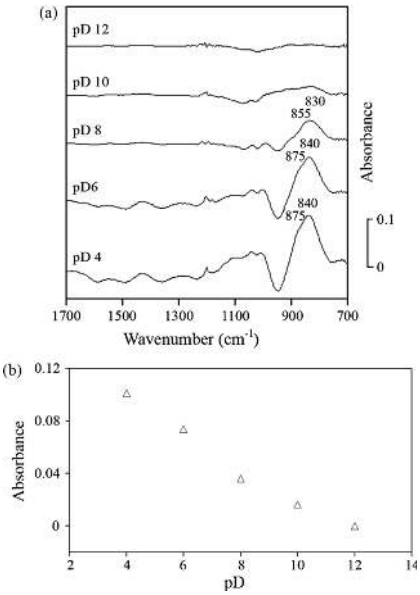

Fig. 9. (a) Spectra of arsenate adsorbed on iron oxide at different pD after 70 min of adsorption from a 0.03 mM arsenate solution in D_2O. (b) pD dependence on the intensity (band height) of the band, at about 840 cm^{-1} wavenumbers, originating from arsenate adsorbed on an iron oxide film from a 0.03 mM solution after 70 min of adsorption.

3.3. Adsorption of As (V) on iron oxide

Fig. 9a shows spectra recorded at different pD after 70 min of adsorption from a 0.03 mM arsenate solution using an iron oxide coated ZnSe crystal. Five background spectra of D_2O flowing over an iron oxide coated ATR element at the same five different pD values, were recorded previous to the adsorption experiment. The adsorption experiments were performed on the same iron oxide and after 70 min of contact with a 0.03 mM arsenate solution. During the course of the experiment the pD was adjusted from the highest pD value, 12, to the lowest, 4. In the pD range 4–10, absorption bands are observed at 875 and 840 cm^{-1} as a result of adsorption of arsenate on the iron oxide. These bands are shifted to slightly lower wavenumbers compared to the bands observed for arsenate in solution. These shifts are caused by a change in the As—O vibrational mode of the As(V) species adsorbed on the iron oxide surface. For the whole pD range, the arsenate species are negatively charged whereas the iron oxide surface is positively charged at low pD and negatively charged at high pD as discussed above. This will of course influence the amount of arsenate species adsorbed as well as the strength of the surface complex formed, as generally accepted for anions adsorbed on iron oxides. [36]

Fig. 9b shows the absorbance at about 840 cm^{-1} versus pD. As expected, the absorbance decreased with pD, as a result of the decreasing amount adsorbed, which in turn probably is a result of that the surface becomes less positively charged and eventually negatively charged (surface complexes I–III above). The surface complexes I and II above admit two types of bonding between iron oxide and arsenate. Either OD or OD_2 is expelled from the surface during reaction with the anion implying an inner-sphere complex or the arsenate species are D-bonded to the surface sites. [20] In the latter case an outer-sphere complex is formed. To distinguish

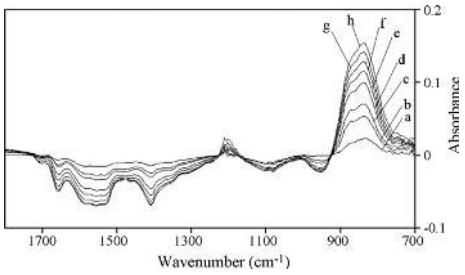

Fig. 10. Spectra of arsenate (0.03 mM, pD 4) adsorbed on an iron oxide film at different times of adsorption. (a) 1.5 min. (b) 6.5 min. (c) 11.5 min. (d) 36.5 min. (e) 66.5 min. (f) 116.5 min. (g) 191.5 min. (h) 300 min.

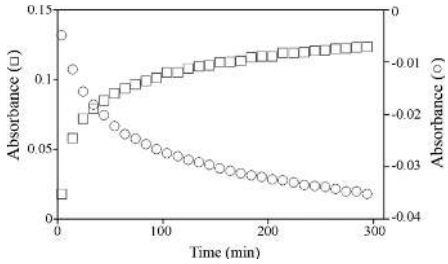

Fig. 11. (□) Peak height of the band at 840 cm^{-1} assigned to arsenate species adsorbed on iron oxide and (○) peak height of the band at 1409 cm^{-1} assigned to carbonate species. Both plotted vs. time with a 0.03 mM arsenate solution flowed over an iron oxide film at pD 4.

between these two possibilities is however not straightforward, especially since both types of bonding may be simultaneously represented at the metal oxide surface. However, D-bonded outer-sphere complexes are expected to be less strongly attached to the surface as compared to inner-sphere complexes, and desorption experiments should at least give a hint to which type of complex dominates (see the discussion under the next subsection).

The absorption bands shifted slightly to lower wavenumber at higher pD values. The most intense band was shifted from 840 to 830 cm^{-1} (10 cm^{-1}) when the pD value was changed from 4 to 8, whereas the shoulder of the peak shifts from 875 to 855 cm^{-1} (20 cm^{-1}). The shift produced in the bands could be due to the deprotonation of the arsenic (V) species adsorbed on the iron oxide particles at higher pD values. The configuration of the complexes formed on the iron oxide seems to be the same at pD 4 and 8.5 because the same number of bands stems from both arsenic complexes which indicates that the complexes have the same symmetry, C_{2v} or lower.

The band at 949 cm^{-1} has been assigned to the Fe—O—D bending vibration. [16] In the present work, a negative band at 949 cm^{-1} appeared simultaneously as the positive band emerged from the arsenate adsorbed on the iron oxide film. The intensity of the negative band at 949 cm^{-1} stemming from Fe—O—D follows the same trend as the intensity of the positive band at 840 cm^{-1} assigned to the arsenate species. This result indicates that arsenate is adsorbed on Fe—O—D and/or Fe—OD_2^+ sites, as has been reported previously. [12] Nevertheless, this (negative) band would also appear if some particles had being expelled constantly from the iron oxide film during the experiment.

In addition, some negative bands in the 1500–1000 cm^{-1} range appeared. These bands were assigned to carbonate species desorbing from the iron oxide film. [16] Hence, in addition to the adsorption sites I–III above, the surface is also characterized by Fe-carbonate sites. The carbonate species may have formed during synthesis of the iron oxide particles or during deposition of these particles on the ATR crystal, since contact with air is hardly avoidable. In these measurements, background spectra were recorded at each pD after equilibrium had been established between pD adjusted D_2O and iron oxide. Hence, the carbonate species adsorbed on the iron oxide film were equilibrated before starting the adsorption of arsenate. Therefore, the negative bands assigned to carbonate species indicate that these species were substituted for arsenate during the adsorption reaction and they may compete for the same adsorption sites.

Fig. 10 shows spectra recorded at different times (from 1.5 to 300 min) during the adsorption on an iron oxide film from a 0.03 mM arsenate solution at pD 4. Previous to the experiment the iron oxide film was in contact with D_2O at pD 4 and a background spectrum was recorded. At $t = 0$ the arsenate concentration in the D_2O was set to 0.03 mM while keeping the pD constant at 4 and the adsorption experiment started. After 1.5 min of adsorption, weak bands at 875 and 840 cm^{-1} were observed. These bands, caused by adsorbed arsenate species, increased in intensity with increasing time of adsorption. Simultaneously, negative absorption bands emerged at 1701, 1657, 1585, 1559, 1534 1464, 1409, 1359, 1068, 1022 and 949 cm^{-1}. The negative band at 949 cm^{-1} has been assigned to the iron oxide Fe—O—D as stated previously. The bands at 1585, 1559, 1534, 1464, 1409 and 1359 cm^{-1} have been assign to both asymmetric and symmetric C—O stretching of carbonate species,[16] whilst the bands observed at 1068 and 1022 cm^{-1} have been assigned to totally symmetric C—O stretching modes.[16]

Fig. 11 shows the intensity (band height) of the absorption band for arsenate at 840 cm^{-1} and the band emerging from carbonate at 1409 cm^{-1} as a function of time. The data was retrieved from the same experiment as the spectra presented in Fig. 10, however for the sake of clarity, not all spectra recorded are shown in Fig. 10. Both adsorption of arsenates and desorption of carbonates are relatively fast within the first 70 min, followed by a slow adsorption as well as desorption process. After 300 min, none of the two processes had reached equilibrium. The declining reaction rates might be due to two different steps. Firstly, desorption of carbonates from the iron oxide surface might be a rate limiting step for the adsorption of arsenate. Secondly, slow diffusion of the arsenate species from solution to the less accessible adsorption sites in the mesoporous iron oxide film as reported earlier. [15]

3.4. Desorption of As (V) from iron oxide

To study the stability of the adsorbed As(V) complexes, in situ FTIR spectra were used for monitoring the stability of the complexes formed as the pD changed. Two different pD's were tested viz. 8.5 or 12. Arsenate was first adsorbed on the iron oxide by exposing the film to a 0.03 mM solution of As (V) at pD 4 for 300 min. Thereafter, the pD was changed to either 8.5 or 12, keeping the As (V) concentration constant at 0.03 mM. The experiment was performed with two different iron oxide films, one for the experiment where the pD was changed to pD 8.5 and the other one when the pD was changed to 12. Only one adsorption curve from a 0.03 mM arsenate solution at pD 4 is shown in Fig. 12, since the two curves obtained were very similar. The peak height of the 840 cm^{-1} band originating from adsorbed arsenate, was then followed as a function of time after the pD change, see Fig. 12. At both pD's, the desorption processes was faster during the first 40 min, followed by a slower process at times >40 min. From the decrease in peak height, it was estimated that approximately 20% of the adsorbed arsenate on the film had desorbed after 200 min at pD 8.5 whilst 65% was desorbed after

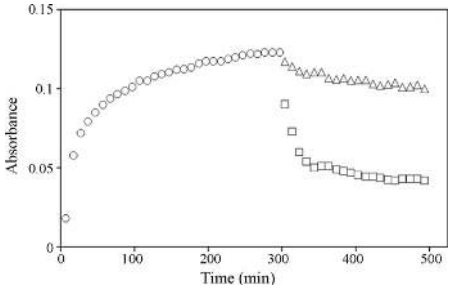

Fig. 12. Adsorption and desorption kinetics followed by monitoring the 840 cm^{-1} absorption band of arsenate. The adsorption (○) was conducted at pD 4 at a concentration of 0.03 mM. At t = 300 min, the pD was changed to either to (△) 8.5 or (□) 12, keeping the concentration of arsenate in the solution constant at 0.03 mM.

200 min at pD 12. The observed decrease in the amount adsorbed was expected since the iron oxide surface is more positively charged at pD 4 than at pD 8.5 and 12. In addition, at higher pD's the concentration of OD^- groups in solution is higher and these ions might also compete with the arsenate species for the iron oxide surface sites.[5,38]

To investigate the stability of the surface complexes formed, a simple rinsing experiment was performed. Two iron oxide films were prepared and a background spectrum of each film was recorded under the flow of D_2O adjusted to pD 4 and pD 8.5 respectively. The two films were subsequently dismounted from the flow cell and equilibrated during 24 h with 0.03 mM arsenate in aqueous solution, one at pH 4 and the other one at pH 8.5. Subsequently the two films were rinsed with water at pH 4 and pH 8.5, respectively, to remove the arsenate in solution and finally the films were dried. The ATR crystals with the films treated at pH 4 and pH 8.5 were then mounted in the spectrometer and in situ FTIR spectra were recorded while the films were flushed with pure D_2O at pD 4 and pD 8.5, respectively. The results obtained from the rinsing experiment at pD 4 are shown in Fig. 13. The arsenate barely desorbed from the film during the first 100 min and no desorption was observed between 100 and 200 min. Approximately 90% of the arsenate previously adsorbed on the iron oxide film was still adsorbed on the iron oxide film after 200 min of flushing at pD 4. These desorption experiments thus suggest a very strong bond of the arsenate to the iron oxide surface at pD 4. These, in turn, indicate a reaction between the surface complex $\equiv Fe{-}OD_2^+$ and $H_2AsO_4^-$ forming a $\equiv Fe{-}O_4H_2As$ complex at the iron oxide surface (inner-sphere).

Fig. 14 shows spectra recorded of the film rinsed at pD 8.5. In this experiment, approximately 60% of the originally adsorbed arsenate

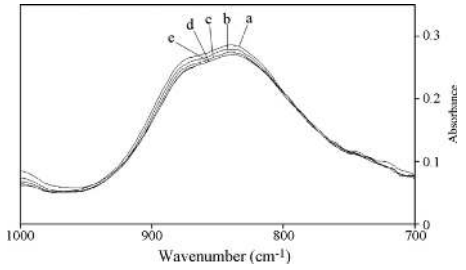

Fig. 13. Spectra recorded after (a) 1.5 min. (b) 20 min. (c) 50 min. (d) 100 min. (e) 200 min of desorption in D_2O at pD 4. Before desorption the iron oxide film was equilibrated for 24 h with a 0.03 mM arsenate solution at the same pD value.

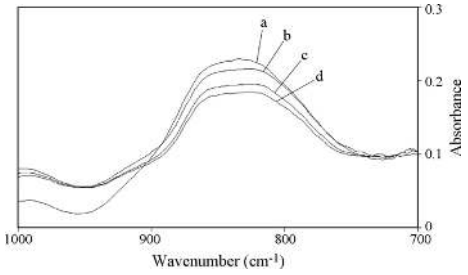

Fig. 14. Spectra recorded after (a) 1.5 min. (b) 75 min. (c) 130 min. (d) 200 min. of desorption in D_2O at pD 8.5. Before desorption the iron oxide film was equilibrated for 24 h with a 0.03 mM arsenate solution at the same pD value.

was still adsorbed on the iron oxide film after 200 min of flushing. Evidently, a fraction of the surface complexes formed at the higher pD value represent more weakly bonded species. It is therefore suggested here that these species could be D-bonded to the iron oxide surface (outer-sphere)

4. Conclusions

In situ ATR-FTIR spectroscopy was proven to be a powerful technique to study the adsorption/desorption of arsenate on an iron oxide films. It was possible to monitor the adsorption/desorption in situ as a function of time as the technique is very sensitive to small amounts of arsenate adsorbed. Moreover, the technique permits simultaneous monitoring of other adsorbed species, e.g. carbonate species, which may interact with the arsenate–ferrihydrite–D_2O system. As the measurements are made in situ, no further sample preparations are needed, thus avoiding any transformation of the sample during preparation.

The desorption experiments indicated that inner-sphere complexes are formed between the iron oxide surface and the arsenate at pD values ranging from 4 and 8.5. Nevertheless, a higher fraction of D-bonded (outer-sphere) complexes seemed to be present at pD 8.5 than pD 4. It was also shown that already adsorbed carbonate species desorbed from the iron oxide surface upon arsenate adsorption.

The technique will be an important tool in forthcoming investigations on how different factors, such as, ionic strength and competitive adsorption with other adsorbates affect the stability of arsenate–iron oxide complexes.

Acknowledgement

The Swedish Research Council Formas, is gratefully acknowledged for financial support.

References

[1] D. Mohan, C.U. Pittman, Arsenic removal from water/wastewater using adsorbents—a critical review, J. Hazard. Mater. 142 (1–2) (2007) 1–53.
[2] B. McAuley, S.E. Cabaniss, Quantitative detection of aqueous arsenic and other oxoanions using attenuated total reflectance infrared spectroscopy utilizing iron oxide coated internal reflection elements to enhance the limits of detection, Anal. Chim. Acta 581 (2) (2007) 309–317.
[3] J. Kumpiene, S. Ore, G. Renella, M. Mench, A. Lagerkvist, C. Maurice, Assessment of zerovalent iron for stabilization of chromium, copper, and arsenic in soil, Environ. Pollut. 144 (1) (2006) 62–69.
[4] D.M. Sherman, S.R. Randall, Surface complexation of arsenic(V) to iron(III) (hydr)oxides: Structural mechanism from ab initio molecular geometries and EXAFS spectroscopy, Geochim. Cosmochim. Acta 67 (22) (2003) 4223–4230.
[5] J. Gimenez, M. Martínez, J. de Pablo, M. Rovira, L. Duro, Arsenic sorption onto natural hematite, magnetite, and goethite, J. Hazard. Mater. 141 (3) (2007) 575–580.

[6] J. Kim, A.P. Davis, Stabilization of available arsenic in highly contaminated mine tailings using iron, Environ. Technol. 37 (1) (2003) 189–195.
[7] W. Hartley, R. Edwards, N.-W. Lepp, Arsenic and heavy metal mobility in iron oxide-amended contaminated soils as evaluated by short- and long-term leaching tests, Environ. Pollut. 131 (3) (2004) 495–504.
[8] M. Mench, Progress in remediation and revegetation of the barren Jales gold mine spoil after in situ treatments, Plant soil 249 (1) (2003) 187–202.
[9] A. Manceau, The mechanism of anion adsorption on iron-oxides—evidence for the bonding of arsenate tetrahedra on free Fe(O,Oh)(6) Edges, Geochim. Cosmochim. Acta 59 (17) (1995) 3647–3653.
[10] S. Fendorf, M.J. Eick, P. Grossl, D.L. Sparks, Arsenate and chromate retention mechanisms on goethite.1. Surface structure, Environ. Technol. 31 (2) (1997) 315–320.
[11] G. Waychunas, B.A. Rea, C.C. Fuller, Surface-chemistry of ferrihydrite. 1. EXAFS studies of the geometry of coprecipitated and adsorbed arsenate, Geochim. Cosmochim. Acta 57 (10) (1993) 2251–2269.
[12] X. Sun, H.E. Doner, An investigation of arsenate and arsenite bonding structures on goethite by FTIR, Soil Sci. 161 (12) (1996) 865–872.
[13] D.G. Lumsdon, A.R. Fraser, J.D. Russel, N.T. Livesey, New infrared band assigments for the arsenate ion adsorbed on synthetic goethite (α-FeOOH), Soil Sci. 35 (1984) 381–386.
[14] P.R. Grossl, M. Eick, D.L. Sparks, S. Goldberg, C.C. Ainsworth, Arsenate and chromate retention mechanisms on goethite.2. Kinetic evaluation using a pressure-jump relaxation technique, Environ. Technol. 31 (2) (1997) 321–326.
[15] C. Luengo, M. Brigante, M. Avena, Adsorption kinetics of phosphate and arsenate on goethite.A comparative study, J. Colloid Interface Sci. 311 (2) (2007) 354–360.
[16] J. Bargar, J.A. Kubicki, R. Reitmeyer, J.A. Davis, ATR-FTIR spectroscopic characterization of coexisting carbonate surface complexes on hematite, Geochim. Cosmochim. Acta 69 (6) (2005) 1527–1542.
[17] K. Dobson, A.J. McQuillan, An infrared spectroscopic study of carbonate adsorption to zirconium dioxide sol–gel films from aqueous solutions, Langmuir 13 (13) (1997) 3392–3396.
[18] Y. Arai, D.L. Sparks, J.A. Davis, Effects of dissolved carbonate on arsenate adsorption and surface speciation at the hematite-water interface, Environ. Technol. 38 (3) (2004) 817–824.
[19] K. Stollenwerk, G.N. Breit, A.H. Welch, J.C. Yount, J.W. Whitney, A.L. Foster, M.N. Uddin, R.K. Majumder, N. Ahmed, Arsenic attenuation by oxidized aquifer sediments in Bangladesh, Sci. Total Environ. 379 (2–3) (2007) 133–150.
[20] A. Roddick-Lanzilotta, A.J. McQuillan, D. Craw, Infrared spectroscopic characterisation of arsenate (V) ion adsorption from mine waters, Macraes mine, New Zealand, Appl. Geochem. 17 (4) (2002) 445–454.
[21] A. Voegelin, S.J. Hug, Catalyzed oxidation of arsenic(III) by hydrogen peroxide on the surface of ferrihydrite, Geochim. Cosmochim. Acta. 68 (11) (2004) A516–A1516.
[22] F.M. Mirabella, Internal Reflection Spectroscopy: Theory and Applications, Marcel Dekker, New York, 1993.
[23] Y.Q. Lu, M.R. Yalamanchili, J.D. Miller, FT-IR internal reflection spectroscopy using regular polygonal internal reflection elements, Appl. Spectrosc. 52 (6) (1998) 851–854.
[24] B.J. Ninness, D.W. Bousfield, C.P. Tripp, In situ infrared technique for studying adsorption onto particulate silica surfaces from aqueous solutions, Appl. Spectrosc. 55 (6) (2001) 655–662.
[25] C. Luengo, M. Brigante, J. Antelo, M. Avena, Kinetics of phosphate adsorption on goethite: Comparing batch adsorption and ATR-IR measurements, J. Colloid Interface Sci. 300 (2) (2006) 511–518.
[26] K. McComb, D. Craw, A.J. McQuillan, ATR-IR spectroscopic study of antimonate adsorption to iron oxide, Langmuir 23 (24) (2007) 12125–12130.
[27] K. Axe, M. Vejgarden, P. Persson, An ATR-FTIR spectroscopic study of the competitive adsorption between oxalate and malonate at the water-goethite interface, J. Colloid Interface Sci. 294 (1) (2006) 31–37.
[28] M.L. Larsson, A. Fredriksson, A. Holmgren, Direct observation of a self-assembled monolayer of heptyl xanthate at the germanium/water interface: a polarized FTIR study, J. Colloid Interface Sci. 273 (2004) 345–349.
[29] A. Fredriksson, A. Holmgren, An in situ ATR-FTIR study of the adsorption kinetics of xanthate on germanium, Colloid Surf. A-Physicochem. Eng. Asp. 302 (2007) 96–101.
[30] A. Fredriksson, P. Hellström, S. Öberg, Comparison between in situ total internal reflection vibrational spectroscopy of an adsorbed collector and spectra calculated by ab initio density functional theory methods, J. Phys. Chem. A 26 (2007) 9299–9304.
[31] M.L. Larsson, A. Holmgren, W. Forsling, Xanthate adsorbed on ZnS studied by polarized FTIR-ATR spectroscopy, Langmuir 16 (2000) 8129–8133.
[32] A. Fredriksson, M.L. Larsson, A. Holmgren, n-Heptyl xanthate adsorption on a ZnS layer synthesized on germanium: An in situ attenuated total reflection IR study, J. Colloid Interface Sci. 286 (2005) 1–6.
[33] J.A. Mielczarski, E. Mielczarski, J. Zachwieja, J. Cases, In Situ and ex situ infrared studies of nature and structure of thiol monolayers adsorbed on cuprous sulfide at controlled potential—simulation and experimental results, Langmuir 11 (7) (1995) 2787–2799.
[34] M. Grahn, A. Lobanova, A. Holmgren, J. Hedlund, Orientational analysis of adsorbates in molecular sieves by FTIR/ATR spectroscopy, Chem. Mater. 20 (19) (2008) 6270–6276.
[35] M. Grahn, A. Holmgren, J. Hedlund, Adsorption of n-hexane and p-xylene in thin silicate-1 films studied by FTIR/ATR spectroscopy, J. Phys. Chem. C 112 (2008) 7717–7724.
[36] R.M. Cornell, U. Schwertmann, The iron oxides: structure, properties, reactions, occurrences and uses, VCH, Weinheim, 1996.
[37] M. Grafe, M.J. Eick, P.R. Grossl, A.M. Saunders, Adsorption of arsenate and arsenite on ferrihydrite in the presence and absence of dissolved organic carbon, J. Environ. Qual. 31 (2002) 1115–1123.
[38] P. Grossl, D.L. Sparks, Evaluation for contaminant ion adsorption-desorption on goethite using pressure-jump relaxation kinetics, Geoderma 67 (1–2) (1995) 87–101.

Paper III

In Situ ATR-FTIR Studies of Competitive Adsorption of Arsenate and Phosphate on Ferrihydrite

Ivan Carabante, Mattias Grahn, Allan Holmgren, and Jonas Hedlund

Journal of Colloid and Inerface Science, 351 (2010) 523-531

Journal of Colloid and Interface Science 351 (2010) 523–531

Contents lists available at ScienceDirect

Journal of Colloid and Interface Science

www.elsevier.com/locate/jcis

Regular Article

In situ ATR–FTIR studies on the competitive adsorption of arsenate and phosphate on ferrihydrite

Ivan Carabante *, Mattias Grahn, Allan Holmgren, Jonas Hedlund

Division of Chemical Engineering, Luleå University of Technology, SE-97187, Luleå, Sweden

ARTICLE INFO

Article history:
Received 21 May 2010
Accepted 28 July 2010
Available online 2 August 2010

Keywords:
Competitive adsorption
ATR–FTIR
In situ
Phosphate
Arsenate
Iron oxide
Ferrihydrite
Film

ABSTRACT

In the present study, in situ ATR–FTIR spectroscopy was used for the first time to study the competitive adsorption of phosphate and arsenate on ferrihydrite. Deuterium oxide was used as solvent to facilitate the interpretations of recorded infrared spectra.

It was found that arsenate and phosphate adsorbed more strongly at lower pD-values, showing similarities in the adsorption behavior as a function of pD. However, arsenate complexes were found to be more strongly adsorbed than phosphate complexes in the pD range studied. About five times higher concentration of phosphate in solution was needed to reduce the absorbance due to pre-adsorbed arsenate to the same relative level as for pre-adsorbed phosphate, which was desorbed using a solution containing equal (molar) concentrations in arsenate and phosphate.

At pD 4, two phosphate complexes were adsorbed on the iron oxide, one deuterated and one de-deuterated. When phosphate was pre-adsorbed and arsenate subsequently added to the system, the deuterated phosphate complex desorbed rapidly while the de-deuterated phosphate complex was quite stable. At pD 8.5, only the de-deuterated phosphate complex was adsorbed on the iron oxide. Moreover, the arsenate adsorbed was also predominantly de-deuterated as opposite to the arsenate adsorbed at pD 4. During the substitution experiments the configuration of these complexes on the iron oxide surface did not change. To the best of our knowledge, this is the first time this difference in stability of the different phosphate complexes is reported and shows the power of employing in situ spectroscopy for this kind of studies.

1. Introduction

Arsenic is a toxic element which may cause blackfoot disease as well as skin-, lung-, bladder- and kidney-cancer, etc. [1]. The routes of exposure to humans are basically by air, drinking-water or food [1]. High arsenic concentration can be found in drinking well-water in many countries, such as; New Zealand, Romania, Argentina, Bangladesh and India but also in mine drainage areas in e.g. Poland, Australia and Sweden [2].

In nature, arsenic is frequently associated with metal sulfides, e.g. lead, silver, copper, cobalt or iron sulfides [1]. However, arsenic may also be a result of anthropogenic activities and may thereby occur in e.g. mining tailings, in agricultural chemicals or in antifungal wood preservatives [1–3]. The use of arsenic compounds in combination with chromate and copper in antifungal wood preservatives, CCA (Copper, Chromate, Arsenate), has been widely used since the 1930s. As a consequence of deficient impregnation methods, many impregnation sites today show high levels of arsenic in the soil.

In most of the contaminated sites, the aim of soil remediation is to recover the ecosystem and soil functionality. For this reason, contaminant mobility and bioavailability should be minimized so as to reduce the toxicity to organisms and improve vegetation establishment. To reduce risks related to arsenic spreading in the environment, the mobility and bioavailability of As in soil can be reduced by the addition of iron compounds [4,5]. Iron is interesting as means for stabilizing arsenic contaminated soil because of its high affinity for arsenic oxyanions in combination with a low cost. However in soil remediation, fertilizer addition is often necessary to improve plant growth on nutrient deficient soils. Phosphate is one of the principal soil nutrients, making it an important component of many fertilizers. Due to the similar behavior of arsenates and phosphates, the presence of phosphorus compounds in fertilizers added to iron oxide stabilized soils may lead to a significant increase of As leaching into the environment as phosphate species compete with arsenate species regarding adsorption on the iron oxide surface [6–8].

The adsorption of arsenic on various iron oxides/oxyhydroxides, for simplicity hereafter referred to as just iron oxides, has been widely studied [9–11]. The adsorption of arsenate anions on iron oxide has been shown to be pH dependent with maximum adsorption at moderately low pH (3–5). The arsenate complexes

* Corresponding author. Fax: +46 920 491199.
E-mail address: ivan.carabante@ltu.se (I. Carabante).

0021-9797/$ - see front matter © 2010 Published by Elsevier Inc.
doi:10.1016/j.jcis.2010.07.064

formed on the surface of iron oxide have been extensively studied using EXAFS (Extended X-ray Absorption Fine Structure) [11–14]. From these studies it was concluded that bidentate binuclear complexes are the predominant complexes. Nevertheless, contradictory information is found in the literature reporting the formation of monodentate as well as bidentate mononuclear complexes on the iron oxide adsorption sites. Loring et al. [15] concluded, by means of ATR–FTIR (Attenuated Total Reflection – Fourier Transform Infrared) spectroscopy and EXAFS data, that arsenate formed monodentate complexes on the goethite surface instead of bidentate binuclear complexes. Furthermore, it was shown that very similar complexes were formed at pD 4 and pD 8.5 and the possible difference between them was the deuteration at lower pD [9]. The hydroxyl sites of the iron oxide were shown to be the active sites on which arsenate adsorbed [16].

The adsorption of phosphate on iron oxides have also been previously studied using ATR–FTIR spectroscopy [17–19]. It was reported that phosphate adsorption on iron oxide showed a pH dependence similar to that of arsenate with higher adsorption at lower pH [17]. Based on FTIR data, the authors concluded that protonated bidentate binuclear complexes were the predominant species adsorbed on iron oxides at pH between 3 and 6 whereas the non-protonated binuclear bidentate complexes were predominant at pH > 7.5.

The adsorption of arsenate and phosphate anions separately onto iron oxides indicated that their adsorption behavior were very similar [20,21]. Both oxoanions adsorbed in very similar amounts on goethite in the pH range 3–5. However, more phosphate than arsenate desorbed from goethite in presence of oxalate ions, indicating that arsenate might be stronger bonded to the iron oxide.

The competitive adsorption of arsenate and phosphate on iron oxides like goethite and ferrihydrite has been studied using batch adsorption experiments [20–24]. When goethite was exposed to a solution of equal molar concentrations of arsenate and phosphate, equal amounts of arsenate and phosphate were adsorbed on the iron oxide at pH > 6, whereas slightly higher amount of arsenate was adsorbed at pH < 6. When arsenate was pre-adsorbed on goethite, the adsorption of phosphate was shown to be highly inhibited. However, if phosphate was pre-adsorbed, its inhibiting effect on arsenic adsorption was much weaker [21].

The main focus of this work was to study the competitive adsorption between arsenate and phosphate on a synthetic iron oxide film using in situ ATR–FTIR measurements. To the best of our knowledge, this is the first report monitoring both arsenate and phosphate species during competitive adsorption onto iron oxide using this in situ method, which is a powerful tool to study adsorption onto and desorption from thin mineral layers [25–30]. The aim was to gain new insight into the stability of adsorbed arsenate and phosphate and simultaneously get molecular information about the surface complexes formed and their stabilities. This information is important in order to get a better understanding of the mobility of these oxoanions in natural soils and especially arsenic contaminated soils treated with iron oxide since phosphate is frequently added to speed up the plant growth. The synthetic iron oxide (ferrihydrite) film was thus used as a model system for natural soils with high iron oxide content. Even though the occurrence of other iron oxides such as goethite or hematite is higher than ferrihydrite due to their higher thermodynamic stability [31], the major difference between them is expected to be the number of adsorption sites.

2. Experimental

2.1. Iron oxide synthesis and film preparation

An iron oxide hydroxide, viz. 6-line ferrihydrite, suspension was synthesised using the same synthesis method as previously reported by the authors [9]. In short, 50 ml of distilled water was heated to boiling, thereafter 1 ml. of a 0.7 M iron (III) chloride ($FeCl_3{\cdot}6H_2O$; Riedel- de Haën, p.a. 99%) solution was added dropwise to the boiling solution. After 5 min of boiling, the solution changed color from yellow to a dark brown-red. The resulting iron oxide suspension was allowed to cool down and was subsequently dialyzed against distilled water for approximately 24 h using a dialysis membrane (MWCO 12-14000; Spectra/Por Dialysis membrane; Spectrum laboratories) in order to reduce the acidity and eliminate possible impurities from the synthesis suspension. As a result of the dialysis, the pH of the suspension changed from approximately 1.5–5.

The dialyzed suspension was subsequently diluted with methanol (CH_3OH; Kebo lab, >99.8%) (1:1 by mass) resulting in an iron oxide content in the suspension of about 2 g/l. To coat the ATR crystal (Crystan, ZnSe, 52 × 20 × 2 mm and 45° cut edges) with a thin layer of iron oxide, 500 µl of the suspension was spread on the ATR crystal using a syringe. About 5 cm^2 of the crystal was covered. The suspension was then allowed to dry under ambient conditions thus forming an even film on the ATR crystal surface. After drying, a similar film was prepared on the other side of the ATR crystal.

2.2. General characterization of the film and iron oxide particles

A FEI Magellan 400 field emission XHR-SEM (Extra high resolution – Scanning electron microscope) was used to investigate the films. Cross sections of the samples were mounted on a holder and investigated using an accelerating voltage of 1 kV without applying any coating on the iron oxide.

Freeze-dried powder of the synthesised iron oxide was characterized with X-ray Diffraction (XRD, Siemens D5000) running in Bragg–Brentano geometry using a step size of 0.02° 2θ.

Nitrogen adsorption at liquid nitrogen temperature was measured on the freeze-dried powder using a Micrometrics ASAP 2010 instrument. The powder was degassed at a temperature of 140 °C for about 24 h.

The zeta potential of the iron oxide particles suspended in 0.01 M KNO_3 was measured with electrophoresis (ZetaCompact, CAD Instrumentation) in the pH range 4–12.

2.3. ATR–FTIR measurements

All spectra were recorded at room temperature using a Bruker IFS 66v/s spectrometer equipped with a DTGS (Deuterated TriGlycine Sulfate) detector. A zero filling factor of two was used and 200 scans were co-added resulting in a resolution of 4 cm^{-1}.

All experiments were performed using deuterium oxide (D_2O, Aldrich, 99 atom% D) as solvent to allow more reliable spectral analysis. Prior to each measurement, a single beam background spectrum of the aqueous ionic medium (0.1 M NaCl, Merck; 99.5%) was recorded. The solution was adjusted to the same pD as in the subsequent experiment viz. pD 4 or pD 8.5 and a single beam spectrum of the sample was recorded. Before recording the background, the system was allowed to equilibrate for 5 h. After recording the background an appropriate amount of a stock solution of sodium hydrogen-arsenate hepta-hydrate ($NaH_2AsO_4{\cdot}7H_2O$; Fluka; p.a. 98.5%) or sodium phosphate monobasic monohydrate ($NaH_2PO_4{\cdot}H_2O$; Sigma–Aldrich; 98–102%) was added to the ionic medium. In the experiments where competitive adsorption was studied, one of the oxoanions was pre-adsorbed from a 0.03 mM aqueous solution onto the ferrihydrite layer for 5 h and subsequently the other oxoanion was added to the working solution resulting in equal (molar) concentration of the two oxoanions (0.03 mM). Sample spectra were recorded every 5 min. The

change in the total ionic strength upon addition of arsenate or phosphate was only 0.06%, and was considered negligible.

Fig. 1 shows a sketch of the experimental set-up. The pD of the solution was controlled with an automatic pH meter (Metler Toledo, T70 pH-stat), which added a 0.01 mM solution of either deuterium chloride (DCl; Aldrich; 99 atom% D) or sodium deuteroxide (NaOD; Aldrich; 99 + atom% D). The solution was pumped by a peristaltic pump, 10 ml/min, from the solution vessel into the stainless steel flow cell. The flow cell was mounted in the spectrometer and contained the iron oxide coated ATR crystal. After passing both sides of the ATR crystal, the solution was recirculated back to the solution vessel. The solutions were continuously bubbled with argon gas (AGA, 99%) in order to minimize absorption of CO_2 from room air.

To verify that the concentration of arsenate and phosphate in the solution did not change during the experiment, the concentrations were analyzed before and after the experiments using Inductively Coupled Plasma–Optical Emission Spectroscopy (ICP–OES, Perkin Elmer optima 2000 DV).

3. Results and discussion

3.1. General characterization of the film

In accordance with previous findings, XRD data (not shown) showed that the iron oxide particles consisted of pure 6-line-ferrihydrite [9]. The point of zero charge (PZC) was determined to be in the pH range 7.5–8.5, which is in accordance with previous reported results for 6-line-ferrihydrite [31]. Fig. 2 shows an SEM image of the cross section of an iron oxide film. The figure illustrates that the film was comprised of small particles forming a film with a thickness of 300–500 nm. From high resolution images, Fig. 2b, the particle size was estimated to ca 10 nm. The specific surface area of the iron oxide was determined by nitrogen adsorption at liquid nitrogen temperature to be 190 m^2/g. By assuming spherical particles, this corresponds to a particle diameter of 8 nm, in agreement with the SEM observations. This particle size is typical for 6-line-ferrihydrite [31].

3.2. Adsorption of arsenate onto iron oxide

Fig. 3 shows the absorbance of the infrared band at ~840 cm^{-1}, assigned to arsenate adsorbed on iron oxide [9], versus arsenate concentration. At each concentration, the adsorption was allowed to equilibrate for 5 h and the pD-value of the aqueous arsenate solutions was either pD 4 (○) or pD 8.5 (■). As reported earlier by the authors, the absorption bands caused by arsenate species adsorbed on iron oxide are clearly distinguishable from the infrared bands recorded for arsenate species in solution [9]. It was also shown that the structure of the adsorbed arsenate complex was the same at the two pD-values studied [9]. The intensity of the band is proportional to the concentration of arsenate species

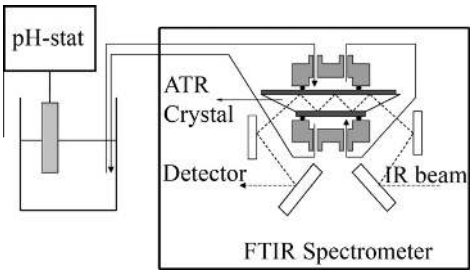

Fig. 1. Sketch of the experimental set-up used to perform the in situ ATR–FTIR measurements. The ATR crystal coated by a thin iron oxide film (dark-gray) was mounted in the flow cell (light gray).

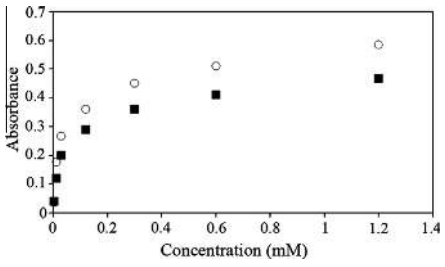

Fig. 3. The Absorbance of the infrared band at 840 cm^{-1} caused by arsenate adsorbed on iron oxide versus arsenate concentration at (○) pD 4 and (■) pD 8.5. Each experimental point corresponds to the amount adsorbed after 5 h of equilibration.

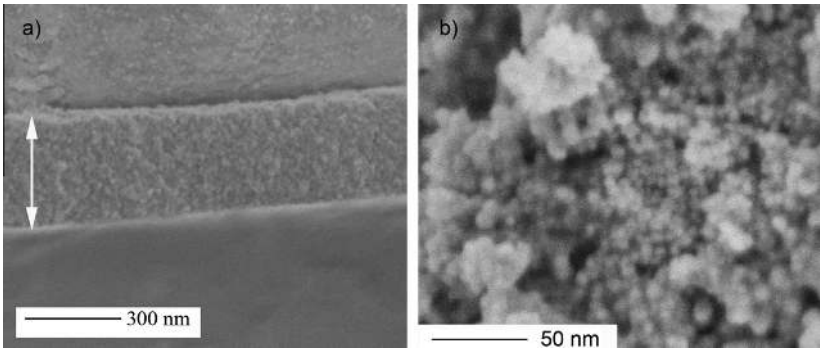

Fig. 2. (a) SEM image of the cross section of the iron oxide film on the ATR crystal in which the film thickness is indicated by the arrow. (b) High resolution SEM image of the iron oxide nanoparticles forming the film.

adsorbed on the iron oxide film according to the Beer–Lambert law [30], presuming that absorption from bulk species can be omitted. Accordingly, by assuming that the molar absorptivities are the same for the adsorbed species at both pD-values, it may be concluded that the amount of arsenate complexes adsorbed on the iron oxide film at a certain concentration is somewhat higher at pD 4 than at pD 8.5 in agreement with data obtained by quantitative methods (the concentrations of the supernatants after batch experiments were measured by means of spectrometric methods) [10,32]. At lower pD the iron oxide surface is more positively charged and the electrostatic attraction between the surface and the oxoanion should facilitate the approach of the latter to the surface [9,31]. The amount of arsenate adsorbed increased with increasing arsenate concentration in solution in the whole concentration range studied suggesting that complete monolayer coverage was not achieved in these experiments. The adsorption isotherms of As(V) on 2-line-ferrihydrite previously published in the literature indicated that complete monolayer coverage is only reached at bulk arsenate concentrations >2 mM, both at pH 4.6 and 9.2 [32]. These results are similar to the ones obtained in the present work for 6-line ferrihydrite. However, it should be noticed that in the present work equilibrium was not reached even after 5 h of equilibration although most of the adsorption seemed to have occurred after this period of time. Similar slow kinetics has been reported in earlier work [33]. Fig. 3 is thus based on pseudo equilibrium data.

3.3. Adsorption of phosphate onto iron oxide

Fig. 4 shows spectra of a 60 mM phosphate solution at pD 4 (spectrum a) and 8.5 (spectrum b) recorded using an uncoated ZnSe crystal, thus showing mainly species in solution. Based on the p*Ka* values for phosphate reported in the literature, viz. 2.2, 7.2, and 12.3, the dominating species in solution at pD 4 and 8.5 would be $D_2PO_4^-$ and $D_2PO_4^{2-}$ [19], respectively assuming that the p*Ka* values are nearly the same for the deuterated species as for the protonated species. At pD 4, three bands at 1180, 1084, and 940 cm^{-1} were observed in the spectrum. These bands were assigned to the PO stretching modes of the $D_2PO_4^-$ species [19]. In the spectrum recorded at pD 8.5, the two bands at 1084 and 988 cm^{-1} were assigned to the PO stretching modes of $D_2PO_4^{2-}$. First the spectrum of phosphate at pD 4 was recorded, thereafter the pD was changed to 8.5 and as the pD changed, the spectrum changed immediately reflecting the fast de-deuteration of $D_2PO_4^-$ to $D_2PO_4^{2-}$. Any adsorption of phosphate on the ZnSe crystal was assumed to be negligible since the intensity of the bands were constant with time and it was thus concluded that virtually all of the signal in spectrum a and spectrum b originated from phosphate species in solution.

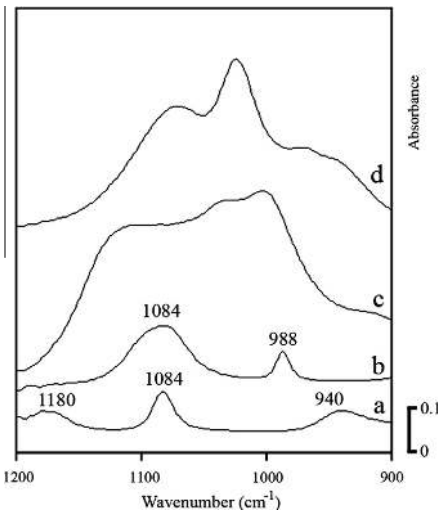

Fig. 4. Infrared spectra of a 60 mM phosphate solution at (a) pD 4 and (b) pD 8.5 recorded using a non coated ATR crystal. The two upper traces show infrared spectra of phosphate adsorbed from a 0.03 mM aqueous phosphate solution at (c) pD 4 and (d) pD 8.5 onto a ferrihydrite coated crystal.

Fig. 4 also shows spectra of phosphate adsorbed on iron oxide from a 0.03 mM phosphate solution at pD 4 (spectrum c) and 8.5 (spectrum d). The bands originating from adsorbed phosphate at pD 4 appeared at different wavenumbers as compared to the bands from phosphate in solution at the same pD. Since the predominant phosphate species in solution at pD 4 is $D_2PO_4^-$, the bands appearing in spectrum c were not caused by phosphate species in solution but from phosphate adsorbed on iron oxide. Moreover, the absorption measured using a crystal coated with iron oxide had approximately three times higher intensity (spectrum c) than a non coated crystal (spectrum a) despite the fact that the phosphate concentration in solution was 2000 times lower (spectrum c), clearly showing that the iron oxide film is interacting with the phosphate species. Similar results were obtained at pD 8.5 (compare spectra b and d in Fig. 4). The change in band shape and peak wavenumbers upon increasing pD from 4 to 8.5 is mainly attributed to the difference in deuteration of the surface complexes formed. However, at the lower pD the strong and broad band appearing at about 1120 cm^{-1}, assigned to the P=O stretch of the phosphate unit, might partly be due to precipitated iron phosphate since the precipitate absorbs infrared radiation in the same spectral region. Other assignments are discussed under Sections 3.4.1 and 3.4.2.

Fig. 5 shows the integrated area (between 1200 and 950 cm^{-1}) of the infrared bands originating from phosphate adsorbed on iron oxide at pD 4 and at pD 8.5 plotted versus phosphate concentration in solution. Following the assumption that the molar absorption coefficient of the different phosphate complexes are very similar [18], it follows that the amount of phosphate adsorbed was higher at pD 4 than at pD 8.5, which is reasonable because of the difference in surface charge. It is also clear that neither the adsorption of phosphate nor the adsorption of arsenate (Fig. 3) follow a Langmuir type of adsorption isotherm since no equilibrium plateau value was reached. This is likely caused by the layer of the synthesised ferrihydrite particles being heterogeneous with respect to the adsorption energy of available surface sites.

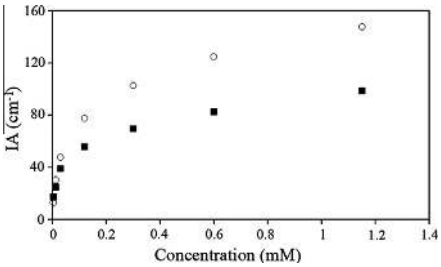

Fig. 5. Integrated absorbance (IA) of the bands between 1200 and 950 cm^{-1}, assigned to adsorbed phosphate on iron oxide, plotted vs. the concentration of phosphate in solution at (○) pD 4 and (■) pD 8.5. At each concentration, the intensity plotted corresponds to the amount of phosphate adsorbed after 5 h of equilibration with the iron oxide film.

3.4. Competitive adsorption of arsenate and phosphate on iron oxide

3.4.1. Substitution of phosphate for arsenate at pD 4

Fig. 6 shows infrared spectra of phosphate adsorbed from a 0.03 mM aqueous solution at pD 4. The iron oxide film was exposed to the solution for 5 h. The infrared bands at 1124, 1084, 1035, 1014, and 998 cm^{-1}, due to phosphate, became more intense with time. The relative intensities of the most intense bands at 1124, 1035 and 998 cm^{-1} were constant during the whole experiment and these bands were thus assigned to the same complex. The band at ~1124 cm^{-1} was previously assigned to the P═O stretching vibration of phosphate species [19]. Since this band is observed, it indicates that the phosphate complex formed on the iron oxide surface did not have a resonance structure involving the P═O bond. Moreover, the number of absorption bands indicates that the symmetry of the species should be C_{2V} or lower. Therefore, the most probable complex generating these IR-absorption bands would be the deuterated bidentate binuclear complex ($(\equiv FeO)_2(OD)PO$) or the monodentate doubly deuterated complex ($(\equiv FeO)(OD)_2PO$) as was suggested previously [18,19]. Further, the relative intensity of the bands at 1084 and 1014 cm^{-1} was also constant, suggesting that these bands originated from one and the same complex. The phosphate complex generating the latter bands have lost their P═O stretching mode due to the formation of a resonance structure since P═O stretching bands appear at higher wavenumber than 1100 cm^{-1} [19]. The de-deuteration of the complexes mentioned previously resulting in either a non-deuterated bidentate binuclear complex ($(\equiv FeO)_2PO_2^-$) or a monodentate mono-deuterated complex ($(\equiv FeO)(OD)PO_2^-$) could both give rise to the two bands [19]. Since the intensity of the bands due to the deuterated phosphate complex (at 1124, 1035, and 998 cm^{-1}) was higher than the intensity of the bands caused by the de-deuterated complex (at 1084 and 1014 cm^{-1}), the concentration of adsorbed deuterated complex appeared higher than the concentration of de-deuterated complex. The opposite phenomenon was reported earlier [18], i.e. bands assigned to deuterated phosphate complexes (at 1123 and 1006 cm^{-1}) were weak, whereas the bands assigned to de-deuterated complexes (at 1084 cm^{-1} and 1044 cm^{-1}) were more intense. However, there was a slight difference in the conditions in those experiments as compared to this work. In the study carried out by Luengo et al. [18], phosphate was adsorbed on goethite at pH 4.5 (i.e. slightly higher pH than in the present work) and from a 0.06 mM phosphate solution. The slight difference in pH may account for the difference in results since the p*Ka* of phosphate complexes adsorbed on the surface of goethite was estimated to be about 4.5 according to titration experiments [19]. It is thus possible that in the adsorption experiment performed by Luengo et al. [18] at pH 4.5 and using goethite as adsorbent, the system was slightly above this p*Ka* value, whereas in the experiments reported here, performed at pD 4 and using ferrihydrite as adsorbent, the system was slightly below the p*Ka* value.

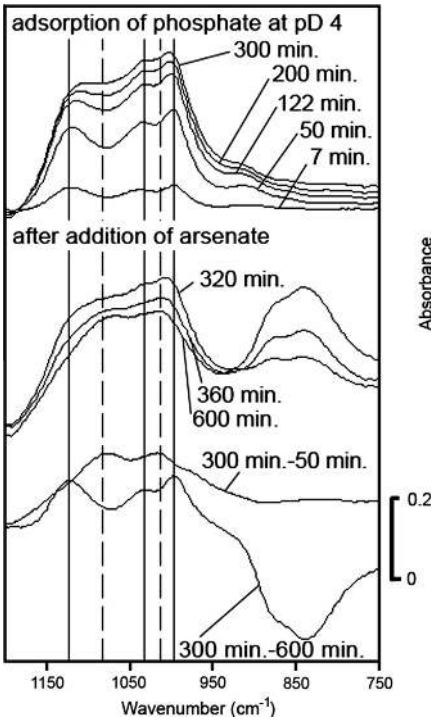

Fig. 6. Infrared spectra of phosphate adsorbed onto iron oxide from a 0.03 mM aqueous phosphate solution. After 300 min arsenate was added arriving at equal (molar) concentration (0.03 mM) solution of phosphate and arsenate and the spectral change was monitored for additionally 300 ' Difference spectra were calculated as indicated in the figure using the OPUS software from Bruker. The vertical lines in the figure mark the frequency positions 1124 cm^{-1}, 1035 cm^{-1}, and 998 cm^{-1} (solid lines) whereas the dashed lines show the wavenumbers 1084 cm^{-1} and 1014 cm^{-1}.

After 50 min of adsorption, only the bands at 1124, 1035, and 998 cm^{-1} were observed. Hence, the deuterated phosphate complex was adsorbed mainly within the first hour of adsorption. On the other hand, the difference spectrum obtained by subtracting the spectrum recorded after 50 min from the spectrum recorded after 5 h shows only the two bands at 1084 and 1014 cm^{-1}, indicating that only the de-deuterated phosphate complex was adsorbed after the first hour (lower part of Fig. 6). This implies a significantly slower kinetics of adsorption for the latter complex as compared to the deuterated phosphate complex, even though these complexes could also interconvert on the surface.

After 5 h, a sufficient amount of arsenate was added to the solution to arrive at equal (molar) concentration of the two oxoanions. Spectra in the middle part of Fig. 6 (320–600 min) were recorded during this second stage of the experiment. The bands already assigned to arsenate adsorbed on iron oxide, in the region 900–800 cm^{-1}, immediately appeared as arsenate was added to the solution and their intensity increased with time. Simultaneously, the bands originating from phosphate complexes (1200–950 cm^{-1}) decreased in intensity as a result of desorption of phosphate species from the iron oxide. Furthermore, from the spectra it was evident that the bands assigned to the deuterated phosphate complex (at 1124, 1035 and 998 cm^{-1}) were reduced much faster than the bands assigned to the de-deuterated complex (at 1084 and 1014 cm^{-1}), which indicates different stability of the two types of complexes. It was very interesting to notice that the first adsorbed phosphate complex was the one that was first out-competed by the arsenate ions. This became clear upon subtracting the spectrum recorded after 300 min, i.e. just before arsenate was added, from the spectrum recorded after 600 min, which highlights only the bands where the intensity decreased by substitution of phosphate for arsenate (Fig. 6, lower part). Only absorption bands assigned to the deuterated complex (1124, 1035, and 998 cm^{-1}) appeared in the difference spectrum indicating that the de-deuterated complex was more stable under these conditions. One reason for this difference might be that the latter complexes are negatively charged whilst the deuterated complexes are neutral. The predominant arsenate species in solution at this pD is the

negatively charged $D_2ASO_4^-$ It should also be noticed here that the point of zero proton charge of the iron oxide was measured to be between pH 7.5 and 8.5.

3.4.2. Substitution of phosphate for arsenate at pD 8.5

Identical experiments as those described under Section 3.4.1 were also performed at pD 8.5 and some of the spectra are shown in Fig. 7. Distinct infrared bands caused by phosphate adsorption appeared at ~1064 cm^{-1} and ~1021 cm^{-1}. Weaker IR-absorption bands, belonging to the adsorbed phosphate complexes appeared at ~965 cm^{-1} as well. The absorption at ~1064 cm^{-1}, ~1021 cm^{-1}, and ~945 cm^{-1} have previously been assigned to the non-deuteurated bidentate binuclear complex ($(\equiv FeO)_2PO_2$) [17–19] on iron oxide or the mono-deuterated mononuclear complex ($((\equiv FeO)(OD)PO_2^-$) [19]. The integrated area of the bands assigned to phosphate species (1200–950 cm^{-1}) increased with time similarly as at pD 4, although the amount adsorbed after 5 h was significantly lower at pD 8.5. Addition of arsenate to the solution again caused desorption of phosphate from the surface of the iron oxide. The major difference between pD 4 and pD 8.5, regarding the infrared absorption of the arsenate species was the shift of the bands to lower frequency (~15 cm^{-1}). These shifts have been reported previously as a consequence of de-protonation of the arsenate adsorbed as compared to the arsenate adsorbed at pD 4. The peak frequencies (1021 cm^{-1} and 1064 cm^{-1}) of the bands assigned to phosphate species shifted to higher wavenumbers during the course of the adsorption experiment. The peak frequency of the 1064 cm^{-1} band shifted about 8 cm^{-1} to higher frequency during 5 h of adsorption. At this point arsenate was added to the system, however, the peak frequency continued to increase to 1081 cm^{-1} during the following 5 h, despite the fact that phosphate desorbed during this time. The most intense band in the spectra shifted from 1021 cm^{-1} to 1027 cm^{-1} after 600 min of adsorption. These spectral shifts could possibly be caused by a change in the interaction between the phosphate species during adsorption (<300 min) and in the interaction between adsorbed phosphate and arsenate species (>300 min). Significant changes of peak frequencies were more easily evaluated at pD 8.5 than at pD 4 because of the broader spectral feature at the latter pD.

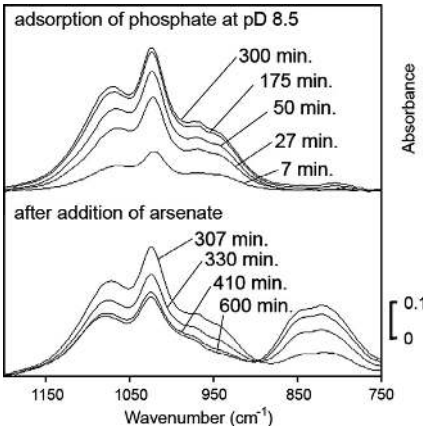

Fig. 7. Infrared spectra of phosphate adsorbed onto ferrihydrite from 0.03 mM aqueous phosphate solution at pD 8.5 (upper part). The adsorption times are shown in the figure. After 300 min arsenate was added to make an equal (molar) concentration (0.03 mM) solution of arsenate–phosphate at the same pD (lower part).

Fig. 8 shows the rate of adsorption/desorption based upon all spectra recorded at various adsorption times, where some results are already described in connection to Figs. 6 and 7. The integrated absorbance between 1200 and 950 cm^{-1} was plotted vs. time, implying the rate curves for phosphate at pD 8.5 and pD 4. As is clear from the graphs, the concentration of phosphate complexes on the iron oxide film increased with time. The slope of the two curves indicates that the initial adsorption rate was higher at pD 8.5 than at pD 4. After about 70 min the rate of adsorption became considerably lower although an equilibrium plateau value was not reached within 300 min. As already discussed, the results indicated the amount of phosphate to be higher at pD 4 than at pD 8.5, which also is in concert with previous findings [31]. When arsenate was added to the solution, the phosphate desorbed from the iron oxide. The peak height of the band at ~840 cm^{-1} assigned to arsenate adsorbed on iron oxide increased in intensity simultaneously as the amount of adsorbed phosphate decreased due to desorption of pre-adsorbed phosphate from the iron oxide layer.

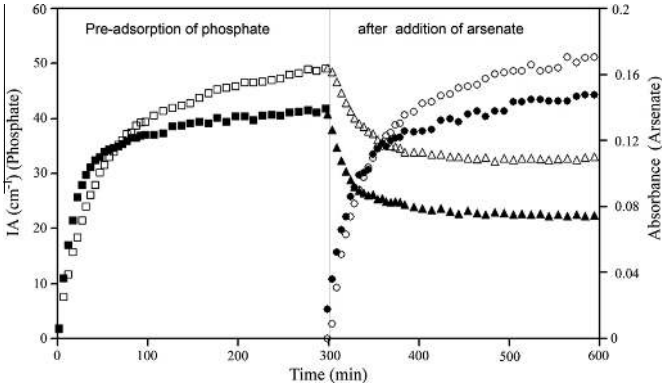

Fig. 8. Integrated absorbance (IA) of adsorbed phosphate versus time showing the results from two different pD-values; pD 8.5 (■) and pD 4 (□). After 300 min of phosphate adsorption, arsenate was added yielding a solution with equal (molar) concentration (0.03 mM) in phosphate and arsenate. The rate of the following phosphate desorption (pD 8.5 (▲) and pD 4 (Δ)) and arsenate adsorption (pD 8.5 (●) and pD 4 (○)) was monitored for 5 h.

The relative desorption of phosphate at pD 4 was 35% whereas at pD 8.5 it was 45%. This relative desorption of phosphate was calculated as the decrease in the integrated absorbance of the bands assigned to phosphate complexes (1200–950 cm^{-1}) after equilibration with arsenate divided by the intensity of the phosphate bands before adding arsenate to the system. The desorption seemed to reach an equilibrium value after about 5 h although the adsorption of arsenate continued after this period of time indicating that arsenate also occupied surface sites not previously occupied by phosphate.

3.4.3. Substitution of arsenate for phosphate at pD 4 and pD 8.5

Infrared spectra recorded during adsorption from a 0.03 mM arsenate solution in D_2O at pD 4 are shown in Fig. 9 (the upper part). As evident from these spectra, the arsenate species adsorbed on iron oxide had two prominent bands at about 875 cm^{-1} and 840 cm^{-1}. Their relative intensities and peak positions remained constant during the course of the experiment, indicating that the arsenate complex formed on the iron oxide surface was not changed. The lower part of the same figure shows spectra of adsorbed phosphate and arsenate after pre-adsorption of arsenate. As phosphate was introduced into the system bands in the region 1200–950 cm^{-1} appeared and their intensity increased with time indicating the adsorption of phosphate species on the iron oxide (the lower part of the figure). Simultaneously, the bands assigned to arsenate (900–800 cm^{-1}) did not undergo any major change in their intensity except for a slight decrease. Regarding the bands associated with phosphate (1200–950 cm^{-1}), the shape of the bands was very similar to that obtained when only phosphate was adsorbed at the same pD, but the band intensities were significantly lower.

Infrared spectra of arsenate (0.03 mM) adsorbed at pD 8.5 are shown in Fig. 10 (the upper part). The lower part of the figure shows the spectra obtained after phosphate was added to the system. Two broad bands appeared at ~855 cm^{-1} and ~830 cm^{-1} in all spectra recorded during the first 5 h. After adding phosphate to the system, bands appeared in the 1200–950 cm^{-1} region. These

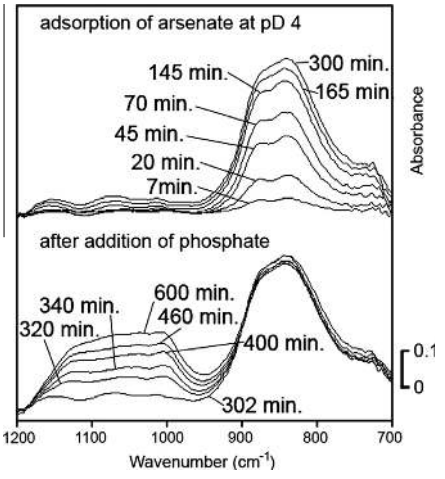

Fig. 9. Infrared spectra of arsenate adsorbed onto ferrihydrite from 0.03 mM aqueous arsenate solution at pD 4 (upper traces). The adsorption times are indicated. After 300 min of adsorption, an equal (molar) concentration (0.03 mM) solution of arsenate–phosphate at pD 4 was brought in contact with the iron oxide layer and spectra were recorded during additionally 5 h.

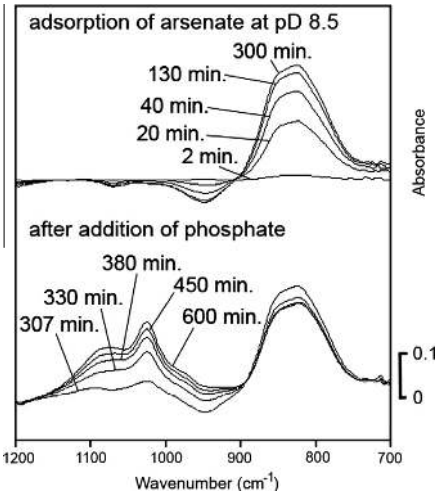

Fig. 10. Infrared spectra of arsenate adsorbed onto ferrihydrite from 0.03 mM aqueous arsenate solution at pD 8.5 (upper part). Adsorption times are indicated. After 300 min phosphate was added to make an equal (molar) concentration (0.03 mM) solution of arsenate–phosphate at the same pD (lower part).

bands increased in intensity with time indicating the adsorption of phosphate on the iron oxide. Simultaneously, the bands assigned to arsenate species decreased slightly in intensity as expected due to some replacement of pre-adsorbed arsenate by phosphate species. However, the pre-adsorbed arsenate species were relatively stable against substitution for phosphate. The frequency position and band shape of the infrared spectra due to arsenate adsorption remained constant during the experiment indicating that the arsenate complex formed on the iron oxide surface did not change upon desorption. The difference in band features at pD 4 as compared to pD 8.5 are most likely a result of de-deuteration of the arsenate complexes at higher pD [9].

Fig. 11 summarizes the adsorption/desorption kinetics based upon all spectra recorded where arsenate was pre-adsorbed onto the iron oxide surface. As observed when phosphate was pre-adsorbed (Fig. 8), the initial adsorption of arsenate was faster at pD 8.5 than at pD 4. The amount of arsenate adsorbed on the iron oxide did not reach an equilibrium plateau value but the slope of the absorbance versus time plot was steeper at pD 4 than at pD 8.5 beyond the initial adsorption (>50 min). Assuming that the arsenate complexes at pD 4 and pD 8.5 have similar molar absorptivities, the concentration of surface complexes adsorbed on the iron oxides after 5 h was higher at pD 4 than at pD 8.5. The higher adsorption at low pD is most probable caused by the surface charge since the more negatively charged surface at high pD should reduce the adsorption of the negatively charged anions. The point of zero charge for this iron oxide was previously determined to be between 7.5 and 8.5. Consequently, at pD 4 the iron oxide surface is positively charged whereas it is neutral-to-negative at pD 8.5. Adding phosphate to the system implied that arsenate desorbed from the surface at both pD 8.5 and pD 4 but only to a minor extent compared to the reverse situation where phosphate was pre-adsorbed.

The relative desorption of pre-adsorbed arsenate caused by the aqueous phosphate solution was estimated to be ~10% at pD 4 and ~20% at pD 8.5, whereas the relative desorption of pre-adsorbed phosphate caused by arsenate was ~35% at pD 4 and ~45% at pD

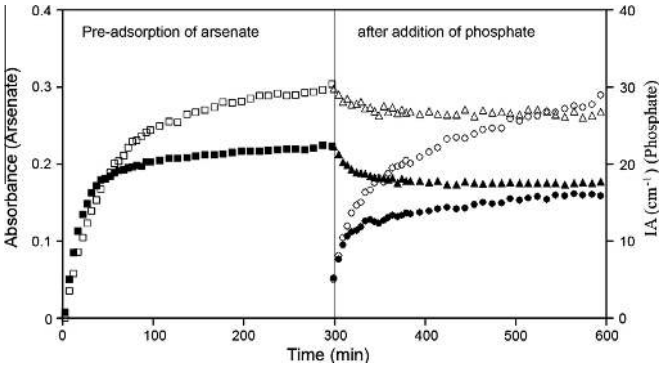

Fig. 11. The figure shows the absorbance of the band at 840 cm^{-1}, assigned to adsorbed arsenate, versus time at both pD 8.5 (■) and pD 4 (□). After 300 min of arsenate adsorption, phosphate was added yielding a solution with equal (molar) concentration (0.03 mM) in phosphate and arsenate. The desorption of arsenate at the two pD-values is shown; pD 8.5 (▲) and pD 4 (Δ). The rate of phosphate adsorption was monitored for 300 min and is shown as the integrated absorbance (IA) between 1200 and 950 cm^{-1} as a function of time; pD 8.5 (●) and pD 4 (○).

8.5. Since a relatively smaller fraction of pre-adsorbed arsenate was replaced at both pD-values, it can be concluded that arsenate was more strongly adsorbed than phosphate. However, the absolute amounts of phosphate and arsenate adsorbed on the iron oxide film can not be compared, since the molar absorptivities of the two species may be different.

The results above showed that arsenate complexes adsorbed on iron oxide were more stable than the adsorbed phosphate complexes at the two pD-values studied. However, the fraction of adsorbed arsenate should vary with increasing the phosphate concentration in solution. Therefore another exchange experiment was performed in order to assess the stability of arsenate complexes at significantly higher phosphate concentrations in solution, a concentration that may be more realistic from a soil stabilization perspective.

To elucidate the influence of phosphate concentration, arsenate was pre-adsorbed on the iron oxide film from a 0.03 mM solution for 5 h as in the previous experiments. Subsequently, phosphate was added to the solution yielding a phosphate concentration of 0.15 mM i.e. five times higher than in the previous experiments. Fig. 12 shows the intensity of the arsenate band at ~840 cm^{-1} plotted vs. time at the two pD-values. For comparison, the desorption kinetics obtained at an aqueous phosphate concentration of 0.03 mM is also shown in Fig. 12. As expected, arsenate desorbed to a larger extent when the concentration of phosphate in the solution was higher. At pD 4, the relative desorption of pre-adsorbed arsenate complexes from the iron oxide film was ~30% of the initial value, whereas at pD 8.5, only about 50% of the initial amount remained after 5 h. As a comparison, the corresponding values at a phosphate concentration of 0.03 mM were 10% and 20% at pD 4 and 8.5, respectively. This confirms the findings that arsenate was much more strongly adsorbed than phosphate at both pD's.

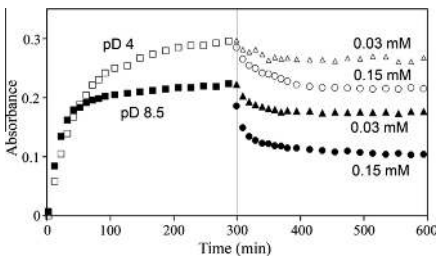

Fig. 12. The absorbance of the arsenate band at 840 cm^{-1} plotted as a function of time. Arsenate was adsorbed from a 0.03 mM aqueous arsenate solution; pD 8.5 (■) and pD 4 (□). At t = 300 min, phosphate was added to make a 0.15 mM phosphate solution. The concentration of arsenate was kept constant at 0.03 mM. The desorption of arsenate from ferrihydrite at pD 4 and pD 8.5 is shown. Phosphate concentrations in the bulk solution are indicated in the figure.

4. Conclusions

The method developed by the authors, based on ATR–FTIR spectroscopy using D_2O as a solvent, showed to be very suitable in order to study the competitive adsorption of arsenate and phosphate onto synthetic ferrihydrite. Indeed, to the best of our knowledge, this is the first study in which the arsenate and phosphate complexes formed on the iron oxide surface have been monitored simultaneously during adsorption/desorption, by using ATR–FTIR spectroscopy.

Evaluation of infrared spectra as a function of adsorption time clearly indicated that the initial rate of adsorption of phosphate as well as arsenate was higher at pD 8.5 as compared with pD 4. During an adsorption time of 300 min neither of the two ionic species reached an equilibrium plateau value. Interestingly, the two phosphate complexes detected on the iron oxide surface at pD 4 showed different adsorption/desorption rates. The first adsorbed phosphate complex was the one that was first out-competed by the arsenate ions. Difference spectra showed that only absorption bands assigned to the deuterated complex (1124, 1035, and 998 cm^{-1}) appeared in the difference spectrum indicating that the de-deuterated complex (1084 and 1014 cm^{-1}) was more firmly attached under the pD conditions of the experiments.

It was also shown that the amount of arsenate and phosphate increased from pD 8.5 to pD 4. However, arsenate complexes showed to be more strongly adsorbed on the iron oxide than phosphate complexes. A five fold increase of the aqueous phosphate concentration implied that about 30% of the originally adsorbed arsenate was desorbed at pD 8.5 and much less at pD 4.

The results of this work confirmed that the pD (pH in a natural system) and the aqueous phosphate concentration in natural systems are critical parameters, which must be controlled in order

to prevent leaching of arsenic to the environment from pre-adsorbed arsenic on iron oxide. The results are therefore of importance in soil remediation or in water purification applications using ferrihydrite as adsorbent.

Acknowledgments

The Swedish Research Council Formas and The Knut and Alice Wallenberg Foundation are gratefully acknowledged for financial support. Dr. Johanne Mouzon and Dr. Jurate Kumpiene are also acknowledged for valuable discussions on this work.

References

[1] Air Quality Guidelines for Europe, WHO Regional Publications, European Series No. 91, 2000.
[2] D. Mohan, C.U. Pittman, J. Hazard. Mater. 142 (1–2) (2007) 1–53.
[3] B. McAuley, S.E. Cabaniss, Anal. Chim. Acta 581 (2) (2007) 309–317.
[4] J. Kumpiene, S. Ore, G. Renella, M. Mench, A. Lagerkvist, C. Maurice, Environ. Pollut. 144 (2006) 62–69.
[5] M. Mench, J. Vangronsveld, C. Beckx, A. Ruttens, Environ. Pollut. 144 (2006) 51–61.
[6] J. Boisson, A. Ruttens, M. Mench, J. Vangronsveld, Environ. Pollut. 104 (1999) 225–233.
[7] X. Cao, L.Q. Ma, Environ. Pollut. 132 (2004) 435–442.
[8] A. Shiralipour, L.Q. Ma, R.X. Cao, Effects of Compost on Arsenic Leachability in Soils and Arsenic Uptake by a Fern, University of Florida, Gainesville, FL, 2002 (Report #02-04).
[9] I. Carabante, M. Grahn, A. Holmgren, J. Kumpiene, J. Hedlund, Colloid Surf. A 346 (2009) 106–113.
[10] J. Gimenez, M. Martinez, J. De Pablo, M. Rovira, J. Hazard. Mater. 141 (3) (2007) 575–580.
[11] D.M. Sherman, Geochim. Cosmochim. Acta 67 (22) (2003) 575–580.
[12] S. Fendorf, M.J. Eick, P. Grossl, Environ. Technol. 31 (2) (1997) 315–320.
[13] A. Manceau, Geochim. Cosmochim. Acta 59 (17) (1995) 3647–3653.
[14] G. Waychunas, B.A. Rea, Geochim. Cosmochim. Acta 57 (10) (1993) 2251–2269.
[15] J.S. Loring, M.H. Sandström, K. Norén, P. Persson, Chem. Eur. J. 15 (2009) 5063–5072.
[16] D.G. Lumsdon, A.R. Fraser, J.D. Russel, N.T. Livesey, Soil Sci. 35 (1984) 381–386.
[17] Y. Arai, D.L. Sparks, J. Colloid Interface Sci. 24 (2001) 317–326.
[18] C. Luengo, M. Brigante, J. Antelo, M. Avena, J. Colloid Interface Sci. 300 (2006) 511–518.
[19] M.I. Tejedor-Tejedor, M.A. Anderson, Langmuir 6 (3) (1990) 602–611.
[20] J. Antelo, M. Avena, S. Fiol, R. Lopez, F. Arce, J. Colloid Interface Sci. 285 (2) (2005) 476–486.
[21] F. Liu, A. De Cristofaro, A. Violante, Soil Sci. 166 (3) (2001) 197–208.
[22] F. Frau, R. Biddau, L. Fanfani, Appl. Geochem. 23 (6) (2008) 1451–1466.
[23] H. Zeng, B. Fisher, D.E. Giammar, Environ. Sci. Technol. 42 (1) (2008) 147–152.
[24] J.S. Zhang, R. Stanforth, S.O. Pehkonen, J. Colloid Interface Sci. 317 (1) (2008) 35–43.
[25] K. Axe, M. Vejgarden, P. Persson, J. Colloid Interface Sci. 294 (1) (2006) 31–37.
[26] A. Fredriksson, A. Holmgren, Colloid Surf. A 302 (2007) 96–101.
[27] M. Grahn, A. Lobanova, A. Holmgren, Chem. Mater. 20 (19) (2008) 6270–6276.
[28] M.L. Larsson, A. Fredriksson, A. Holmgren, J. Colloid Interface Sci. 273 (2004) 345–349.
[29] A. Roddick-Lanzilota, A.J. McQuillan, Appl. Geochem. 17 (4) (2002) 445–454.
[30] F.M. Mirabella, Internal Reflection Spectroscopy: Theory and Applications, Marcel Dekker, 1993.
[31] R.M. Cornell, U. Schwertmann, The Iron Oxides: Structure, Properties, Reactions, Ocurrences and Uses, VCH, Weinheim, 1996.
[32] K.P. Raven, A. Jain, R.H. Loeppert, Environ. Sci. Technol. 32 (3) (1998) 344–349.
[33] C. Luengo, M. Brigante, M. Avena, J. Colloid Interface Sci. 311 (2) (2007) 354–360.

Paper IV

Influence of Zn (II) on the adsorption of arsenate onto ferrihydrite

I. Carabante, M. Grahn, A. Holmgren, J. Kumpiene, J. Hedlund

Submitted to Environmental Science and Technology.

Influence of Zn(II) on the adsorption of arsenate onto ferrihydrite

Ivan Carabante [a*], Mattias Grahn [a], Allan Holmgren [a], Jurate Kumpiene [b] and Jonas Hedlund [a]

[a]*Chemical Technology, Luleå University of Technology, SE-97187, Luleå, Sweden*

[b]*Division of Geoscience and Environmental Engineering, Luleå University of Technology, SE-97187, Luleå, Sweden*

Abstract

Addition of iron oxide to arsenic contaminated soil has been proposed as a means of reducing the mobility of arsenic in the soil. Arsenic and zinc are common co-existing contaminants in soils. The presence of zinc therefore may affect the adsorption properties of arsenic on iron oxide, and may thus affect its mobility in the soil. The influence of Zn(II) on the adsorption of arsenate ions on iron oxide was studied.

Batch adsorption experiments indicated that Zn(II) increased the arsenate removal from a solution by ferrihydrite at pH 8. However, ATR-FTIR spectroscopy showed that no adsorption of arsenate on a ferrihydrite film occurred at pD 8 in the presence of Zn(II). Precipitation of zinc hydroxide carbonate followed by arsenate adorption onto the precipitate was found to be a plausible mechanism explaining the arsenate removal from a solution in the presence of Zn(II) at pH/pD 8. The previously suggested mechanisms attributing the enhanced removal of arsenate from solution in the presence of Zn(II) to additional adsorption on iron oxides could not be verified under the experimental conditions studied. It was also shown that at pH/pD 4, the presence of Zn(II) in the system did not significantly affect the adsorption of arsenate on ferrihydrite.

1 Introduction

Iron oxides show a high adsorption capacity towards arsenic (V) oxoanions.[1-3] Therefore, the addition of iron oxide to soil has been proposed as a remediation technique to reduce the leachability of arsenic from contaminated soils, for instance, CCA (chromate, copper, arsenate) contaminated soils.[4] However, changes in chemical parameters of the soil such as redox potential, pH or concentration of ions that adsorb competitively on iron oxides may increase the mobility of previously immobilized arsenic.

The adsorption of arsenate on iron oxide is pH dependent, with larger adsorption at low pH values (around pH 4) than at higher pH values (around pH 8) and therefore an increase in the pH value in the soil may lead to desorption of arsenic from the iron oxide.[5] A more extensive knowledge of the different chemical parameters

which could affect the leaching of arsenic from iron oxide stabilized soils is crucial to establish amendment of arsenic contaminated soil by iron oxides as a standard remediation technique.[4]

Arsenic contaminated soils often contain high concentrations of zinc, e.g. soils exposed to leaching water from mine tailings and CCA contaminated soils, since CCA often contained zinc oxide or zinc sulphate. [6-7] The presence of Zn(II) could affect the adsorption/desorption properties of arsenate on iron oxides and it is therefore important to study the Zn(II) / arsenate / iron oxide system.

Arsenic speciation on CCA contaminated soils was studied, concluding that arsenic was mostly bonded to Cu precipitates as well as to goethite (iron oxy-hydroxide).[8]

The co-adsorption of Zn(II) and arsenate ions on iron oxide (goethite) has been studied by means of batch experiments and subsequent analysis of the aqueous phase after separation.[6] It was reported that the adsorption of arsenate on goethite was enhanced by 30% at pH 4 and by more than 500% at pH 7 in the presence of Zn(II). [6] Complementary EXAFS measurements were performed in order to explain the results obtained by batch adsorption experiments. It was proposed that arsenate could form bridging complexes on iron and zinc sites at lower concentrations while the subsequent co-precipitation of Zn(II) and arsenate on the hydroxyl groups of the iron oxide could form a surface precipitate ($Zn_2(AsO_4)OH$) at higher concentrations.[6] The adsorption of arsenate on magnetite in the presence of Zn(II) has also been studied by means of batch adsorption experiments and an enhanced adsorption of arsenate at pH 8 was reported whereas no effects of zinc on the arsenate adsorption on magnetite at pH 4 were reported.[9] Moreover, it was concluded that the formation of a ternary zinc-arsenate-iron oxide complex was the most plausible explanation for the enhanced adsorption of arsenate onto magnetite at pH 8.[9] Cu(II) ions and arsenate were also found, by means of EXAFS measurements, to form surface precipitates on the goethite surface, enhancing arsenate removal at pH 5.65.[10]

The Zn(II)/arsenate / ferrihydrite system in aqueous (H_2O/D_2O) suspension was studied by means of batch adsorption experiments and in situ Attenuated Total Reflection - Fourier Transform Infrared (ATR-FTIR) spectroscopy. These two complementary techniques enabled the study of the processes involved in the arsenate removal from aqueous solution in the presence of Zn(II).

2 Experimental

2.1 Batch experiments

Iron oxide in the form of ferrihydrite nanoparticles were synthesized following the method previously described by McComb et al.[11] 1 ml of an aqueous 0.7 M iron chloride ($FeCl_3 \cdot 6H_2O$, Riedel-de Haën, >99%) solution was added dropwise to 50 ml of boiling distilled water and the solution was allowed to boil for 5 minutes. During this time, ferrihydrite nanoparticles were formed. The synthesis solution was dialyzed against distilled water using a polymeric membrane (MWCO 12-14000; Spectra/Por Dialysis membrane; Spectrum laboratories) in order to remove remaining ions (iron, chloride) from the synthesis solution.

Two batch adsorption experiments were first performed without any Zn(II), one at pH 4 and the other one at pH 8. The concentration of ferrihydrite was 56 mg/l and the concentration of arsenate ($NaH_2AsO_4 \bullet 7H_2O$; Fluka; p.a. 98.5%) was 0.06 mM. Two more batch adsorption experiments, at the same pH values, were performed using the same concentrations of ferrihydrite and arsenate and with a concentration of 1.2 mM of Zn(II) ($ZnCl_2$; Merck;

p.a. 98 %). Four additional experiments were performed in the absence of ferrihydrite at pH 8. First, 0.06 mM arsenate was in solution with either 0.06 mM Zn(II), or 1.2 mM Zn(II), and the precipitate that formed was collected by centrifugation, redispersed in distilled water at pH 8 and then freeze dried. Finally, 0.06 mM arsenate in a 650 mg/l suspension of either zinc hydroxide carbonate ($Zn_x(CO_3)_y(OH)_z$, Merck; p.a. 98%, the Zn content of the salt was 58%) or zinc oxide (ZnO; Merck;p.a. 99.0%).

All batch experiments were carried out for 72h to ensure that equilibrium was established and the pH values of the suspensions were controlled and adjusted every 24 hours. After the experiment, the solid phase was removed by filtration using a 0.2 µm cellulose acetate filter (FP30/0,2 CA-S, Whatman). The remaining concentration of arsenic and zinc in the filtrate was determined by means of Induced Coupled Plasma – Optical Emission Spectroscopy (ICP-OES, Perkin Elmer optima 2000 DV). Blank experiments with and without ferrihydrite and without filtering were also performed to obtain the initial arsenic and Zn concentration prior to adsorption, as well as to rule out filtration as a reason for the decrease in the concentration of arsenic or zinc in the supernatant.

2.2 In situ ATR-FTIR measurements

The dispersion of ferrihydrite nanoparticles obtained after purification by dialysis was diluted adding 50 wt. % methanol (CH_3OH; Kebo lab, >99.8 %). A 500 µl drop of the diluted suspension was spread on both sides of the ATR crystal (Crystran, ZnSe, 52×20×2 mm with 45° cut edges). After the drop had dried, a thin layer of ferrihydrite coated each side of the ATR crystal. The ATR-FTIR spectrum of the ferrihydrite film in vaccum showed no detectable bands originating from methanol.

A film of zinc hydroxide carbonate on an ATR crystal was prepared by spreading 200 µl of a 400 mg/l solution of the zinc hydroxide carbonate on only one side of the ATR crystal. The same procedure was used to obtain a zinc oxide (ZnO; Merck;p.a. 99.0%) film on the ATR crystal.

ATR-FTIR spectra were recorded using a Bruker IFS 66v/s spectrometer equipped with a DTGS (Deuterated Tryglicine Sulphate) detector by co-adding 200 scans at a resolution of 4 cm^{-1} and a zero-filling factor of two. The in situ ATR-FTIR measurements were performed using the same experimental set up described in detail in a previous report.[5] Briefly, the solution containing the arsenate and/or Zn(II) was kept in a beaker where the pD of the solution was controlled by an automatic pH controller (Metler Toledo, T70 pH-stat). The solution was continuously pumped into the flow cell inserted in the FTIR spectrometer and subsequently re-circulated to the beaker. The ATR crystal coated with ferrihydrite film was assembled in the flow cell situated inside the spectrometer, where the flowing solution was in contact with the film. Deuterium oxide (D_2O, Aldrich, 99 atom % D) was used as a solvent in order to decrease the spectral noise that water would cause due to absorption of infrared radiation in the spectral region below 1000 cm^{-1}. Before each adsorption experiment, a single beam background spectrum was recorded after an equilibration time of 5 hours between a 0.1 M sodium chloride (0.1 M NaCl, Merck; 99.5%) solution in D_2O and the ferrihydrite film in the flow cell. A small volume of a stock solution of either arsenate or Zn(II) was first added to the ionic medium. After 5 hours, the other ion was added to the solution and spectra were recorded every 5 minutes during the course of the adsorption experiments. The concentration of arsenate in solution after addition of the stock solution was 0.03 mM. The concentrations for Zn(II) were 0.03 mM or 1.2 mM.

2.3 Characterisation

The particle size in the purified suspension of 6-line ferrihydrite was measured by Dynamic Light Scattering (DLS) using a Malvern, Zetasizer nano ZS instrument. The iron oxide film and the freeze dried precipitate were analysed by Scanning Electron Microscopy/Energy Dispersive X-ray Spectroscopy (SEM/EDS) using a Magellan 400 field emission XHR-SEM equipped with a 80 mm^2 Oxford X-max EDS detector. The samples were not coated. Images were recorded using an accelerating voltage of 3kV, and 20 kV was used when recording spectra. X-ray diffraction data were recorded with a PANalytical Empyrean instrument, equipped with a PIXcel3D detector and a Cu LFF HR X-ray tube. Diffuse Reflectance Infrared-Fourier Transform Spectroscopy (DRIFT) data of the precipitate was recorded with a Bruker IFS 66v/s spectrometer equipped with a DTGS (Deuterated Tryglicine Sulphate) detector by co-adding 124 scans at a resolution of 4 cm^{-1}. Adsorptionof N_2 at 77K on the precipitate, zinc hydroxide carbonate and zinc oxide was measured using a Micrometrics ASAP 2010 after degassing at 250°C.

3 Results and Discussions

3.1 Batch adsorption experiments

The results of batch adsorption experiments are summarized in Table 1

3.1.1 Arsenate removal by ferrihydrite

At both pH values studied, the concentration of arsenate in solution (supernatant) was considerably reduced from the initial concentration of 60 μM by the presence of ferrihydrite suspended in solution. Arsenate removal was greater at pH 4 than at pH 8, with a final arsenate concentration in solution of 4.1 μM and 11.1 μM, respectively (Table 1, batch experiments 1 and 2). These results agree with previously reported data.[5] At lower pH values, ferrihydrite surface is positively charged and electrostatic attraction between the surface and the oxoanion would facilitate adsorption on the ferrihydrite surface.[5,12]

3.1.2 Effect of Zn(II) on the arsenate removal at pH 8

The presence of Zn(II) in the system (1200 μM) considerably enhanced the removal of arsenate from solution at pH 8, with a concentration of arsenate in the supernatant of 11.1 μM in the absence of Zn(II), and 2.3 μM in the presence of Zn(II) (batch experiments 2 and 4). In the latter case, the concentration of Zn(II) was also reduced from 1200 μM to 45.8 μM. These results are in agreement with previously reported data.[6,9] In those previous works, [6,9] the formation of ternary complexes of zinc, arsenate and iron oxide was suggested as the most likely explanation for the enhanced arsenate adsorption on iron oxide by Zn(II). An experiment was also performed without any ferrihydrate (batch experiment 5). A decrease in the concentration of both ions in solution, from 60 μM to 7.0 μM for arsenate and from1200 μM to 41.2 μM for Zn(II), was observed. The final concentrations are only slightly higher than the corresponding concentrations in the presence of ferrihydrite. From this observation,

it is reasonable to conclude that only the presence of Zn(II) at high concentrations could reduce the aqueous arsenate concentration, and thus the ternary zinc–arsenate-ferrihydrite complex, previously reported,[6,9] may not be the only possible mechanism explaining the arsenate removal in the zinc-arsenate-ferrihydrite system.

However, when the initial concentration of Zn(II) was reduced to 60 μM (without ferrihydrate) only a slight decrease in the concentration of arsenate was observed, from 60 to 55.7 μM (batch experiment 6). On the other hand, the concentration of Zn(II) decreased to 22.7 μM, which suggests that Zn(II) precipitates.

Moreover, a reduction in the concentration of Zn(II) (without arsenate and ferrihydrite) from an initial concentration of 1200 μM to 34.5 μm (batch experiment 7) was observed. The concentration of Zn(II) also decreased to 29.6 μM when the initial Zn(II) concentration was 60 μM (batch experiment 8) which is about the same as the reduction observed in the presence of arsenate (batch experiment 6). These results again suggest that Zn(II) formed a precipitate.

To investigate the precipitation of Zn(II) further, an aqueous system comprising 0.1 M NaCl, 60 μM arsenate and 1200 μM Zn(II) in contact with a non-absorbing gas having a CO_2 partial pressure of 0.00038 atm, i.e. as in ambient air, was simulated in the pH range from 3 to 10, using the chemical equilibrium modelling software, Visual Minteq (version 3.0, beta).[13] The calculations result in the saturation index. Positive values for the saturation index of a solid phase indicate that precipitation of this phase is thermodynamically favoured whereas negative values of the saturation index indicate that the formation of the precipitate is not thermodynamically favoured. It was found that formation of zinc carbonate, especially hydrozincite ($Zn_5(OH)_6(CO_3)_2$) was the most thermodynamically favoured phase between pH 8 and 10. The formation of zinc oxides, e.g. zincite, was also thermodynamically favoured in the pH range 8 -10. The formation of zinc arsenate at pH 8 could not completely be ruled out, since the saturation indexes for this phase were very close to 0, although negative. The saturation indexes for the different phases vs. pH (Figure S1, Supporting Information) are in agreement with published data in which the predominant phase in a 100 μM aqueous Zn(II) solution was calculated to be a solid phase of $ZnCO_3$, $Zn_5(OH)_6(CO_3)_2$ or ZnO, depending on the CO_2 pressure, at pH values higher than 7.5.[14] Figure 1 (a) shows the DRIFT spectrum recorded of the precipitate formed from a 60 μM arsenate and 1200μM Zn(II) solution at pH 8. An ATR-FTIR spectrum (b) was recorded of a film prepared from a commercial zinc hydroxide carbonate. Both spectra showed very similar bands situated at 1300 to 1500 cm^{-1} assigned to carbonate asymmetric stretching modes, a band at 1040 cm^{-1} corresponding to the symmetric stretching vibration and a band at 835 cm^{-1} assigned to the carbonate out-of-plane bending mode.[15] The spectroscopic data thus suggest that the precipitate formed in solution was zinc hydroxide carbonate.

Figure 2 shows the XRD pattern recorded of the precipitate and for commercial ZnO and $Zn_x(CO_3)_y(OH)_z$. The peak positions and relative intensities of the main peaks for the precipitate agreed well with those for the commercial ZnO, while the broad peaks of low intensity at about 13, 33 and 60 degrees most likely stem from zinc hydroxide carbonate. The sinuous baseline of the diffractogramm from the precipitate shows that XRD-amorphous material was also present in the precipitate. The amorphous signal may originate from the zinc hydroxide carbonate identified by DRIFT. Figure 3 shows SEM images of the precipitate. Two different kinds of aggregates were observed, star shaped and irregular aggregates. Two star-like aggregates are illustrated in the low magnification image (a), one of which is indicated with a white circle. However, the SEM image shown in (a) is

not a representative image, since the number of star-like aggregates was small. The high magnification SEM images (b, c) reveal that the particles with irregular shape were comprised of smaller crystals with a platelet habit. This habit has previously been reported as typical for hydrozincite.[16] The star-like aggregates on the other hand were comprised by small particles with a cubic habit. This habit have previously been reported for ZnO particles.[16,17] EDS spectra (Figure S2-S3, Supporting Information) from the two types of aggregates indicated that the content of Zn and O was higher in the star-like aggregates supporting the morphological identification of the two phases. EDS spectra also showed a higher content of As in the irregular shaped aggregates, zinc hydroxide carbonate, than in the star-like aggregates, zinc oxide.

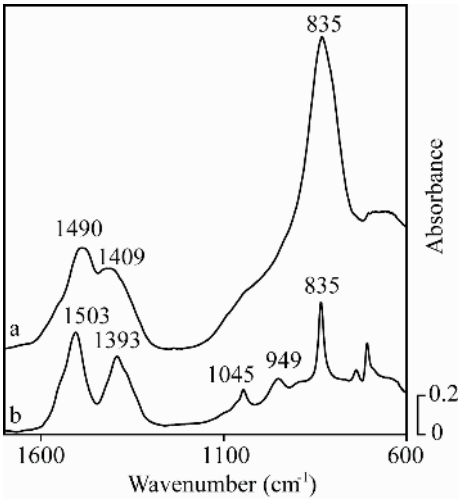

Figure 1. (a) DRIFT spectrum of the precipitate formed from a 60 μM arsenate and 1200μM Zn(II) solution at pH 8. (b) ATR-FTIR spectrum recorded of a film prepared from a commercial zinc hydroxide carbonate ($Zn_x(CO_3)_y(OH)_z$, Merck; p.a. 98%, corresponding to a Zn content of 58%).

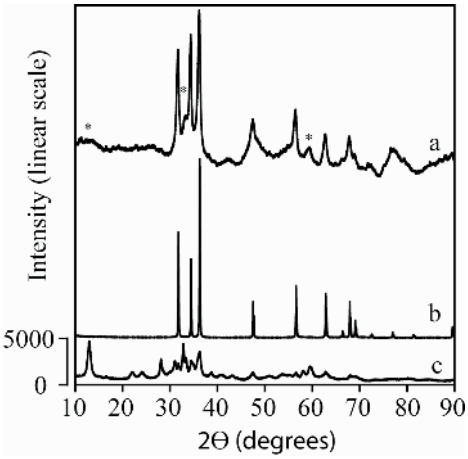

Figure 2. X-ray diffractogramm (a) of the precipitate formed from a 60 µM arsenate and 1200µM Zn(II) solution at pH 8, (b) of commercial zinc oxide and c) of commercial zinc hydroxide carbonate. Peaks labelled with an asterisk in diffractogramm (a) correspond to the positions 13, 33 and 60. Notice that the intensity in diffractogramm (b) is divided by a factor of 3.

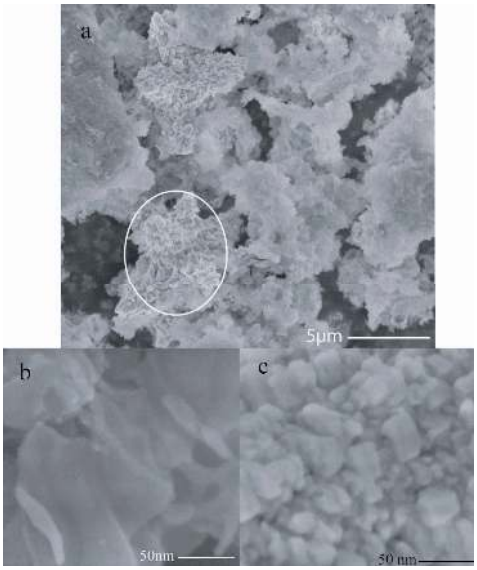

Figure 3. a) Low magnification SEM image of the precipitate formed from a 60 µM arsenate and 1200µM Zn(II) solution at pH 8. The white circle indicates a star-like aggregate found in the sample. b) and c) High magnification SEM image of the particles composing the irregular shaped aggregates and the star-like aggregates, respectively.

It was shown that zinc hydroxide carbonate and zinc oxide precipitated at pH 8 (60 µM arsenate and 1200µM Zn(II)) and the removal of arsenate from solution was also enhanced in the presence of only Zn(II) at this pH

value. A batch experiment with a suspension of $Zn_x(CO_3)_y(OH)_z$ (650 mg/l) and arsenate (60 µM) in solution therefore was performed at pH 8 in order to assess its influence in the removal process. The arsenate concentration decreased to 5.6 µM and the final concentration of Zn(II) was 0.09 µM (batch experiment 9). This result indicates that the arsenate ions interact with the solid, possibly by adsorbing to the solid zinc hydroxide carbonate.

A similar batch experiment was carried out albeit substituting the zinc hydroxide carbonate for zinc oxide (650 mg/l). In this case, the concentration of arsenate decreased to 35.6 µM whereas the Zn(II) concentration was 0.5 µM (batch experiment 10). This indicates that the arsenate ions may also interact with the solid zinc oxide.

To conclude, the removal of arsenate at pH 8 was enhanced by the presence of Zn(II) in the system. The interaction of arsenate with zinc precipitates, such as zinc hydroxide carbonate, zinc oxide or the precipitation of zinc arsenates may be the possible mechanism explaining the arsenate removal by Zn(II) at pH 8. However, the presence to a lower extent of surface complexes of zinc, arsenate and iron oxide, as has been reported earlier[6,9] cannot be dismissed.

3.1.3 Effect of Zn(II) on the arsenate removal at pH 4

At pH 4, the presence of Zn(II) had no significant effect on the removal of arsenate from solution using ferrihydrite, since the final concentration of arsenate in the supernatant was 4.1 µM in the absence of Zn(II) and 5.8 µM in the presence of Zn(II) in the system (batch adsorption experiments 1 and 3). This result is in agreement with previously reported data for ferrihydrite.[9] However, in another study using goethite as adsorbent, a slight improvement of arsenic removal was observed in the presence of Zn(II). The use of a different iron oxide phase might explain the differences from our results.

Table 1. Summary of experimental conditions and final ion concentration for the batch adsorption experiments.

Experimental conditions (initial concentrations)							Final concentrations	
Batch experiment	As µM	Zn µM	Ferrihydrite mg/l	$Zn_x(CO_3)_y(OH)_z$ mg/l	ZnO mg/l	pH	As µM	Zn µM
1	60	-	56	-	-	4	4.1	< 0.03
2	60	-	56	-	-	8	11.1	< 0.03
3	60	1200	56	-	-	4	5.8	1136
4	60	1200	56	-	-	8	2.3	45.8
5	60	1200	-	-	-	8	7.0	41.2
6	60	60	-	-	-	8	55.7	22.7
7	-	1200	-	-	-	8	< 0.01	34.5
8	-	60	-	-	-	8	< 0.01	29.6
9	60	-	-	650	-	8	5.6	0.09
10	60	-	-	-	650	8	35.6	0.5

3.2 In situ ATR-FTIR measurements

Films of ferrihydrite, zinc hydroxide carbonate and zinc oxide were probed using in situ ATR-FTIR spectroscopy in order to obtain information on species adsorbed on the surface of the films. The results from these experiments may give a hint about which processes occur and to their extent.

SEM images of the ferrihydrite film on a ZnSe ATR element showing that the ferrihydrite film comprised particles smaller than 10 nm and that the film thickness was about 250nm (Figure S4, Supporting Information). The average size of the ferrihydrite particles was determined to about 8 nm by DLS, which confirmed the SEM observations regarding particle size. The specific surface area of the freeze dried powder obtained from this synthesis route was estimated to be 190 m2/g by means of N_2(g) adsorption and the iron oxide phase was determined to be 6-line ferrihydrite by means of XRD.[5]

3.2.1 Effect of Zn(II) on the arsenate adsorption on ferrihydrite at pD 8

A solution containing only 0.03 mM arsenate was in contact with the ferrihydrite film for 5 hours and a spectrum was then recorded, see spectrum (a) in Figure 4. This Figure shows the spectral region between 1000 cm^{-1} to 700cm^{-1} since no interesting features were observed elsewhere, besides negative bands appearing in the 1600 to 1200 cm-1 range corresponding to desorbed carbonate species from ferrihydrite.[5]. Two broad absorption bands at about 855 and 830 cm^{-1} which were previously assigned to adsorbed arsenate species on deuterated ferrihydrite[5,18] and deuterated goethite,[19] were observed in the spectrum. The position of the bands, their band shapes and their relative intensity showed in the spectrum and the one observed for arsenate adsorbed on deuterated goethite[19] at the same pD value were very similar, indicating that the coordination environment of arsenate adsorbed on ferrihydrate and goethite was the same. As reported in a previous study,[5] arsenate species in solution were not detectable at a concentration below 1mM when the measurement were performed using the same equipment and the same ATR elements without any ferrihydrite coating. The spectrum of arsenate species in solution at pD 8 only showed a single band at about 856.[5,20] The bands originating from species adsorbed on ferrihydrite differed significantly from the arsenate species in solution and became somewhat broader.[5,19-20] Subsequently, Zn(II) (1.2 mM) were added to the solution, keeping the pD and the arsenate concentration constant. Spectrum (b) was recorded 5 hours after the addition of Zn(II). The intensity of the bands (855 and 830 cm^{-1}) assigned to adsorbed arsenate decreased slightly upon the addition of Zn(II), indicating that only a very small amount of arsenate species previously adsorbed on the ferrihydrite was desorbed after the addition of Zn(II). According to batch experiments (subsection 3.1.2), the addition of 1.2 mM Zn(II) to the arsenate-ferrihydrite system results in reduction of the concentration of arsenate ions in solution. However, a reduction in the arsenate concentration in solution may also cause a very slight desorption of arsenate from ferrihydrite as shown previously in desorption experiments by flushing the ATR cell with the pure solvent.[5] Accordingly, the reduction of arsenate concentration in solution upon addition of Zn(II) in the present work did not result in an increased arsenate sorption on the ferrihydrite film. Notice here that the intensity of the absorption bands should be proportional to the amount of species adsorbed onto ferrihydrite.[21] This statement is true provided that the infrared absorption from species in solution and the change of the refractive index of the sample with time can be neglected. Even though the intensity of the bands at about 855 cm^{-1} and 830 cm^{-1} decreased slightly upon desorption of arsenate, the bands

position and their relative intensity were constant with time, which indicates that the addition of Zn(II) did not change the chemical structure of the arsenate complexes formed on the ferrrihydrite surface.

To investigate if the order of addition of zinc and arsenate was important, an experiment was carried out where a solution containing only Zn(II) at a concentration of 0.03 mM was allowed to flow over the ferrihydrite film for 5 hours, after which arsenate at a concentration of 0.03 mM was introduced to the system while keeping the Zn(II) concentration and the pD of the solution constant. Spectrum (c) in Figure 4 was recorded 5 hours after the addition of arsenate to the solution. This spectrum shows two bands at about 855 and 830 cm^{-1} with a band shape slightly different from the bands discussed above, indicating that the arsenate species adsorbed had a slightly different chemical environment depending on the order of addition of the reactants Zn(II) and arsenate ions. The relative intensities of the two bands changed slightly, and they became better resolved. Simultaneously, the half-width of the band increased. A tentative explanation to this small difference may be that a co-precipitation/complexation of zinc and arsenate occurred on the surface of the ferrihydrite induced by the increase of their surface concentration, mainly due to pre-adsorbed Zn(II). Spectrum d, shown in Figure 4, was recorded after 5 hours of arsenate adsorption (0.03 mM at pD 8) when the ferrihydrite film had previously been exposed to a high concentration (1.2 mM) of Zn(II). No absorption bands were observed in the 900-800 cm^{-1} region of the spectrum, implying no adsorbed arsenate on the ferrihydrite surface. This indicates that a high concentration of Zn(II) prevents adsorption of arsenic on ferrihydrite, presumably due to the formation of a precipitate in solution involving arsenate ions as discussed above.

3.2.2 Spectroscopic evidence of the adsorption of arsenate on zinc hydroxide carbonate at pD 8.

While arsenate removal at pH 8 was enhanced by the presence of Zn(II) at a concentration of 1.2 mM according to batch experiments, in situ ATR-FTIR indicated no adsorption of arsenate on the ferrihydrite surface under the same conditions. The formation of zinc hydroxide carbonate or zinc oxide as discussed above, and the subsequent adsorption of arsenate on this phase might explain the differences in results between the batch- and ATR-FTIR experiments. Therefore, ATR-FTIR experiments using both a $Zn_x(CO_3)_y(OH)_z$ and a ZnO film were performed.

Figure 4 shows the spectrum recorded after 5 hours of contact between a 0.03 mM arsenate solution and a $Zn_x(CO_3)_y(OH)_z$ film (e). Negative IR absorption bands appeared at 950 cm^{-1} and 833 cm^{-1} and they were assigned to the $Zn_x(CO_3)_y(OH)_z$ as shown earlier in Figure 1. The appearance of these negative bands indicated that some particles from the film were re-suspended in the arsenate solution and/or that a small amount of the particles were dissolved. However, a broad band from about 900 cm^{-1} to 750 cm^{-1} was clearly distinguished in the spectrum. This band was assigned to arsenate species adsorbed on the $Zn_x(CO_3)_y(OH)_z$ surface. Arsenate ions free in solution at a concentration of 0.03 mM are not detected if the ATR crystal is not coated with any material,[5] such as ferrihydrite or zinc hydroxide carbonate. Moreover, the intensity of these bands located between 900 cm^{-1} and 750 cm^{-1} increased with adsorption time. Although the negative bands made the resolution of the vibrations bands originating from arsenate adsorbed on zinc hydroxyl carbonate difficult, the bands appeared to be rather similar to the ones originating from arsenate adsorbed onto ferrihydrite, spectrum a-c. Arsenate is known to

adsorb on ferrihydrite via the hydroxide group on its surface.[5,12,20] According to the similarities in spectral features, arsenate could possibly adsorb via the hydroxide group also on zinc hydroxyl carbonate. It was shown in subsection 3.1.2, by simulations, DRIFT, SEM/EDS and XRD that zinc hydroxide carbonate was formed at a Zn(II) concentration of 1.2 mM, pH/pD 8, and a 0.00038 atm pressure of CO_2. Furthermore the spectroscopic investigation showed that pre-addition of Zn(II) at this concentration prevented adsorption of arsenate on ferrihydrite. Adsorption of arsenate on zinc hydroxide carbonate thus may be a mechanism preventing the adsorption of arsenate on ferrihydrite. However, other mechanisms like precipitation of zinc arsenate cannot be completely dismissed.

A similar experiment in which the arsenate solution (0.03mM at pD8) was in contact with a ZnO film was also performed. After 5 hours of contact, spectrum (f) in Figure 4, was recorded. No bands in the spectral range between 900 cm^{-1} and 800 cm^{-1} could be observed indicating that no arsenate species adsorbed on the ZnO surface in detectable amounts. ZnO has previously been reported to show a very low arsenate adsorption capacity.[9] However, from the batch experiment presented in subsection 3.1.2, it was observed that the arsenate concentration was reduced in a ZnO suspension. No adsorption of arsenate on the ZnO film was observed (if there was any adsorption at all). An explanation might be that the specific surface area, as measured by nitrogen adsorption, of the commercial ZnO was much too low, i.e. 4.7 m^2/g. This is to be compared to the specific surface area of the commercial $Zn_x(CO_3)_y(OH)_z$ which was 71.2 m^2/g.

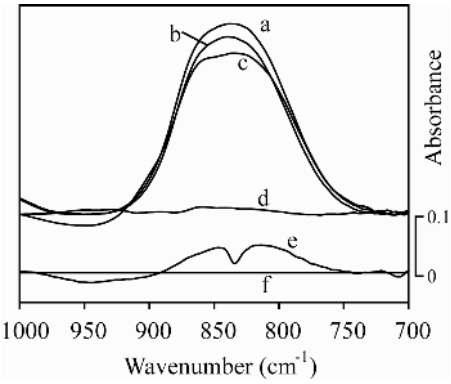

Figure 4. a) Spectrum of arsenate adsorbed on the ferrihydrite film from a 0.03 mM solution at pD 8 after 5h. Thereafter, 1.2 mM Zn(II) were added, and a spectrum b) was recorded 5h after the addition of Zn(II). c) and d) were the spectra recorded after 5 hours of arsenate adsorption from a solution of 0.03 mM at pD 8 when the film first had previously been equilibrated for 5 hours with 0.03 mM and with 1.2 mM Zn(II), respectively. ATR spectra recorded after 5 hours of contact between a 0.03mM arsenate solution at pD 8 and e) a $Zn_x(CO_3)_y(OH)_z$ film, f) a ZnO film.

In all the experiments performed at pH/pD 8 the presence of Zn(II) and the order of addition of the two ions to the system played an important role in the arsenate adsorption onto ferrihydrite. Pre-adsorbed arsenate species on ferrihydrite did not easily desorb from the ferrihydrite surface upon addition of Zn(II). On the other hand, when a high concentration of Zn(II) was added prior to arsenate addition, arsenate did not adsorb on the ferrihydrite even at a high zinc concentration (1.2 mM). The formation of zinc hydroxide carbonate at this pD was found to play a crucial role in the arsenate speciation of the system studied, since spectroscopic evidences indicated the

adsorption of arsenate ions on zinc hydroxide carbonate, whereas no adsorption of arsenate on ZnO was detected. The results presented here are important if an arsenic contaminated soil is to be remediated by the addition of ferrihydrite based adsorbents. The speciation of zinc in the soil prior to the remediation may be one of the factors leading to the success/failure of the subsequent remediation.

3.2.3 Effect of Zn(II) on the adsorption of arsenate on ferrihydrite at pD 4

The effect of Zn(II) and the order in which Zn(II) was added to the solution on the adsorption of arsenate on the ferrihydrite film at pD 4 was also investigated. A solution containing only arsenate (0.03 mM) was first added and the adsorption of the anion on the ferrihydrite film took place during 5 hours, after which spectrum (a), shown in Figure 5, was recorded. This Figure shows the spectral region between 950 cm^{-1} to 750cm^{-1} since no interesting features were observed elsewhere, besides negative bands appearing in the 1600 to 1200 cm-1 range, corresponding to desorbed carbonate species from ferrihydrite.[5] Two broad bands, situated at 875 cm^{-1} and 840 cm^{-1}, previously assigned to adsorbed arsenate on the deuterated surfaces of ferrihydrite[5,18] and goethite[19] were observed in the spectrum. The position of the bands, band shapes and their relative intensity showed in the spectrum and the one observed for arsenate adsorbed on deuterated goethite[19] at the same pD value agreed, indicating that the adsorbed arsenate coordination was the same on ferrihydrite as on goethite. As reported in a previous study,[5] arsenate species in solution were not detectable at concentrations below 1mM using uncoated ATR elements. At higher concentration, the arsenate species in solution at pD 4 showed three absorption bands originating from As-O stretching with peaks at 908 cm^{-1}, 875 cm^{-1} and 730 cm^{-1}.[5,20] The spectral feature was very different from the broad feature shown in Figure 5 a), indicating that the latter bands stem from adsorbed species.[20] The position of the two bands originated from adsorbed species at pD 4 were shifted to higher wavenumber as compared to the bands observed for arsenate adsorbed on ferrihydrite at pD 8 (855 and 830 cm-1, Figure 4 spectrum a). The reason for this shift has been attributed to de-deuteration of the arsenate complexes adsorbed on the iron oxide as pD increased.[5,19,20] After spectrum (a) was recorded, Zn(II) (1.2 mM) was added to the solution while keeping the arsenate concentration and the pD of the solution constant. After 5 hours of equilibrium time spectrum (b) was recorded. The intensity of the absorption bands emanating from arsenate ions adsorbed on the ferrihydrite film increased within the 5 hours, indicating that the concentration of arsenate ions adsorbed on the ferrihydrite surface increased within the time frame of the experiment. In precious studies, the adsorption of arsenate on the ferrihydrite film from a 0.03 mM solution did not reach equilibrium after 5 hours.[5,18] The increase of the arsenate concentration on the ferrihydrite surface thus was not necessarily induced by the addition of Zn(II), since the plots of the kinetics of adsorption (Figure S5, Supporting Information) were continuous before and after Zn(II) addition.

The effect of reversing the order of addition of arsenate and zinc on the arsenate adsorption on the ferrihydrite film was also studied. Accordingly, the film was first pre-treated with a solution containing only 1.2 mM Zn(II), which after 5 hours equilibrium time was followed by the addition of arsenate (0.03 mM) while keeping the concentration of Zn(II) and the pD constant. Spectrum (c), in Figure 5, was recorded 5 hours after the addition of arsenate to the system. The spectrum showed the absorption bands, at 875 cm^{-1} and 840 cm^{-1}, assigned to arsenate adsorbed on the ferrihydrite film. The arsenate complexes formed on the ferrihydrite surface thus would appear to

have the same chemical structure as when the ferrihydrite film was not pre-treated with Zn(II). The intensity of the absorption bands, even though not exactly the same, were reasonably similar in both spectra (a and c), indicating that pre-treatment with Zn(II) did not significantly change the arsenate adsorption on the ferrihydrite film.

Accordingly, the results of the spectroscopic experiments were in agreement with the results obtained from the batch experiments. No effects of Zn(II) on the arsenate adsorption on ferrihydrite were found at pH/pD 4 and at the concentrations studied.

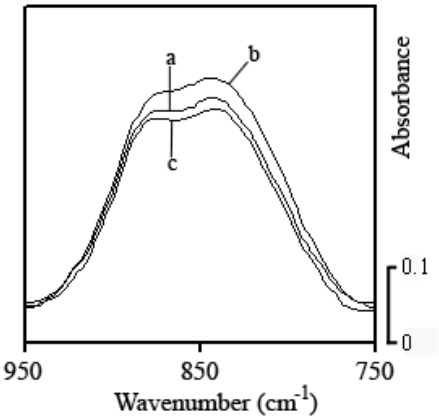

Figure 5. a) Spectrum of arsenate adsorbed on the ferrihydrite film from a 0.03 mM solution at pD 4 after 5h., time after which 1.2 mM Zn(II) were added and b) a spectrum was recorded 5h. after this addition. c) Spectrum recorded after 5 hours of arsenate adsorption from a solution of 0.03 mM at pD 4 when the film first had been equilibrated for 5 hours with a 1.2 mM Zn(II) solution at the same pD.

Batch adsorption experiments indicated that Zn(II) increased the arsenate removal from a solution by ferrihydrite at pH 8. In situ ATR-FTIR spectroscopy showed that no adsorption of arsenate on a ferrihydrite film occurred at pD 8 in the presence of Zn(II). The seemingly contradictory data could be explained by the precipitation of zinc hydroxide carbonate which was found to play a crucial role in the arsenate removal from a solution in the presence of Zn(II) at pH/pD 8. On the other hand, the formation of surface precipitates and ternary complexes Zn(II)/arsenate/iron oxide as suggested previously[6,8] were not detected in the conditions studied. At pH/pD 4, the presence of Zn(II) in the system did not have any significant effect of the adsorption of arsenate on ferrihydrite.

Acknowledgements

The Knut and Alice Wallenberg foundation and the Kempe foundation are greatfully acknowledged for the financial support given to purchase instruments used. Dr. Johanne Mouzon is acknowledged for assistance performing SEM measurements.

Supporting Information

Figures S1, S2, S3, S4 and S5 are found in Supporting Information.

References

(1) Giménez J.; Martínez M.; De Pablo J.; Rovira M.; Duro L.; Arsenic sorption onto natural hematite, magnetite and goethite. *J. Hazard Mater.* **2007** 141 (3), 575-580.

(2) Mohan D.; Pittman C.U.; Arsenic removal from water/wastewater using adsorbents- a critical review. *J. Hazard. Mater*. **2007** 142 (1-2), 1-53.

(3) Sherman D.M.; Randall S.R.; Surface complexation of arsenic(V) to iron(III) (hydr)oxides: Structural mechanism from ab initio molecular geometries and EXAFS spectroscopy. *Geochim. Cosmochim. Acta* **2003** 67(22), 4223-4230.

(4) Kumpiene J.; Assesment of Trace Element Stabilization in Soil. Doctoral Thesis, Luleå University of Technology, 2005:38, ISSN:1402-1544.

(5) Carabante I.; Grahn M.; Holmgren A.; Kumpiene J.; Hedlund J.; Adsorption of As(V) on iron oxide nanoparticle films studied by in situ ATR-FTIR spectroscopy. *Colloid Surf. A-Physicochem. Eng. Asp.* **2009** 346, 106-113.

(6) Gräfe M.; Nachtegaal M.; Sparks D.L.; Formation of Metal-Arsenate Precipitates at the Goethite –Water Interface. *Environ. Sci. Technol*. **2004** 38, 6561-6570.

(7) Bhattacharya P.; Mukherjee A.B.; Jacks G.; Nordqvist S.; Metal contamination at a wood preservation site: characterisation and experimental studies on remediation. *Sci. Tot. Environ.* **2002** 290, 165-180.

(8) Gräfe M.; Tappero R.V.; Marcus M.A.; Sparks D.L. Arsenic speciation in multiple metal environments II. Micro-spectroscopic investigation of a CCA contaminated soil. *J. Coll. Interf. Sci.* **2008** 321, 1-20.

(9) Yang W.; Kan A.T.; Chen W.; Tomson M.B.; pH-dependent effect of zinc on arsenic adsorption to magnetite nanoparticles. *Water Research.* **2010** 44, 5693-5701.

(10) Gräfe M.; Beattie D.A.; Smith E.; Skinner W. Copper and arsenate co-sorption at the mineral-water interfaces of goethite and jarosite. *J. Coll. Interf. Sci.* **2008** 322, 399-413.

(11) McComb K.; Craw D.; McQuillan J.A.; ATR_FTIR spectroscopic study of antimonate adsorption to iron oxide, *Langmuir* **2007** 23 (24),12125-12130.

(12) Cornell R.M., Schwertmann U., The iron oxides: structure properties, reactions, occurrences and uses, VCH, Weinheim, 1996.

(13) Kungliga Tekniska Universitet (KTH) Website; Visual Minteq webpage; http://www2.lwr.kth.se/English/OurSoftware/vminteq.

(14) Preis W.; Gamsjäger H.; (Solid+solute) phase equilibria in aqueous solution. XIII. Thermodynamic properties of hydrozincite and predominance diagrams for (Zn(II) + H2O + CO2). *J. Chem. Thermodynamics.* **2001** 33, 803-819.

(15) Frost R.; Hales M.; Synthesis and vibrational spectroscopic characterization of synthetic hydrozincite and smithsonite. *Polyhedron.* **2007** 26 (17), 4955-4965.

(16) Wahad R.; Ansari S.G.; Young Soon Kim; Dar M.A.; Hyung-Shink Shin; Synthesis and characterization of hydrozincite and its conversion into zinc oxide nanoparticles. *J. Alloys Comp.* **2008** 461, 66-77.

(17) Gupta A.; Bhatti H.S.; Verma N.K.; Tandon R.P.; Nano and bulk crystals of ZnO: Synthesis and characterization. *Digest Journal of nanomaterials and Biostructures.* **2006** 1 (1), 1-9.
(18) Carabante I.; Grahn M.; Holmgren A.; Hedlund J.; In situ ATR-FTIR studies on the competitive adsorption of arsenate and phosphate on ferrihydrite. *J. Coll. Interf. Sci.* **2010** 351 (2), 523-531.
(19) Loring J.S.; Sandström M.H.; Norén K.; Persson P. Rethinking arsenate coordination at the surface of goethite. Chem. Eur.J. **2009**, 15, 5063-5072.
(20) Roddik-Lanzilotta A.; McQuillan A.J.; Craw D. Infrared spectroscopic characterisation of arsenate(V) ion adsorption from mine waters, Macraes mine, New Zealand. *Appl. Geochem*. **2002** 17 (4) 445-454.
(21) Mirabella F.M., Internal Reflection Spectroscopy: theory and applications, Marcel Dekker, 1993.

Supporting Information

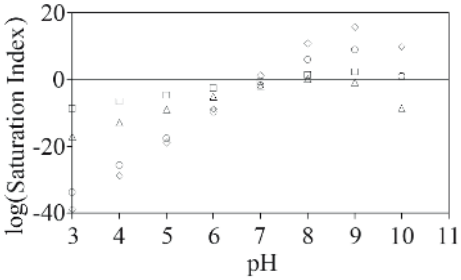

Figure S1. Saturation index for (□) zincite (ZnO), (○) zinc hydroxide chloride $Zn_5(OH)_8(Cl)_2$, (◊) hydrozincite ($Zn_5(OH)_6(CO_3)_2$) and (Δ) zinc arsenate ($Zn_3(AsO_4)_2 \cdot 2.5H_2O(s)$) calculated using Visual Minteq for an aqueous system containing 0.1M NaCl, 0.06 mM arsenate and 1.2 mM Zn^{2+} in contact with an atmosphere containing 0.00038 atm CO_2 and inert gas.

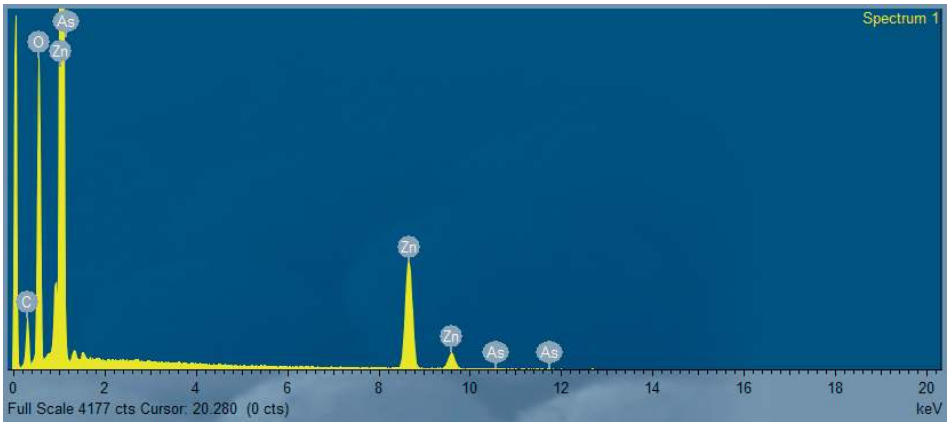

Figure S2. EDS X-ray spectrum from the like-star aggregate

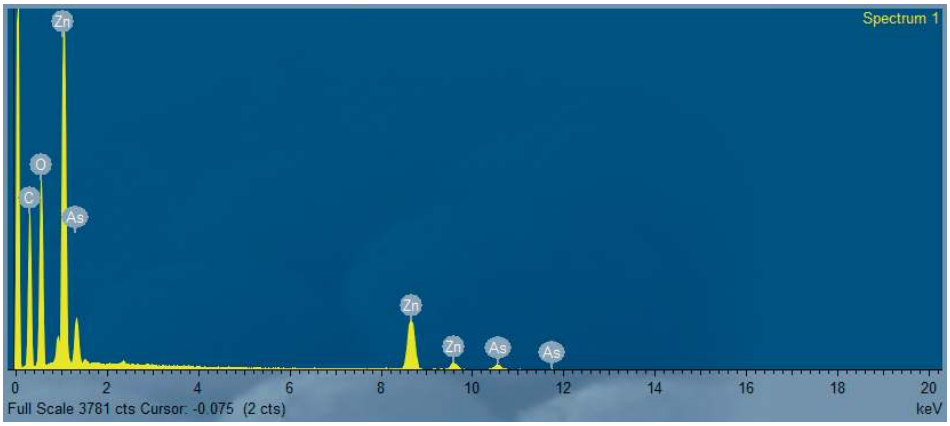

Figure S3. EDS X-ray spectrum from the non-defined aggregate

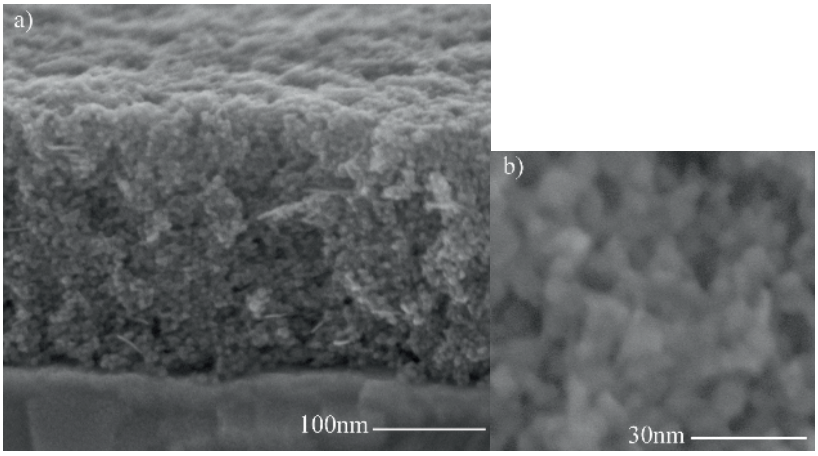

Figure S4. a) cross-sectional SEM image of the ferrihydrite film and b) high magnification SEm image of the ferrihydrite particles comprising the ferrihydrite film.

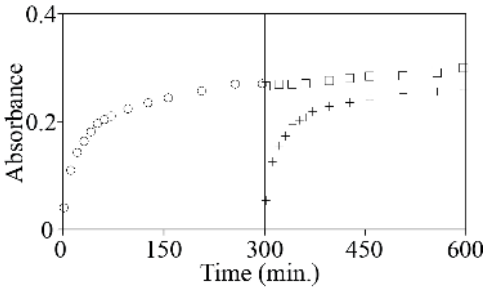

Figure S5. (○) kinetics of adsorption of arsenate onto the ferrihydrite film from a 0.03 mM arsenate solution at pD 4 followed by (□) kinetics of desorption upon addition of Zn^{2+} (1.2 mM). at the same pD. (+) Adsorption of arsenate (0.03 mM at pD 8) when the iron oxide was pre-treated for 5hours with 1.2 mM Zn^{2+}. The kinetic curves were obtained by plotting the height of the absorption band situated at ~ 840 cm^{-1} (assigned to arsenate adsorbed on the iron oxide) vs. time.

Paper V

An Effective Adsorbent prepared from Hematite for Removal of Arsenic (V) from Water

I. Carabante, J. Mouzon, J. Kumpiene, M. Grahn, A. Holmgren, A. Fredriksson, J. Hedlund

Manuscript in preparation.

An Effective Adsorbent prepared from Hematite for Removal of Arsenic (V) from Water

Ivan Carabante[a*], Johanne Mouzon[a], Jurate Kumpiene[b], Mattias Grahn[a], Andreas Fredriksson[c], Jonas Hedlund[a]

[a] *Chemical Technology, Luleå University of Technology, SE-97187, Luleå, Sweden*

[b] *Division of Geoscience and Environmental Engineering, Luleå University of Technology, SE-97187, Luleå, Sweden*

[c] *LKAB, SE-981 86 Kiruna*

Abstract

Iron oxides have been reported as efficient adsorbents for the removal of arsenic from drinking water. However a high specific surface area of the iron oxide is necessary to achieve sufficiently high specific adsorption capacity. In this work, a method was developed to enhance the specific surface area of porous bodies of sintered hematite. The method comprised partial dissolution of the raw material using hydrochloric acid followed by the formation of a coating of iron oxide nanoparticles on the raw material by precipitation. The nanoparticles comprising the coating showed two distinct habits: spherical habit with a diameter of about 8 nm and acicular habit with a length of about 35 nm and a diameter of about 13 nm. The spherical nanoparticles are likely ferrihydrite and the acicular particles are likely goethite and/or akaganéite. The specific surface area of the hematite raw material increased from 0.5 m^2/g to 3.75 m^2/g and the weight fraction of nanoparticles in the adsorbent was about 1 (w) %. Equilibrium adsorption data of arsenate on the adsorbent from a solution at pH 5 followed the Langmuir model and the monolayer adsorption capacity was estimated to be 0.65 mg[As]/g adsorbent. The adsorption capacity of the raw material was negligible. Breakthrough adsorption data for a 500 µg[As]/l arsenate solution at pH 5 showed sharp breakthrough fronts and a Thomas model could be fitted to the experimental data. The adsorption capacity estimated from the break through experiments was about 0.6 mg[As]/g adsorbent which agrees well with the estimated capacity from the batch adsorption experiments. The adsorbed arsenic could be desorbed using distilled water at pH 12.

1. Introduction

Arsenic is a hazardous element and ingestion of low amounts may, in the long term, lead to severe diseases such as cancer, pigmentation changes, skin thickening, neurological disorders and muscular weakness [1-4]. Ingestion of arsenic in sufficiently high amounts is acute toxic and may be lethal [1].

Arsenic in natural water is mainly found in two oxidation states: As (III) which dominates under reducing conditions, and As (V) which dominates in oxidative environments [1]. The inorganic species, arsenite (H_3AsO_3; As (III)) and arsenate (H_3AsO_4; As (V)), are the predominant species in natural waters while the organic species of arsenate, such as monomethylarsenate (MMA) and dimetylarsenate (DMA), are normally found at lower concentrations [5].

High occurrence of arsenic in natural waters has been reported in many countries worldwide, such as; USA, China, Chile, Bangladesh, Taiwan, Mexico, Argentina, Poland, Canada, Hungary, New Zealand, Japan, India and Sweden [1, 6]. The West Bengal in India and Bangladesh are the areas in which the greatest population is exposed to arsenic contaminated groundwater [1]. The origin of arsenate contamination in natural waters is basically due to: weathering of rocks, geochemical reactions, contact of arsenic bearing sediments with aquifers, industrial waste discharges, volcanic emissions, fertilizers, mining and smelting operations, and deficient industrial practice of wood impregnation by CCA (Copper, Chromium, Arsenate) wood preservatives [1,6,7]. While the USEPA lowered the permissible limit in drinking water to 10 µg/l following the WHO recommendations, still some countries, such as Argentina, Bangladesh, China and Mexico, have kept the maximum permissible limits for drinking water at 50 µg/l [1,8]. One of the reasons that these countries have kept their limits to 50 µg/l is their high concentration of arsenic in natural waters in combination with the lack of efficient and cost-effective methods for reducing the arsenic levels in the drinking water [1].
Iron oxides have shown high adsorption capacity towards arsenate [7, 9-12]. The affinity of arsenate to iron oxide depends on the pH value. At moderately acidic conditions (about pH 4) a maximum in the adsorption capacity is observed, while the extent of adsorption decreases as the pH value increases [9,11,13]. The presence of other species, such as phosphates, carbonates, zinc and/or humic acid in the aqueous solution has also been reported to affect the adsorption of arsenate on iron oxides [7,14,15]. The specific surface area will ultimately define the arsenate adsorption capacity by the iron oxide, with higher specific adsorption capacity as the specific surface area increases (or as the particle size decreases) [8,13,16].

Iron oxide adsorbents have been proposed as potentially inexpensive and efficient adsorbents to purify arsenic contaminated water [1]. Iron oxide showing a high specific adsorption capacity is typically comprised of very fine powders which are often difficult to separate from the solution after the adsorption process [1]. A common strategy when developing adsorbents which can easily be separated from solution is to coat an inert material by active iron oxide nanoparticles with high specific surface area, normally by a quick precipitation from Fe (III) salts. Examples of these kind of adsorbents are, for instance, iron oxide coated sand [17-19], iron oxide coated cement [20,21], Fe (III) modified natural zeolite tuff [22], iron hydroxide coated alumina [23], iron salt pre-heated activated carbon [1] or iron oxide coated glass fibers [24]. Another strategy to facilitate the collection of the adsorbent from the solution is to granulate fine iron oxide powder in a high pressure process obtaining so-called granular ferric hydroxide [25].

Iron oxides are relatively inexpensive and very abundant [8]. However, only iron oxide nanocrystals, especially poorly crystalline ferrihydrite, with specific surfaces areas over 200 m^2/g [13], has been reported to be suitable in arsenic removal processes [13]. Hydrochloric acid has been reported to dissolve Fe (III) from hematite [26]. The reported mechanisms of dissolution involve fully protonation of the oxide surface together with a formation of Cl-Fe bonds, which leads to breaking of Fe-O bonds [26]. Subsequent hydrolysis of Fe(III) ions in solution leads to precipitation of iron oxide nanocrystals, such as ferrihydrite, goethite or akaganeite (formation in Cl^- rich environments) [13]. The goal of the present work was to develop a simple and inexpensive method to increase the surface area of iron oxide crystals produced by a mining company to increase the adsorption capacity of arsenate. In the present study, the specific surface area of sintered iron oxide crystals was increased by first treating the raw material with hydrochloric acid, and in the next step, a coating of iron oxide nanoparticles was formed by precipitation. As a result, the arsenate adsorption capacity of the material significantly increased. An advantage of using Fe (III) oxide as a support material, is that it can be used as an Fe (III) source and the adsorbent easily could be regenerated by the same method once the life time of the adsorbent has been reached, without using any other Fe (III) sources. Another advantage is that by-products from mining companies comprised of undersized sintered iron oxide particles can be used as raw materials for preparation of valuable adsorbents.

2. Experimental & Models

2.1 Adsorbent synthesis and characterization

Fine powder of magnetite (MagnaChem 10, > 98.7 %, > 95 (w) % larger than 50 μm, > 55 (w) % larger than 20 μm) was placed in a crucible and sintered using a heating rate of 3.5 ºC/min, the temperature was kept constant at 1200 °C for 24 h, and thereafter the sample was cooled to room temperature at a cooling rate of 10 ºC/min. As will be shown below, the iron oxide was converted to hematite during the sintering process. The porous sintered body was crushed using a jaw crusher and particles in the size range -1.2 mm to +0.59 mm were selected by sieving. This size fraction of particles was used in the experiments and will hereafter be referred to as sintered hematite particles in the text.

A measuring cylinder was filled with sintered hematite particles. A sufficient amount of a 6 M hydrochloric acid (HCl, Merck, fuming 37 %) solution was added to the cylinder in order to cover all the sintered hematite particles. The particles were left in the solution for 3 h and subsequently, the wet particles were placed on a glass plate and dried at 50 ºC in a heating cabinet. After drying, the particles were rinsed with small amounts of a 12 M sodium hydroxide (NaOH, Sigma-Aldrich; p.a. > 98 %) solution. The amount of NaOH solution used was just sufficient to wet the particles in order to not rinse out nanoparticles from the material. After rinsing, the particles were again dried at 50 ºC. The cycle composed of rinsing with alkaline solution followed by drying at 50 ºC was repeated 5 times. Finally, the particles were rinsed with generous amounts

of distilled water until the supernatant became clear. The particles were thereafter dried at 50 ºC and kept in a refrigerator until use (within 2 months). The resulting particles will hereafter be named as adsorbent particles for the sake of simplicity.

2.2 Materials characterization

The magnetite fine powder, the sintered hematite particles and the adsorbent particles were characterised by means of Scanning Electron Microscopy (SEM) using a Magellan 400 field emission XHR-SEM without any coating. X-ray diffraction data of the three samples were recorded with a PANalytical Empyrean instrument, equipped with a graphite monocromator and a PIXcel3D detector and a Cu LFF HR X-ray tube. The specific surface areas of the samples were determined by adsorption of N_2 at 77 K using a Micrometrics ASAP 2010 instrument. The sintered hematite particles were degassed at 250 °C for about 12 h prior to analysis. The adsorbent particles were degassed using two protocols: One sample was degassed at 55 °C for about 7 days whereas the other sample was degassed at 100 °C for 3 days. Thermo Gravimetry (TG) data of the sintered hematite particles and the adsorbent particles were obtained using a Netzch STA 449 C instrument, by heating the sample from room temperature to 900 ºC with a constant heating rate of 10 ºC/min and recording the change in mass using synthetic air (AGA, 21 % O_2, 79 % N_2) in the sample environment.

2.3 Batch Adsorption experiments

For batch adsorption experiments at room temperature, glass flasks were filled with 100 ml of distilled water and 3 g adsorbent. The pH was kept constant at 5 during the first 3 h of the experiment using an automatized titrator equipment (TitroWico, Wittenfeld and Cornelius). After 3 h, a certain volume (0.25 ml, 0.5 ml, 0.75 ml, 1.5 ml, 2 ml, 5 ml and 8 ml, respectively) of a 0.48 g[As]/l arsenate stock solution ($NaH_2AsO_4 \cdot 7H_2O$; Fluka; p.a. 98.5 %)) was added to each of the flasks. The pH was again kept at 5 during 24 h. After 24 h of equilibration time, the supernatant was filtered with a 0.45 µm cellulose filter (Pall Corporation, Acrodisc 25 mm, w/ 0.45 µn Supor Membrane). The concentration of arsenate in the supernatant was subsequently analyzed by means of Induced Coupled Plasma – Optical Emission Spectroscopy (ICP-OES) using a Perkin Elmer Optima 2000 DV instrument. Arsenate concentrations of blank samples (without any adsorbent present) were analyzed before and after filtering in order to dismiss any influence of filtering on the arsenate analysis. Experiments using sintered hematite particles were also performed to assess the adsorption capacity of the iron oxide before coating with a film of iron oxide nanoparticles.

2.4 Column experiments

A vertical glass column (i.d. = 1.9 cm) was filled with 45 g of adsorbent for flow adsorption experiments at room temperature. The height of the adsorbent bed in the column was about 10 cm. The adsorbent bed was

fixed by two beds of about 5 cm height of silica beads (MERCK, Ø ca. 3 mm), one below and the other above the adsorbent bed. Filter paper was used both at the inlet and at the outlet of the column in order to filter out any particles from the stream. A 500 µg[As]/l arsenate solution in distilled water was adjusted to pH 5 by adding small amounts of a 0.1 M HCl solution. The arsenate solution was pumped through polypropylene tubes from the feed tank to the lower end of the column with a peristaltic pump at three different flow rates: 3.5 ml/min, 12.5 ml/min and 21.7 ml/min. The effluent solution from the top of the column was transported through the propylene tube to a 2 ml open vessel from where small aliquots were automatically taken for analysis every 15 minutes using an online arsenic analyzer (Istran, EcaMon SaFIA, equipped with a E-T Au electrode and an analytical range from 5 µg[As]/l to 500 µg[As]/l). The concentration of arsenate in the effluent was monitored well beyond the time when the concentration approached the concentration in the feed. In the next step, desorption experiments were carried out by flushing the column with distilled water adjusted to pH 12 or pH 5 at a flow rate of 21.7 ml/min.

2.5 Models

The Thomas Model has been widely applied to adsorption and ion exchange column breakthrough data [18, 27-32]. The model is based on the assumptions plug flow in the bed, that the adsorption equilibrium follows the Langmuir adsorption model and that the kinetics of adsorption follows a second-order reversible reaction [27]. The Thomas model is given by equation 1 [27]:

$$\frac{C}{C_o} = \frac{1}{1+exp\left(\frac{K_{tho}}{Q}(q \cdot W - C_o \cdot V)\right)} \qquad (1)$$

In this equation, C is the effluent adsorbate concentration (µg/l), C_o is the adsorbate concentration in the feed (µg/l), K_{tho} is the Thomas rate constant (l/min µg), q the amount adsorbed in equilibrium with the concentration in the feed (mg/g), W is the mass of the adsorbent (g), V throughput volume (l), and Q is the volumetric flow rate (l/min).

The linearized version of the Thomas Model, the so-called Yoon-Nelson model, described by equation 2 [32], was used in order to determine q_o and K_{YN} from the breakthrough adsorption data by linear regression.

$$Ln\left(\frac{C_o}{C} - 1\right) = -K_{YN} \cdot (t - \tau) \qquad (2)$$

In this equation, τ $\left(\frac{q \cdot W}{Q \cdot C_o}\right)$ is the time required to reach 50 % of the influent concentration in the effluent, i.e. C/C_o=0.5. K_{YN}($K_{tho} \cdot C_o$) is the Yoon-Nelson rate constant (min^{-1}).

Adsorption isotherm data often follows by the Langmuir Adsorption Model which is described by equation 3 [13].

$$q = \frac{K \cdot q_o \cdot C}{1 + K \cdot C} \qquad (3)$$

In equation 3, q is the equilibrium concentration adsorbed (mg/g); K is the Langmuir adsorption constant (l/mg [As]); q_o is the monolayer adsorption capacity (mg/g) and C is the adsorbate (arsenic) concentration in solution (mg/l) in equilibrium with the adsorbent.

Linear regression of the experimental data to the linearized version of the Langmuir Adsorption model, equation 4, was performed in order to determine K and q_o from the experimental adsorption data.

$$\frac{C}{q} = \frac{1}{q_o} \cdot C + \frac{1}{q_o \cdot K} \qquad (4)$$

3. Results and discussion

3.1 Characterization of the materials

Figure 1 shows an X-ray diffractogram of the magnetite raw material. The positions of the peaks and their relative intensities agree well with the reference pattern (pattern number 01-086-1362) for randomly oriented magnetite crystals, the latter represented by filled circles. No signal from amorphous material is observed. This shows that the raw material is comprised of pure magnetite crystals without amorphous material. The sintered hematite particles were crushed to obtain a fine powder suitable for analysis by XRD and the diffractogram of this sample is shown in Figure 1. The peak positions and relative intensities agree well with the reference pattern (pattern number 01-085-0599) for randomly oriented hematite crystals, the latter represented by filled triangles. This shows that the magnetite oxidized and converted to hematite during sintering in air as expected [13,33].

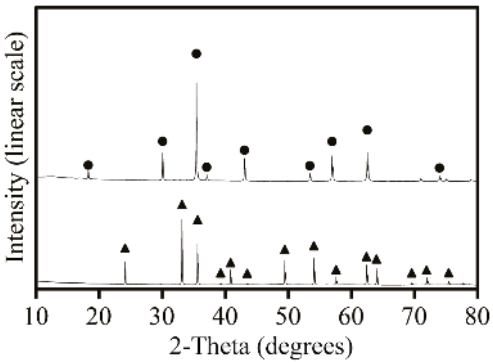

Figure 1. XRD pattern of the magnetite powder (top) and crushed porous sintered hematite particles (bottom). The black circles indicate the peak positions and relative intensities of the database XRD pattern of randomly oriented magnetite. The black triangles indicate the peak positions and relative intensities of the database XRD pattern of randomly oriented hematite.

Figure 2 shows a SEM image of the magnetite raw material (left) prepared from grinded iron ore. The image shows that the powder as expected is comprised of irregular-shaped crystals, with varying size up to ca. 50 µm. No aggregates were observed. A SEM image of the sintered hematite particles is shown in Figure 2 (right). The image shows that the original particles sintered at 1200 ºC as expected [33]. However, the SEM image also illustrates clearly that the sintered body is still very porous.

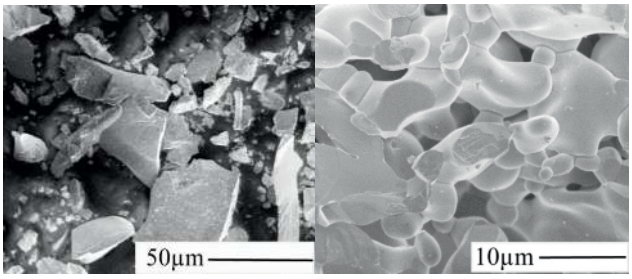

Figure 2. SEM image of the magnetite raw material (left) and sintered hematite particles (right).

Figure 3 shows SEM images of the adsorbent particles. The exterior of the adsorbent particles was completely covered by nanoparticles as illustrated in the top-left image. The formation of the coating was accompanied by a change of color of the sample from black-red to brown-yellow. The nanoparticles probably formed as a result of dissolution of Fe^{3+} from the sintered body by the action of HCl [25] followed by hydrolyzation of the Fe^{3+} ions and further crystallization to iron oxide nanoparticles while neutralizing with NaOH and/or drying at 50 ºC [13]. Images of fracture surfaces of adsorbent particles (top-middle image) show that the nanoparticles were also coating the pore walls inside the adsorbent particles. A thourough inspection by SEM was performed on 3 different adsorbent particles and the conclusion from this

inspection is that a nano particle film was fully coating both the outside and the interior of the particles. The top-right image illustrates the film at higher magnification. The film thickness varied between ca 10 nm up to 150 nm throughout the samples. Moreover, larger agglomerates were found on top of the films at some spots (not shown). By closer inspection it was found that the film was comprised of nanoparticles with two different habits, spherical and acicular. The bottom-left image illustrates small crystals of spherical habit with a particle size of about 8 nm, typical for ferrihydrite ($Fe_5O_8H{\cdot}H_2O$) [7,9,13]. Particles with acicular habit of about 35 nm in length and 13 nm in diameter are shown in the bottom-middle image. Both goethite (α-FeOOH) and akaganéite (β-FeOOH) crystals may display acicular habit[13, 34-36]. Most likely, both ferrihydrate and goethite (α-FeOOH) and/or akaganéite (β-FeOOH) (may form in solutions rich in Cl^- as in the present work) was precipitated during the neutralization step with NaOH [13]. The latter two images were recorded at specific locations where crystals with the two habits were segregated. However, usually, crystals with the two habits were coexisting, as shown in the bottom-right image.

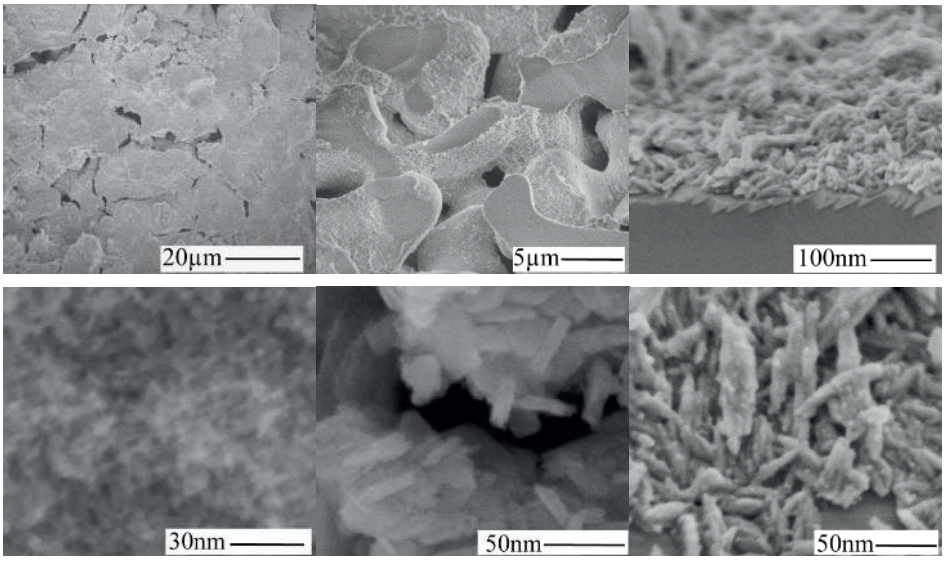

Figure 3. **top:** SEM images of the exterior (left) and fracture surface at low (center) and high (right) magnification of adsorbent particles. **Bottom:** SEM images recorded at high magnification illustrating ca. 8 nm crystals with spherical habit (left), crystals with acicular habit (middle), and crystals displaying both acicular and spherical habit in the same spot (right)

Figure 4 (a) shows a TG curve obtained from the sintered hematite particles. The weight loss during the thermal treatment was insignificant, which is expected for hematite as it does not undergo any phase transformations at these temperatures in air [13]. On the other hand, the adsorbent particles lost some weight loss upon heating, Figure 4 (b). The initial weight loss, from 25 ºC to about 200 ºC, most likely corresponds to desorption of water from the nanoparticles coating the hematite particles [13]. At temperatures exceeding 200 ºC the iron oxide nanoparticles probably underwent a phase transformation to hematite [13]. The total weight loss between 200 ºC and 900 ºC was about 0.2 %. The phase transformation of ferrihydrite into

hematite can be described by reaction 1 which represents a 25 % weight loss, while the phase transformation of goethite (or akaganéite) into hematite can be described by reaction 2 which represents a 10 % weight loss. By assuming that the nanoparticle coating was comprised of 50 (w) % ferrihydrite and 50 (w) % goethite (or akaganéite) the amount of nanoparticles in the adsorbent can be estimated from the weight loss between 200 ºC and 900 ºC to about 1 (w) %.

No differences between the two materials were observed in the recorded DSC curves, probably because of the low amount of nanoparticles in the adsorbent sample.

$$Fe_5O_8H{\cdot}H_2O\ (s) \rightarrow 2.5\ Fe_2O_3\ (s) + 1.5\ H_2O\ (g) \qquad (1)$$

$$FeOOH\ (s) \rightarrow 0.5\ Fe_2O_3\ (s) + 0.5\ H_2O\ (g) \qquad (2)$$

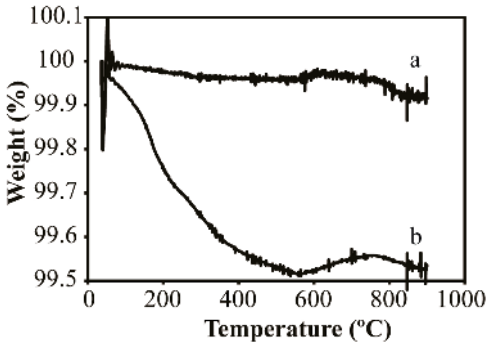

Figure 4: TG curves recorded of the sintered hematite particles (a) and the adsorbent particles (b).

The specific surface area of the sintered hematite particles increased from 0.5 m^2/g to 3.75 m^2/g as a result of the acid treatment and re-precipitation. Different degassing temperatures were used for the different samples. While the sintered hematite particles were degassed at 250 ºC, the adsorbent particles were degassed at 55 ºC or at 100 ºC in order to prevent transformation of the nanoparticles into hematite before the measurement. Similar specific surface areas of the adsorbent were observed after degassing at 55 ºC and at 100 ºC. However, the real specific surface area could perhaps be higher if the nanoparticles were not fully degassed at these temperatures.

The amount of nanoparticles in the adsorbent was estimated from gas adsorption data as follows. The spherical particles were assumed to be non-porous spheres with a diameter of 8 nm (as observed by SEM) and with a particle density corresponding to that of ferrihydrite, 3.96 g/cm^3 [13]. Under these assumptions, the specific surface area of the spherical crystals will be 474 m^2/g. The acicular particles were assumed to be non-porous cylinders with a length of 35 nm and a diameter of 13 nm (as observed by SEM) and with a particle density corresponding to that of goethite, 4.26 g/cm^3 [13]. Under these assumptions, the specific surface area of the acicular crystals will be 86 m^2/g. By again assuming that the nanoparticle coating was

comprised of 50 (w) % ferrihydrite and 50 (w) % goethite the amount of nanoparticles in the adsorbent was estimated from the change in surface area from 0.5 m^2/g (sintered hematite) to 3.75 m^2/g (adsorbent) to about 1 (w) % in good agreement with the estimation from the weight loss during the TG experiment.

The phase of the nanoparticles could not be determined by XRD, DRIFT and Raman measurements, probably due to the small amount of nanoparticles present in the adsorbent.

3.2 Adsorption experiments

3.2.1 Batch adsorption experiments

No removal of arsenate from solution was observed when the sintered hematite particles were used as adsorbent in batch adsorption experiments. Even though hematite adsorbs arsenate [37], the low specific surface area (0.5 m^2/g) of the sintered hematite particles used in the present work resulted in negligible adsorption. Figure 5 shows the experimental data (points) for adsorption of arsenate on the adsorbent particles at pH 5. The isotherm is typical for adsorption data following the Langmuir adsorption model, described by equation 3. Batch adsorption data for arsenate has previously been shown to follow the Langmuir adsorption model, for pure iron oxides, such as hematite, magnetite, goethite and ferrihydrite [11,18,37] and also for iron oxide-coated cement [21].

Figure 5 shows that a Langmuir model can be fitted to the experimental data very well with a regression coefficient (R^2) of 0.9998. The monolayer adsorption capacity, q_o, was fitted to be 0.65 mg[As]/g while the Langmuir adsorption constant, K, was fitted to 15.0 l/mg[As]. Table 1 shows the adsorption capacity per gram adsorbent reported for different iron-based adsorbents found in literature as compiled by Mohan et al. [1] together with the result from this study. The adsorption capacity per gram adsorbent of the adsorbent developed in the present work was significantly higher than the adsorption capacities reported for iron oxide coated sand while it was lower than that reported for waste of Fe(III)/Cr(III), iron oxide coated melted slag, granular ferric hydroxide, iron oxide coated cement, iron oxide coated alumina and iron-containing fly ash. The adsorption capacity, of course, depends on the density of the inert support of the adsorbent. The bulk density of the hematite particles was estimated to be 3.2 g/cm^3 as calculated from weighting a known volume of sintered hematite. The bulk density of sand, cement, ashes, slag and waste of Fe(III)/Cr(III) has been reported to be 1.4 - 1.7 g/cm^3, 2.2 - 2.4 g/cm^3, 0.64 - 0.72 g/cm^3, 1.1 -1.2 g/cm^3 and 0.895 g/cm^3 respectively [38,39]. These densities are significantly lower than the specific density of the sintered iron oxide particles. Table 1 also shows the adsorption capacities per volume adsorbent estimated from the data compiled by Mohan et al. [1] by considering the bulk densities of the materials. The adsorption capacity per volume adsorbent for the adsorbent prepared in the present work is now more appealing in comparison with the other adsorbents.

The arsenate adsorption capacity of ferrihydrite has been reported to be 111 mg[As]/g [11] and the arsenate adsorption capacity of goethite was reported to be 65 mg/g [40]. By again assuming that the nanoparticle film in the adsorbent developed in the present work was a mixture of 50 (w) % ferrihydrite and 50 (w) % goethite and the adsorption capacity of the adsorbent was 0.65 mg[As]/g, and the adsorption of arsenate on the sintered hematite particles was negligible, the amount of nanoparticles in the adsorbent was again estimated to be about 1 (w) %, in accordance with the estimations presented above based on nitrogen adsorption and TG measurements.

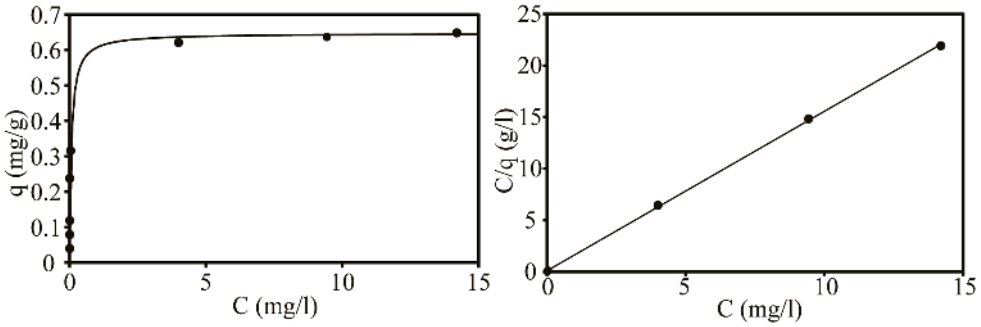

Figure 5. Adsorption isotherm of arsenate on the adsorbent at pH 5 at room temperature (left). Adsorption data plotted according to the linearized Langmuir model (right). Experimental data are represented by points and the fitted Langmuir model by curves.

Table 1. Adsorption capacities of iron oxide based adsorbent.

Adsorbent description	**Adsorption capacity (mg[As]/g)** as compiled by Mohan et al. [1]	**Adsorption capacity (mg[As]/cm^3)**
Adsorbent developed in present work	0.65	2.1
Iron oxide coated sand	0.043	0.065
Iron oxide coated sand	0.008	0.012
Iron oxide coated sand	0.018	0.027
Waste Fe(III)/Cr(III)	11.02	9.862
Iron oxide coated melted slag	18.8 - 78.5	20 - 80
Granular ferric hydroxide	8.5	
Iron oxide coated cement	6.43	15
Iron oxide coated alumina	36.64	
Iron-containing fly ash	19.46	13

3.2.2 Column experiments

First a breakthrough adsorption experiment using the sintered hematite particles as adsorbent was performed (data not shown). The breakthrough time obtained when a 500 µg[As]/l arsenate solution at pH 5 was pumped through the bed was very similar to the time taken by distilled water to fill the system, indicating that the adsorption of arsenate on the sintered hematite particles was negligible, in concert with the results from the batch adsorption measurements.

The points in Figure 6 shows the experimentally determined breakthrough curves obtained when a 500 µg[As]/l arsenate solution at pH 5 was pumped through the adsorbent bed. The scattering in the experimental data at high concentrations is probably a result of that the analysis instrument is operating close to its upper detection limit. The breakthrough curves showed the characteristic S-shape as expected for this kind of experiments. At the beginning of the experiment, the concentration in the effluent was very low, since all the arsenate was adsorbed on the adsorbent. At a certain point, arsenate starts to break through as the bed approaches saturation. To best utilize the adsorption capacity of the adsorbent, it is desirable with an as sharp breakthrough curve as possible. A sharp breakthrough curve is observed when the dispersion in the system is small (plug flow with no channeling etc.) and when the flow rate is sufficiently small compared to the rates of adsorption and diffusion (i.e. when the ratio K_{tho}/Q in equation 1 is large). Figure 6 shows that the sharpest breakthrough curve was observed for the lowest flow rate and that the width of the curve increased as the flow rate was increased, as expected. This is best visualized when the breakthrough curves are plotted versus volume of solution.

According to WHO, the arsenic guideline concentration for drinking water is 10 µg/l [1], which is 2 % of the influent concentration ($C/C_0 = 0.02$). The experimental point at which the effluent concentration reached 2 % of the influent concentration is known as the 2 % breakthrough point. The 2 % breakthrough volume (the volume of solution pumped through the bed) and the 2 % breakthrough time are presented in Table 2. It can be observed that the 2 % breakthrough volume ($V_{b2\%}$) decreased when increasing the flow rate, in fact when the lowest flow rate was used about twice the volume of water could be processed as compared to when the highest flow rate was used. The adsorption capacity at the 2 % breakthrough point ($q_{b2\%}$), which can be determined by integrating the breakthrough curve function [41] and represents the usable adsorption capacity of the adsorbent bed, decreased as the flow rate increased, see Table 2.

The total adsorption capacity of the adsorbent bed was determined by integrating the experimental breakthrough curves, yielding values in the range 0.50 - 0.54 mg[As]/g for the three flow rates. This adsorption capacity is similar to the loading of the adsorbent, q = 0.571 mg[As]/g, for a 500 µg[As]/l arsenate solution at pH 5 calculated from the Langmuir equation using the Langmuir adsorption constants determined from equilibrium data discussed earlier viz. $q_o = 0.65$ mg[As]/g and K = 15.01 l/mg[As].

The lines in Figure 6 represent the Thomas Model fitted to the experimental data and it is clear that the model fits the experimental data very well. The linearized Thomas Model was used to estimate τ and K_{YN},

from equation 2. τ represents the time required to reach 50 % of the feed concentration in the effluent, i.e. $C/C_o = 0.5$, and is reported in Table 3. The experimentally observed $t_{b50\%}$, reported in Table 2 agreed with the fitted parameter, τ, in the Thomas Model as expected considering the good fit between the model and experimental data. The adsorption capacity of the bed was calculated from the fitted parameter, τ (q_oW/QC_o), and reported in Table 3. The adsorption capacities calculated from the Thomas Model (0.60 – 0.61 mg[As]/g) were very similar, although slightly higher, than the value estimated from the Langmuir adsorption model fitted to the batch experiments of 0.571 mg[As]/g at a concentration in solution of 500 µg[As]/l. The adsorption rate constant, $K_{YN,}$ were also estimated for each flow rate and are reported in Table 3. Interestingly, K_{YN} increased linearly with flow rate ($R^2 = 1$), which has previously been reported [32]. This shows that the rate limiting step in the adsorption process is diffusion of arsenic through the liquid film surrounding the particles.

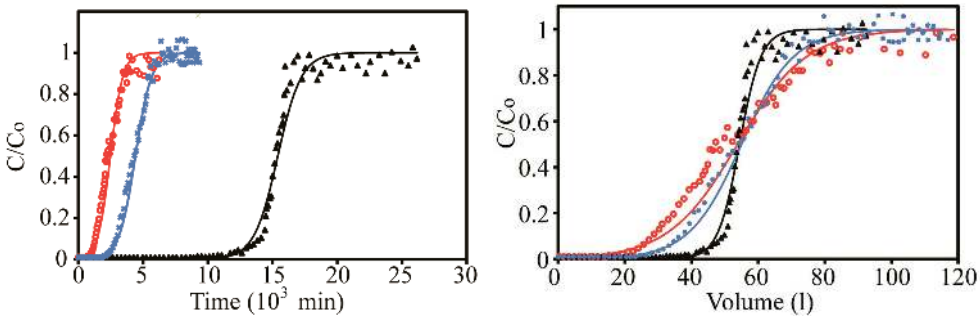

Figure 6. Breakthrough curves obtained for a feed with a concentration of 500 µg[As]/l at pH 5 pumped through the adsorbent bed at a flow rate of 21.7 ml/min (red), 12.5 ml/min (blue) and 3.5 ml/min (black). To the left the curves are represented by plotting the ratio between the effluent and the influent arsenic concentration vs. time. The dots represent experimental data, while the lines represent the Thomas Model fitted to the experimental data. To the right the breakthrough curves are plotted vs. the throughput volume.

Table 2. Summary of parameters obtained from the experimental breakthrough data

Flow rate (ml/min)	$V_{b2\%}$ (l)	$t_{b2\%}$ (min)	$q_{b2\%}$ (mg[As]/g)	$t_{b50\%}$ (min)	q_b (mg[As]/g)
3.5	41.5	11740	0.42	15160	0.54
12.5	27.9	2236	0.28	4330	0.54
21.7	19.3	889	0.19	2340	0.50

Table 3. Parameters of the Thomas Model obtained by fitting the model to experimental data.

Flow rate (ml/min)	τ (min)	K_{YN} (min^{-1})	q_o (mg[As]/g)	R^2
3.5	15400	0.0021	0.60	0.898
12.5	4400	0.0016	0.61	0.979
21.7	2480	0.0011	0.60	0.947

Two desorption experiments were performed to monitor the desorption/regeneration properties of the adsorbent. Figure 7 shows the curves obtained from both experiments where the effluent concentration from the column was plotted versus the throughput volume. First, the bed of adsorbent was saturated with a 500 µg[As]/l arsenate solution at pH 5 through the system. Then the feed was changed to water at pH 12 (filled triangles) or water at pH 5 (open squares), at a flow rate of 21.7 ml/min. The concentrations of arsenate in the effluent when the column was flushed by water at pH 12 was very high, up to 12000 µg/l (Figure 7 to the left), at the beginning (low throughput volumes) of the desorption. The concentration of arsenate in the effluent decreased very fast and was below 500 µg/l within the first 6 liters pumped through the column. By integrating the desorption curve, it was estimated that about 25 mg[As] was desorbed during the duration of the desorption experiment (flushing with about 50 liters) while about 17 mg[As] were desorbed within the first 5 liters. These values should be compared to the total amount of arsenic adsorbed estimated to be about 27 mg (45 g adsorbent · 0,6 mg[As]/g). It can thus be concluded that most of the arsenate adsorbed on the iron oxide bed was desorbed during the desorption experiment with distilled water at pH 12 and about 65 % of the arsenate was desorbed within the first 5 liters of the desorption experiment. This experiment thus showed that water at pH 12 could be used in a regeneration step for this kind of adsorbent, in accordance with previously reported data [9,17].The desorption curve obtained when distilled water at pH 5 was pumped through the system showed much lower concentrations in the effluent stream than the ones obtained at pH 12. As reported earlier, the arsenate complexes formed on the iron oxide at moderate acidic condition (pH 4) showed good stability in desorption experiments [9]. The total amount of arsenic desorbed during this experiment after flushing with about 50 liter corresponded to about 3 mg[As] (from integration of the desorption curve) which only represents 11 % of the previously adsorbed arsenic. This value is in line with the reported value of 10 % of arsenate desorbed from synthetic ferrihydrite after 200 min of flushing with D_2O at pD 4 [9]. These results illustrate that desorption/regeneration of the adsorbent with water should be conducted at high pH.

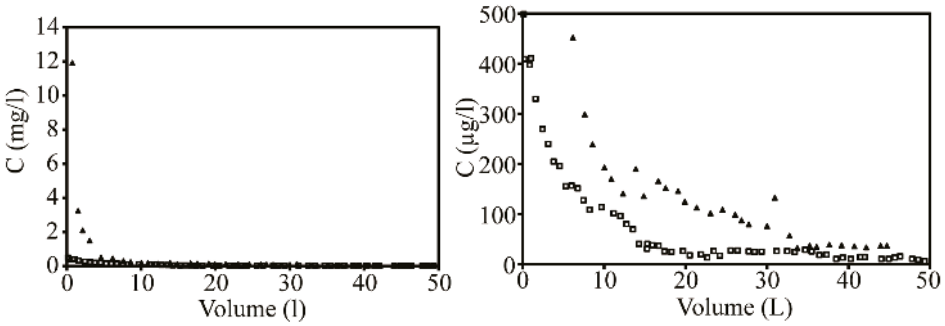

Figure 7. Desorption curves obtained by flushing water with a flow rate of 21.5 ml/min through the bed at pH 5 (open squares) and at pH 12 (filled triangles). Prior to the desorption, the adsorbent was saturated with a 500 µg[As]/l arsenate solution at pH 5. The desorption curve is plotted in the concentration range 0 -14 mg/l (to the left) and in the concentration range 0 – 500 µg/l (to the right) to better resolve the data at low concentrations.

4. Conclusions

A novel method for preparing an iron oxide based adsorbent for removal of arsenic from water was developed. The method was based on partial dissolution of Fe^{3+} from hematite by treatment with hydrochloric acid followed by hydrolysis leading to the formation of a coating of iron oxide nanoparticles. The coating was comprised of ferrihydrite and goethite and/or akaganéite crystals and the amount of nanoparticles in the adsorbent was about 1 (w) %. The adsorbent performed very well in both equilibrium and dynamic adsorption experiments using arsenate solutions at pH 5. The arsenate adsorption capacity was about 0.65 mg[As]/g. The adsorption rate was limited by diffusion of arsenic through the liquid film surrounding the particles. Desorption experiments with water at pH 12 showed that the adsorbent can be regenerated easily.

5. Acknowledgments

Luossavaara Kiirunavaara AB (LKAB) and CAMM are gratefully acknowledged for financial support. Dr. Evelina Bränvall and Lic. Engineer Iftekhar Bhuiyan, are also acknowledged for their helpful assistance in the laboratory.

6. References

(1) Mohan D.; Pittman C.U.; Arsenic removal from water/wastewater using adsorbents- a critical review. *J. Hazard. Mater*. **2007** 142 (1-2), 1-53.

(2) Mandal, B.K.; Suzuki, K.T.; Arsenic round the world: a review, Talanta **2002** 58, 201-235.

(3) Jain, C.K.; Ali, I., Arsenic occurrence toxicity and speciation techniques, Water Res. **2000** 34, 4304-4312.

(4) Ng J.C.; Wang, J.; Shraim, A., A global health problem caused by arsenic from natural sources, Chemosphere **2003** 52 (9), 1353-1359.

(5) Thirunavukkasaru, O.S.; Viraghavan, T.; Subramanian, K.S.; Removal of Arsenic in Drinking Water by Iron Oide-Coated Sand and Ferrihydrite – Batch Studies. *Water Qual. Res. J. Canada.* **2001** 36 (1), 55-70.

(6) Bhattacharya P.; Mukherjee A.B.; Jacks G.; Nordqvist S.; Metal contamination at a wood preservation site: characterisation and experimental studies on remediation. *Sci. Tot. Environ.* **2002** 290, 165-180.

(7) Carabante I.; Grahn M.; Holmgren A.; Hedlund J.; In situ ATR-FTIR sudies on the competitive adsorption of arsenate and phosphate on ferrihydrite. *J. Coll. Interf. Sci.* **2010** 351 (2), 523-531.

(8) Aredes S.; Klein B.; Pawlik M.; The removal of arsenic from water using natural iron oxide minerals. *J. Cle. Prod.* 2012 29-30, 208-213.

(9) Carabante I.; Grahn M.; Holmgren A.; Kumpiene J.; Hedlund J.; Adsorption of As(V) on iron oxide nanoparticle films studied by in situ ATR-FTIR spectroscopy. *Colloid Surf. A-Physicochem. Eng. Asp.* **2009** 346, 106-113.

(10) Luengo, C.; Brigante, M.; Avena, M., Adsorption kinetics of phosphate and arsenate on goethite. A comparative study, *J. Colloid Interface Sci.* **2007** 311 (2), 354-360.

(11) Rave, K.P.; Jain, A.; Loeppert, R.H.; Arsenite and Arsenate Adsorption on Ferrihydrite: Kinetics, Equilibrium, and Envelopes. *Environ. Sci. Technol.* **1998** 32, 344-349.

(12) Choong, T.S.Y.; Chuah, T.G.; Robiah, Y.; Koay, F.L.G.; Azni, IArsenic toxicity, health hazards and removal techniques from waer: an overview. *Desalination.* **2007** 217, 139-166.

(13) Cornell R.M., Schwertmann U., The iron oxides: structure properties, reactions, occurrences and uses, VCH, Weinheim, 1996.

(14) Visanu, T.; Nurak, G.; Chih-Hsiang, L.; Background species effect on aqueous arsenic removal by nano zero-valent iron using fractional factorial design. *J. Haz. Mat.* **2012** 205, 40-46.

(15) Yang, W.; Kan, A.T.; Chen, W.; Tomson M.B.; pH-dependent effect of zinc on arsenic adsorption to magnetite nanoparticles. *Water Research.* **2010** 44, 5693-5701.

(16) Waychunas, G.A.; Kim, I.; Banfield, J.; Nanoparticulates iron oxide minerals in soils and sediments: unique properties and contaminant scavenging mechanisms. *J. Nanopart. Res.* **2005** 7, 409-433.

(17) Joshi, A.; Chaudhuri, M; Removal of Arsenic from ground water by iron oxide-coated sand. *J. Environ. Eng.* 1996 122 (8), 769-771.

(18) Thirunavukkarasu, O.S.; Viraraghavan, T.; Subramiam, K.S.; Arsenic removal from drinking water using iron oxide-coated sand. *Wat. Air Soil Pol.* **2003** 142, 95-111.

(19) Vaishya, R.C.; Gupta, S.K.; Arsenic removal by sulfate modified iron oxide coated sand (SMIOCS) in Fixed Bed Column. *Water Qual. Res. J. Canada.* **2006** 41 (2) 157-163

(20) Kundu, S.; Gupta. A.K.; Adsorptive removal of As(III) from aqueous solution using Iron Oxide Coated Cement (IOCC): Evaluation of Kinetic, equilibrium and thermodynamic models. *Separation and Purification Technology*. **2006** 51, 165–172.

(21) Kundu, S.; Gupta. A.K.; Arsenic adsorption onto iron oxide coated cement (IOCC): regression analysis of equilibrium data with several isotherm models and their optimization. *Chemical Engineering Journal*. **2006** 122, 93–106..

(22) Stanić, T.; Daković, A.; Živanović, A.; Tomašević-Čanović, M.; Dondur, V.; Milićević, S.; Adsorption o arsenic (V) by iron (III)-modified natural zeolite tuff. Environ. Chem. Lett. 2009 7, 161-166.

(23) Hlavay, J.; Polyák, K.; Determination of surface properties of iron hydroxide-coated alumina adsorbent prepared for removal of arsenic from drinking water. *J. Coll. Interf. Sci.* **2005** 284, 71-77.

(24) Kumar, A.; Gurian, P.L.; Bucciarelli-Tieger, R.H.; Mitchell-Blackwood, J.; Iron oxide-coated fibrous sorbents for arsenic removal. *Am. Water Works Ass. J.* **2008** 100 (4), 151-164.

(25) Banerjee, K.; Amy, G.L.; Prevost, M.; Nour, S.; Jekel, M.; Gallagher, P.M.; Blumenschein, D., Kinetic and thermodynamic aspects of adsorption of arsenic onto granular ferric hydroxide (GFH), *Water Res*. **2008** 42, 3371-3378.

(26) Cornell, R.M; Giovanoli, R.; Acid Dissolution of Hematites of Different Morphologies. *Clay Minerals* **1993** 28, 223-232.

(27) Lezehari, M.; Baudu, M.; Bouras, O.; Basly, J.P.; Fixed-bed column studies of pentachlorophenol removal by use of alginate-en-capsulated pillared clay microbeads. *J. Coll. Interf. Sci.* **2012** 379 (1), 101-106.

(28) Yahaya, N.K.E.M; Abusta, I.; Latiff, M.F.P.M.; Bello, O.S.; Ahmad, M.A.; Fixed-bed column study for Cu(II) removal from aqueous solutions using rice husk based activated carbon. *Int. J. Eng. Tech.* **2011** 11 (1), 248-252.

(29) Suksabye, P.; Thirvetyan, P.; Nakbanpote, W.; Column study of Chromium (VI) adsorption from electroplating industry by coconut coir pith. *J. Hazard Tech.* **2008** 160, 56-62.

(30) Sansalone, J.; Asce, M.; Ma, J.; Parametric Analysis and Breakthrough Modeling of Phosphorous from Al-Oxide Filter Media. *J. Environ. Eng.* **2011** 137 (2), 108-118.

(31) Sulaiman, A.; Gupta, A.K.; Basheer, A.B.; A fixed bed sorption system for defluoridation of ground water. *J. Urban Environ. Eng.* **2009** 3 (1), 17-22.

(32) Luo, W.; Wei, P.; Chen, H.; Fan, L.; Huang, L.; Huang, L.; Huang, J.; Xu, Z.; Cen, P.;Kinetics and optimization of L-tryptophan separation with io-exchange chromatography. *Korean J. Chem. Eng.* **2011** 28 (5), 1280-1285.

(33) Forsmo, S.P.E.; Forsmo, S.-E.; Samskog, P.-O.; Björkman, B.M.T.; Mechanisms in oxidation and sintering of magnetite iron ore green pellets. *Powder Tech.* **2008** 183, 247-259.

(34) Schwertmann, U.; Murad, E.; Effect of pH on the Formaion of Goethite and Hematite from ferihydrite. *Clays Clay Min.* **1983** 31, 4, 277-284.

(35) Montes-Hernandez, G.; Beck, P.; Renard, F.; Quirico, E.; Lanson, B.; Chiriac, R.; Findling, N.; Fast Precipitation of Acicular Goethite from Ferric Hydroxide Gel under Moderate Temperature (30 and 70 ºC). *Crystal Growth Des.* **2011** 11, 2264-2272.

(36) Glotch, T.D.; Kraft, M.D.; Thermal transformations of akaganéite and lepidocrocite to hematite: assessment of possible precursors to Martian crystalline hematite. Phys. Chem. Minerals. **2008** 35, 569-581.

(37) Gimenez, J.; Martinez, M.; de Pablo, J.; Rovira, M.; Duro, L.; Arsenic sorption onto natural hematite, magnetie, and goethite. *J. Hazard. Mat.* **2007** 141, 575-580.

(38) Perry R.H., Green D.W., Perry's Chemical Engineers' Handbook, McGraw-Hill, 5th edition, **1973**.

(39) Namasivayan, C.; Senthilkumar, S.; Removal of Arsenic(V) from Aqueous Solution Using Industrial Solid Waste: Adsorption Rates and Equilibrium Studies. Ind*. Eng. Chem. Res.* **1998** 37, 4816-4822.

(40) Asta, M.P.; Cama, J. Martinez, M.; Gimenez, J. Arsenic removal by goethite and jarosite in acidic conditions and its environmental implications. *J. Hazard. Mat.* **2009** 171, 965-972.

(41) Crittenden, B.; Thomas, W.J., Adsorption Technology and Design, Buterworth-Heinemann, 1st edition, **1998**.